UNIVERSITA' DEGLI STUDI DEL PIEMONTE ORIENTALE

"AMEDEO AVOGADRO"

Dottorato in Medicina Molecolare XIX ciclo

TESI DI DOTTORATO

LA RISPOSTA BIOLOGICA ALLO STRETCHING MECCANICO IN

COLTURE CELLULARI DINAMICHE

Candidata: Francesca Boccafoschi

Anno Accademico: 2006-2007

INDICE

1. INTRODUZIONE

1.1 STATO DELL'ARTE

La biomeccanica è lo studio scientifico delle forze e degli effetti che esse hanno sul corpo umano. Questa scienza ha avuto riscontri molto interessanti in diversi campi quali la medicina, lo sport, la riabilitazione e la ricerca di base. La ricerca scientifica classica, infatti, negli ultimi anni ha sviluppato strumenti di laboratorio più o meno empirici al fine di applicare ai modelli oggetto di studio stress meccanici di varia natura (*shear stress*, stiramento, compressione, etc.) e di verificarne la risposta biologica. In letteratura diverse pubblicazioni riportano come il comportamento cellulare sia a livello morfologico così come a livello molecolare subisca delle profonde modificazioni quando in presenza di un ambiente dinamico, cioè in cui le cellule vengono meccanicamente sollecitate, rispetto alla colture classiche per così dire "statiche" [Chiquet et al., 2007; Helderman et al., 2007; Marotti et al., 2007].

In particolare, l'ingegneria tessutale fornisce un nuovo approccio all'attuale problema della rigenerazione degli organi e all'eventuale utilizzo di biomateriali appropriati al fine di ristabilire l'ottimale funzionalità dei diversi apparati. Ma nonostante i numerosi sforzi fatti negli ultimi anni per ottenere la rigenerazione di organi e tessuti in ambiente statico, una sfida tuttora da vincere è la rigenerazione di questi in ambienti dinamici atti a riprodurre e mantenere le condizioni fisiologiche dinamiche normalmente presenti nel corpo umano. Vi è, dunque, una crescente attenzione da parte del mondo scientifico volta da una parte allo studio del comportamento cellulare in presenza di stress meccanici di vario tipo, dall'altro uno sforzo notevole al fine di ideare ed utilizzare strumentazioni adatte alla riproduzione il più possibile fedele degli stress meccanici fisiologici (ad esempio bioreattori, colture cellulari su substrati deformabili meccanicamente, etc.).

1.2 I TESSUTI

Il concetto di tessuto è relativamente recente ed il primo che ne introdusse il termine fu il giovane anatomista francese François Xavier Bichat (1771-1802) che, in base a criteri puramente macroscopici, si convinse dell'esistenza, in tutti gli organismi animali, di costituenti fondamentali comuni, che ritenne formassero la base di una ventina di tessuti i quali, combinandosi variamente tra loro, formavano degli organi. Fu così che, pubblicando nel 1800 il suo "Traitè des Membranes", introdusse nelle scienze la nozione di tessuto, spostando l'attenzione dei morfologi dagli organi ai tessuti che li componevano.

François Xavier Bichat (1771-1802)

Tuttavia, criteri di ordine microscopico per una più accettabile classificazione dei tessuti compariranno nella "Allgemeine Anatomie" di Friedrich Gustav Jacob Henle (1809-1885). Poco dopo, Rudolf Virchow (1821-1902), considerando l'organismo come "uno stato di cellule" riconobbe che i tessuti fossero costituiti sempre e senza eccezione, dalle individualità elementari della sostanza organizzata, cioè da cellule e da sostanze da esse elaborate.

I grandi istologi del XIX secolo erano in prevalenza morfologi e, pertanto, ritenevano che lo studio delle strutture dovesse essere fine a se stesso. Questo modo di concepire l'istologia aveva le sue limitazioni nell'investigare il nesso tra struttura e funzione e non consentiva di cogliere le

condizioni biologiche profonde. Cominciò così a manifestarsi il desiderio di ricercare il significato funzionale delle strutture biologiche e la necessità di ricorrere al metodo sperimentale. Si giunse così a stabilire che, per la specifica architettura morfo-funzionale, ciascuno dei tessuti fondamentali rispondeva ad un'altrettanto specifica attività biomeccanica.

Per finalizzare le proprie funzioni, le cellule devono essere in grado di utilizzare le informazioni genetiche per sintetizzare, immagazzinare e trasportare biomolecole, convertire diverse forme di energia, trasdurre segnali, mantenere le strutture interne e rispondere a segnali provenienti dall'ambiente esterno. Molti di questi processi coinvolgono gli stress meccanici. Il campo della meccanica cellulare, che fa parte di un più ampio campo interdisciplinare, riguarda lo studio delle caratteristiche del movimento cellulare, delle deformazioni ed interazioni, così come le cellule stesse percepiscono, generano e rispondono alle forze meccaniche. Negli anni '90, il campo della meccanica cellulare ha subito una rapida crescita. Sviluppi recenti riguardano studi sulle dinamiche citoscheletriche e l'interazione cellula-matrice extracellulare in relazione alla forma, la funzione, la deformabilità e le proprietà meccaniche dell'intera cellula; la viscoelasticità e le connessioni delle strutture subcellulari come microtubuli, filamenti di actina, filamenti intermedi; gli aspetti biochimici dell'adesione cellulare e della locomozione cellulare a livello sia cellulare sia molecolare; danni cellulari dovuti a forze meccaniche; e gli effetti delle perturbazioni meccaniche sui processi cellulari, quali la crescita, il rimodellamento, la meccanotrasduzione del segnale e l'espressione genica. Questi nuovi sviluppi della ricerca hanno avuto un impatto significativo sull'ingegneria cellulare e tessutale, sulla biomeccanica cardiovascolare, sulla biomeccanica dei tessuti molli e duri, sulla modellizzazione biomedica e sulla studio dei biomateriali.
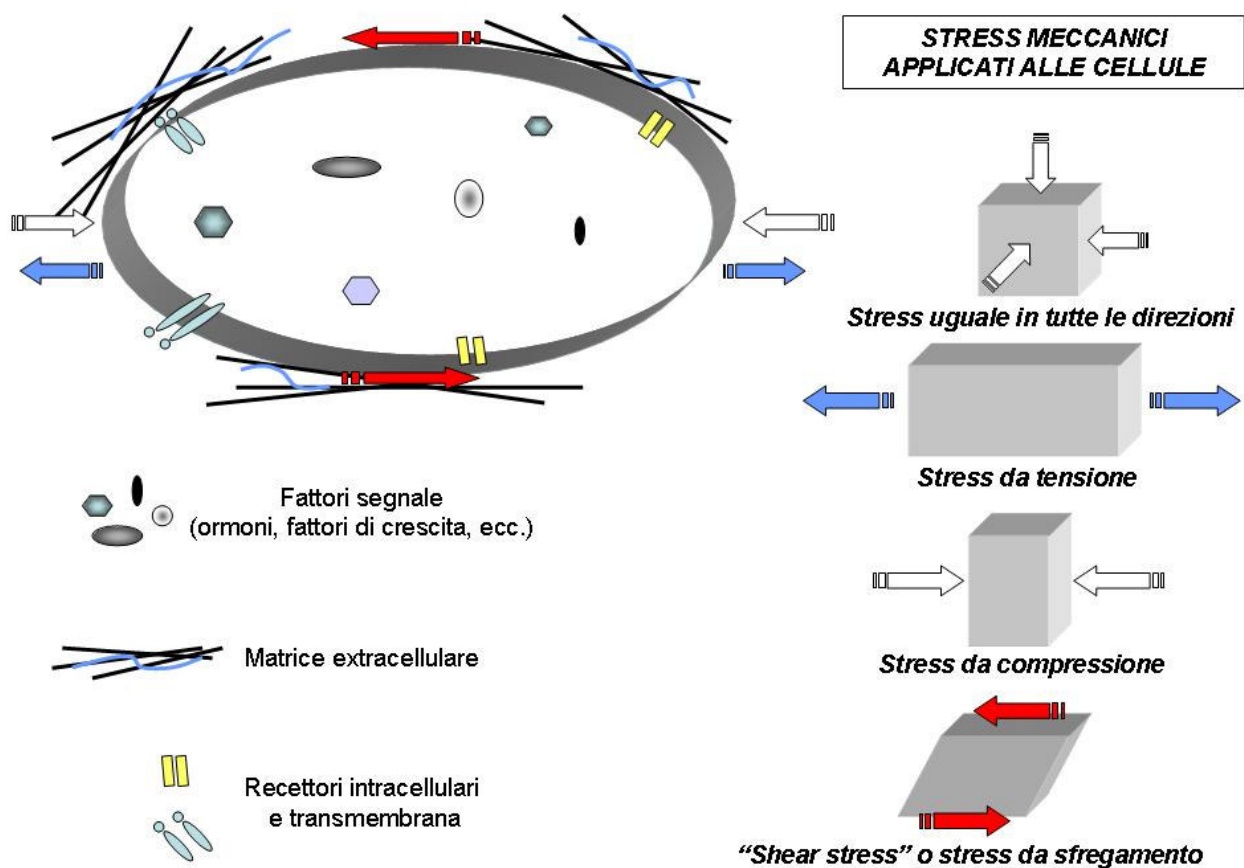
1.3 TESSUTI, CELLULE E STRESS MECCANICI

Le cellule si deformano quando forze esterne agiscono su di loro. Questi comportamenti sono descritti dalle proprietà meccaniche delle cellule e sono determinate dalla composizione e dalle strutture cellulari così come dall'ambiente che le circonda e con il quale le cellule interagiscono. Il contributo dovuto alle diverse componenti varia. Ci sono strutture specifiche nella cellula che garantiscono la deformabilità. Allo stesso modo, le proprietà meccaniche dei tessuti contribuiscono alla deformazione dell'intero tessuto sottoposto a forze meccaniche [Kreplak et al. 2007] .

Dunque, le forze meccaniche inducono nelle cellule risposte biologiche specifiche. Ci sono crescenti evidenze che condizioni fisiologiche o patologiche delle cellule dipendono o sono regolate dall'ambiente meccanico circostante. La regolazione delle funzioni cellulari da parte delle forze meccaniche applicate è di grande interesse nella biomeccanica cellulare. Le questioni critiche includono il modo in cui le forze sono applicate ai tessuti cellulari aderenti alla matrice extracellulare, come queste forze sono trasmesse e distribuite alle cellule e come queste vengono trasformate in segnali biochimici atti ad indurre le risposte cellulari [Wang et al., 2006]. Da questo punto di vista, identificare specifici "pathway" molecolari coinvolti nella trasmissione delle forze meccaniche è altrettanto importante quanto identificare le molecole coinvolte nella cascata di eventi biochimici intracellulari.

Il citoscheletro è sicuramente il candidato più indicato come regolatore dei meccanismi meccanici. Questo è costituito da un sistema strutturale organizzato che consiste di filamenti di actina (6-10nm di diametro), filamenti intermedi (7-11nm) e microtubuli (25nm). Le proprietà meccaniche del citoscheletro hanno un ruolo chiave non solo nel determinare la forma cellulare, ma anche in altre funzioni cellulari quali lo "spreading", la migrazione, l'orientamento o la citochinesi [Kreplak et al., 2007].

Lo shear stress o stress da sfregamento può inoltre indurre il rimodellamento citoscheletrico, portando all'allungamento ed all'allineamento delle cellule endoteliali nella direzione del flusso. Il

rimodellamento citoscheletrico viene inibito dalla depolimerizzazione dei microtubuli ed inoltre è stato dimostrato che l'attività tirosina-chinasi e il calcio intracellulare giocano un ruolo fondamentale in questo meccanismo, mentre i meccanorecettori quali i canali ionici, la proteina-chinasi C e i filamenti intermedi non intervengono nel cambiamento morfologico e nel rimodellamento citoscheletrico. Al contrario, lo stiramento ciclico del substrato induce le cellule endoteliali ad orientarsi perpendicolarmente rispetto alla direzione dello stiramento e le risposte allo stiramento vengono inibite utilizzando il gadolinio (inibitore dei canali ionici) [Shikata et al., 2004]. Dunque, sembra che meccanismi diversi vengano coinvolti a seconda del tipo di stress meccanico applicato, risultando in risposte biologiche sensibilmente differenti.

STRESS MECCANICI APPLICATI ALLE CELLULE

Stress uguale in tutte le direzioni

Stress da tensione

Stress da compressione

"Shear stress" o stress da sfregamento

Fattori segnale (ormoni, fattori di crescita, ecc.)

Matrice extracellulare

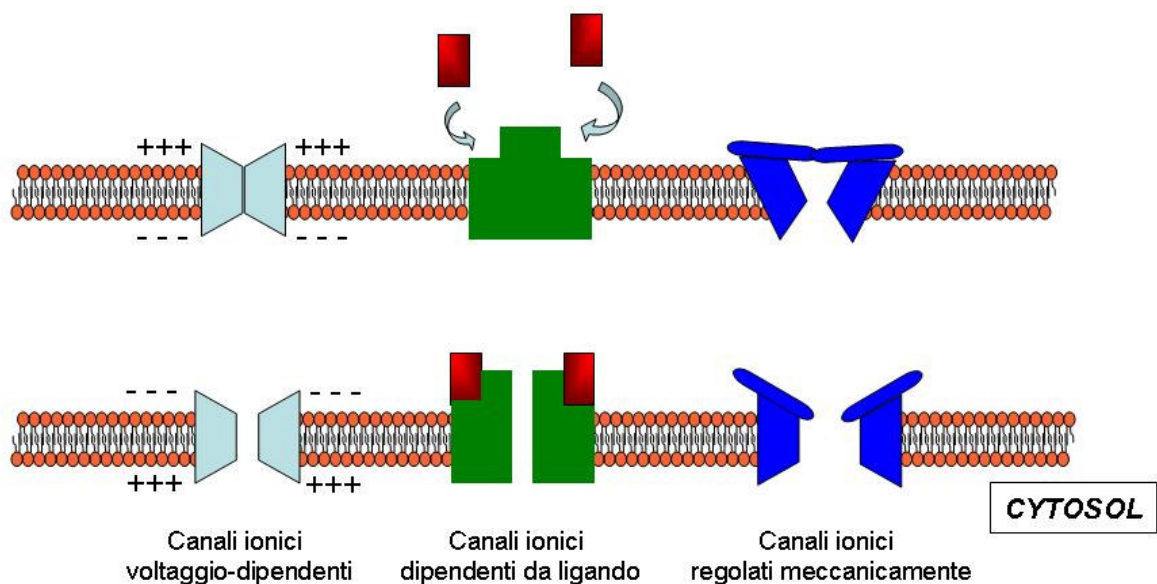Recettori intracellulari e transmembrana

I meccanismi tramite i quali le cellule identificano e convertono gli stimoli meccanici in risposte elettrofisiologiche e biochimiche rimangono non del tutto chiare. Molecole esposte sulla superficie

cellulare possono essere attivate direttamente dallo spostamento fisico (cambiamento conformazionale) o indirettamente tramite gradienti di trasferimento di massa che cambiano le interazioni recettore-ligando. Queste strutture di membrana (o meccanorecettori) includono canali ionici, recettori legati a proteine G, recettori tirosina-chinasi e integrine coinvolte nelle adesioni focali. Questi meccanorecettori possono generare una cascata biochimica di risposte nella faccia citoplasmatica della membrana cellulare, tramite secondi messaggeri, l'attivazione di proteine chinasi seguite dall'attivazione nel citosol di fattori trascrizionali, e/o dalla regolazione di geni per la trascrizione a livello nucleare. Un'altra via di traduzione dei segnali meccanici coinvolge le interazioni tra i meccanorecettori attivati e gli elementi citoscheletrici. La trasmissione può avvenire tramite qualsiasi connessione con il citoscheletro (per esempio siti di adesione focale, giunzioni cellula-cellula, etc.) e può portare ad un'enorme varietà di risposte cellulari. Alcune delle risposte generate da molecole di segnale intracellulari (secondi messaggeri) sono rapide, nell'ordine di secondi o minuti (per esempio cambi di permeabilità ionica, generazione di inositolotrifosfato, liberazione di calcio intracellulare, attività adenilato-ciclasica), mentre altri si sviluppano nel corso di alcune ore (alterazione dell'espressione genica, ridistribuzione delle proteine citoscheletriche, cambiamenti morfologici cellulari).
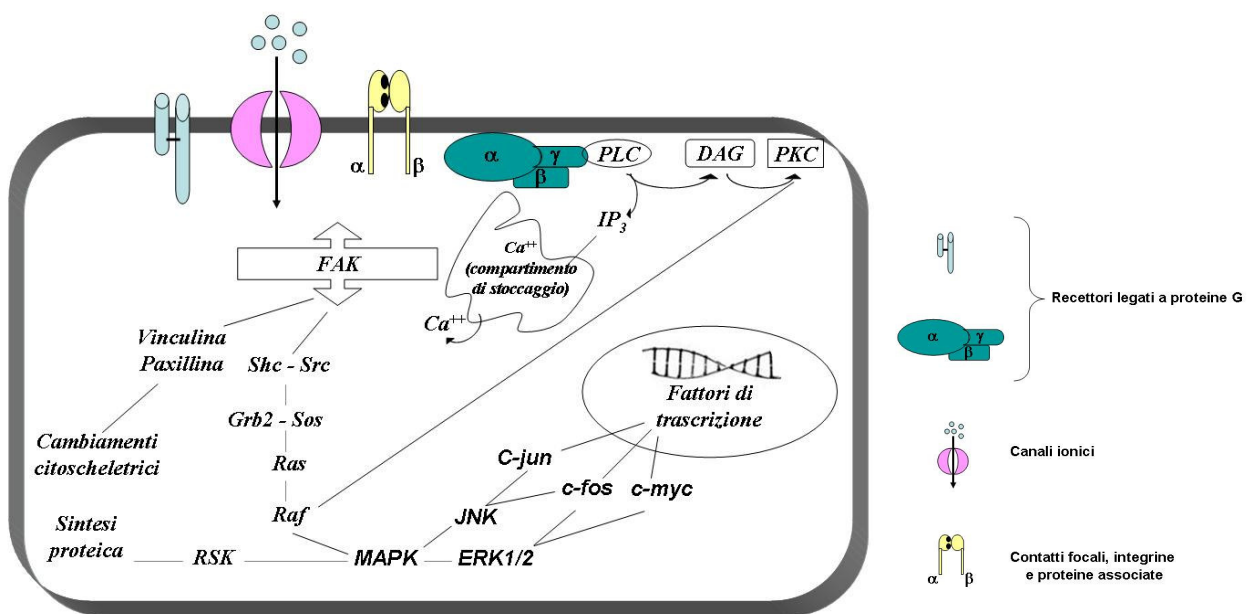
1.3.1 Canali ionici.

Il doppio strato lipidico delle membrane cellulari è altamente permeabile a molecole idrofobiche e poco polari mentre è altamente impermeabile a molecole cariche e ionizzate, funzione cruciale per il mantenimento di differenti concentrazioni di soluti rispetto a quelle presenti nei fluidi extracellulari. Proteine di membrana specializzate (canale e trasportatrici) sono responsabili del trasporto di specifici ioni attraverso la membrana cellulare. Le proteine canale non legano gli ioni ma formano pori idrofobici attraverso la membrana, che, in conformazione aperta, permettono il trasporto, mentre le proteine trasportatrici si legano agli ioni e cambiano la loro conformazione al fine di trasportare attraverso la membrana gli ioni legati. Il trasporto tramite i canali ionici ed alcune proteine trasportatrici è a diffusione facilitata, in cui cioè la forza di trasporto del soluto è data dal suo stesso gradiente elettrochimico attraverso la membrana. Le proteine trasportatrici possono anche trasportare attivamente il soluto contro gradiente elettrochimico, attraverso l'utilizzo di fonti energetiche quali ATP o GTP [Gautam M et al., 2006].

Canali ionici
voltaggio-dipendenti

Canali ionici
dipendenti da ligando

Canali ionici
regolati meccanicamente

CYTOSOL

1.3.2 Recettori legati a proteine G.

I recettori legati a proteine G, che appartengono alla famiglia dei recettori con sette domini transmembrana, alterano la concentrazione dei secondi messaggeri, che a loro volta influenzano il

comportamento di altre proteine bersaglio nella cellula. Le interazioni tra i recettori e i secondi messaggeri sono mediate da enzimi o canali ionici, attivati proteine regolatorie leganti GTP (proteine G). Le proteine G sono eterodimeri legati tramite una catena specifica alla faccia citoplasmatica della membrana cellulare. La proteina G attivata lega GDP al posto di una molecola di GTP in seguito all'attivazione del recettore. Questo fa sì che le subunità formanti la proteina G si dissocino attivando il *downstream* di attivazione dei secondi messaggeri. Il segnale citoplasmatico coinvolge la trasduzione di segnali quali: a) l'attivazione della fosfolipasi C (PLC); b) l'attivazione di canali per il calcio e l'inibizione dell'adenilato ciclasi; c) la stimolazione dei canali per il potassio. La PLC stimola diverse risposte cellulari formando inositolo-1,4,5-trifosfato (IP_3) e diacilglicerolo (DAG) da fosfotidilinositolo-4,5-bifosfato. IP_3 diffonde rapidamente nel citosol dalla membrana cellulare e rilascia Ca^{2+} dai compartimenti di deposito del calcio intracellulari. L'attivazione del DAG è transiente, ed entro pochi secondi può a) essere successivamente clivato per rilasciare acido arachidonico (AA) successivamente trasformato in prostacicline (PGI2) e nelle relative molecole di segnale lipidiche; b) essere fosforilato per formare fosfatidato (PA); o c) attivare la proteina chinasi C (PKC) (proteina chinasi serina/treonina specifica). PKC può fosforilare molte proteine con differenti funzioni nella cellula e può aumentare la trascrizione di alcuni geni [Li et al., 2007].
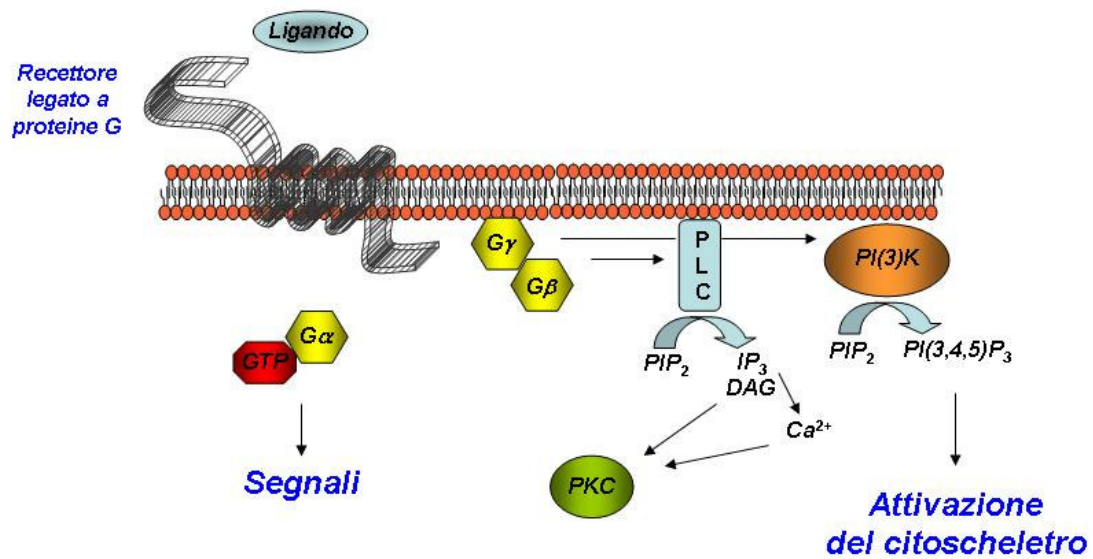
1.3.3 Proteine chinasi.

Gli eventi precoci della trasduzione del segnale attivati da stress meccanici portano ad una cascata di eventi a valle la maggior parte dei quali sono mediati da proteine chinasi attivate in maniera sequenziale. L'attivazione completa delle proteine chinasi richiede la fosforilazione di residui di tirosina e treonina. Una volta attivate le chinasi trasmettono il segnale a valle fosforilando a loro volta altre proteine chinasi e fattori di trascrizione. Queste chinasi vengono spente dall'attivazione di specifiche fosfatasi.

Le MAPK sono le chinasi più studiate nel campo degli stress meccanici e sono state originariamente identificate come chinasi associate ai microtubuli a causa del loro coinvolgimento nel citoscheletro [Li et al., 2007].

1.3.4 Contatti focali, integrine e proteine associate.

Numerosi studi hanno dimostrato che gli stress meccanici quali lo shear stress causano la riorganizzazione del citoscheletro e l'allineamento delle cellule in direzione dello stress. La redistribuzione delle fibre da stress di F-actina o microfilamenti, dei microtubuli, dei filamenti intermedi in risposta allo stress, in aggiunta ai dati che confermano che la rottura dei filamenti

citoscheletrici utilizzando specifiche molecole chimiche inibisce le risposte intracellulari indotte dallo stress, fornisce forti evidenze che il citoscheletro è il maggiore meccanotrasduttore. I siti di contatto (per esempio i contatti di adesione focale, i contatti cellula-cellula) tra citoscheletro e i meccanorecettori sono strutturalmente connessi, il che implica che la trasduzione del segnale attraverso il citoscheletro sia decentrata. Le adesioni focali sono le strutture maggiormente studiate come potenziali meccanotrasduttori per il citoscheletro. Esse forniscono un *continuum* tra il citoscheletro e le proteine della matrice extracellulare, e sono formate nella porzione di legame della parte citoplasmatica delle integrine con le proteine del citoscheletro stesso. I contatti focali sono responsabili dell'adesione cellulare ed hanno un ruolo chiave nei segnali cellulari, nella morfologia, nella proliferazione, nella migrazione e nel differenziamento. Le integrine sono eterodimeri formate da glicoproteine transmembrana che servono da recettori di adesione. La subunità α determina la specificità del recettore per le componenti della matrice extracellulare (per esempio fibronectina, collagene, laminina, etc.).
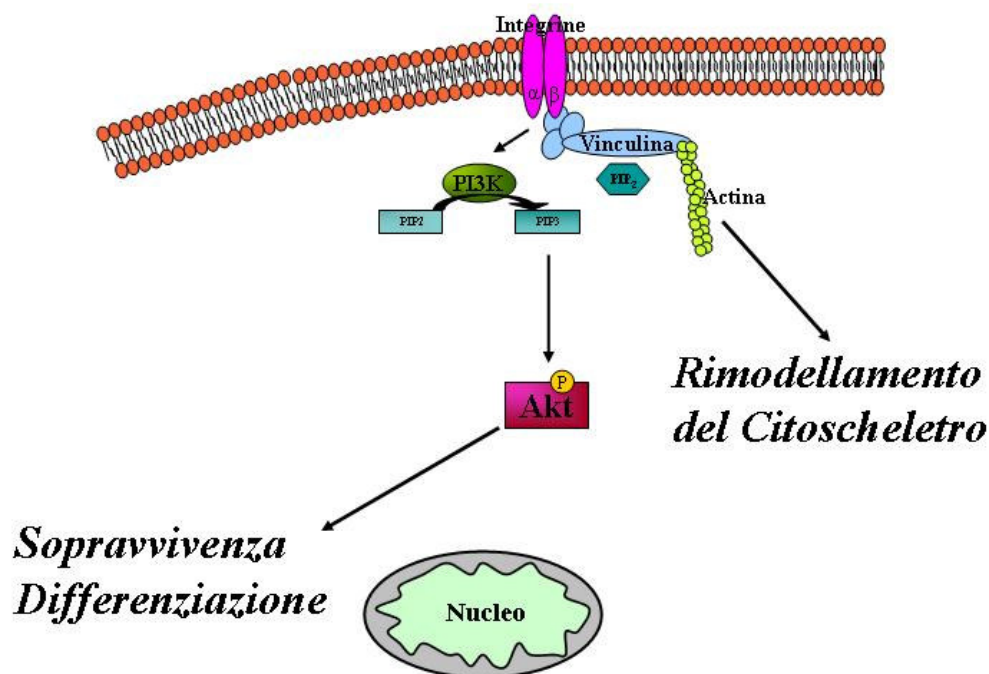
L'attivazione delle integrine avviene tramite l'interazione del recettore integrinico con i ligandi della matrice extracellulare e il reclutamento delle tirosina-chinasi intracellulari. Una proteina-

chinasi Ca^{2+}indipendente, FAK (Focal Adhesion Kinase), localizzata sulle adesioni focali, viene autofosforilata dopo l'attivazione delle integrine con meccanismi ancora sconosciuti. La fosforilazione di FAK recluta altre proteine chinasi Ca^{2+}indipendenti come ad esempio src. L'attivazione di FAK e src provoca la fosforilazione di altre proteine di adesione quali la paxillina, la vinculina, l'α-actinina, che interagiscono anch'esse con il citoscheletro. La fosforilazione delle tirosine delle proteine delle adesioni focali può indurre cambiamenti nell'assemblamento/disassemblamento dinamico del network dei microfilamenti e dei microtubuli e può causare il rimodellamento delle adesioni focali e la conseguente modificazione della morfologia cellulare. Recenti evidenze dimostrano che la traduzione del segnale attraverso le interazioni cellula-matrice sono correlate al metabolismo dei fosfolipidi. Questa correlazione è mediata da rho, una piccola proteina legante GTP. Essa appartiene alla famiglia delle GTPasi monometriche, che può alternare due stati conformazionali: attivo quando si lega una molecola di GTP e inattivo quando si lega una molecola di GDP. Rho, attraverso una cascata di eventi intracellulari, regola la fosfatidilinositolo-5-chinasi che fosforila il fosfatidilinositolo-4-fosfato per ottenere il fosfatidilinositolo-4,5-bifosfato (PIP_2). PIP_2 è il substrato per PLC e può formare IP_3 e diacilglicerolo (DAG). In letteratura è riportato che le interazioni indotte da stress da sfregamento tra matrice ed integrine stimolano un membro della famiglia delle MAPK, Erk 1/2, attraverso l'attivazione della chinasi src. E' stato proposto che l'attivazione di src, attraverso FAK, induce la fosforilazione di una proteina c linker shr. Shr fosforilata può reclutare in membrana il complesso Grb2/Sos, dove Sos può attivare Ras. Questa proteina, simile a Rho, appartiene alla famiglia delle GTPasi monomeriche. Attraverso una cascata di eventi, ras attiva Erk 1/2.

Le cascate intracellulari finora nominate indicano che esistono interazioni sinergiche o additive tra integrine, recettori accoppiati a proteine G, e il pathway di segnali rho-ras-Erk 1/2 in seguito a stimolazioni meccaniche delle cellule [Geiger et al., 2001; Katsumi et al., 2004].
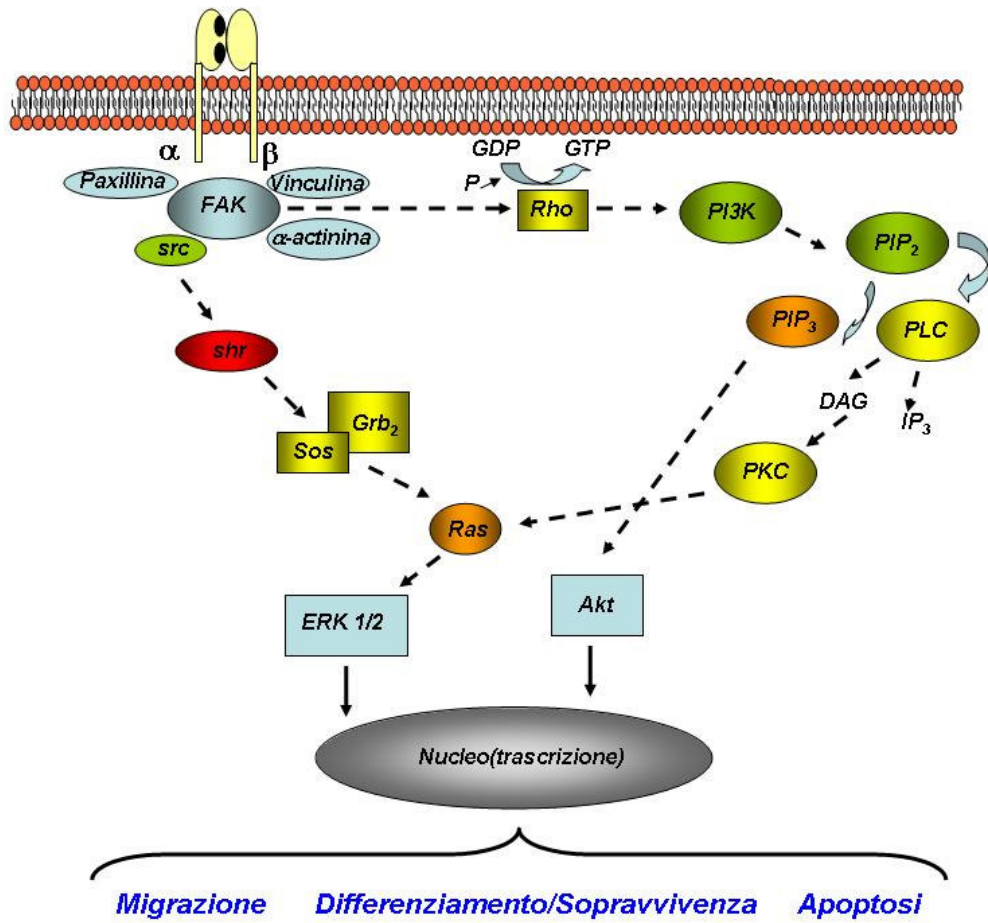
2. MATERIALI E METODI

2.1 Materiali

Fogli di silicone trattati per l'adesione cellulare (0.010" Non-Reinforced Vulcanized, SMI Specialty Manufacturing Inc**.** Saginaw, MI, USA) sono stati utilizzati quale substrato deformabile. I fogli sono stati sterilizzati in autoclave per 20' a 121°C e rivestiti in condizioni di sterilità con fibronectina 10μg/ml (Sigma, Milano, Italia) per 1 ora a temperatura ambiente prima della semina cellulare.

2.2 Colture cellulari

E' stata utilizzata una linea cellulare di fibroblasti di origine umana MRC5 (ATCC CRL 171) derivanti da tessuto polmonare normale. Le concentrazioni utilizzate variano a seconda del tipi di esperimento: $15x10^3$ cells/cm^2 per gli esperimenti riguardanti l'orientamento, la morfologia e i contatti focali; $15x10^3$ cells/cm^2 per gli esperimenti riguardanti l'analisi delle proteine tramite western blot e RT-PCR.

Le cellule sono state coltivate in DMEM arricchito con 10% di siero bovino fetale, glutammina (2mM), penicillina (100U/ml) e streptomicina (100μg/ml) (Euroclone, Italia). Al fine di ottenere un'adesione ottimale alle membrane deformabili, le cellule sono state mantenute sul silicone, adeguatamente trattato come in precedenza descritto, a 37°C in atmosfera umida al 5% CO_2 in condizioni statiche per 12 ore prima di applicare sulle stesse gli stress meccanici da stiramento.

Negli esperimenti di inibizione della proteina Akt è stato utilizzato il reagente Wortmannina (Alexis Biochemicals, CA, USA) alla concentrazione finale 10μM addizionato 30 minuti prima di applicare gli stress meccanici al substrato.

2.3 Applicazione degli stress meccanici alle cellule

Per imporre una trazione controllata ai substrati deformabili è stata utilizzata la strumentazione Instron 5564 (Instron Corporation, Canton, MA, USA). Lo strumento comprende una console di controllo elettronico con una cella di carico con una capacità di 2,5N in tensione o compressione e 2500mm/min-0.05mm/min rispettivamente come velocità massima e minima di spostamento del braccio mobile. I campioni di silicone adeguatamente seminati con le cellule e connessi tramite delle pinze alla cella di carico dell'Instron, sono stati immersi per tutta la durata degli esperimenti in una camera d'organo verticale (Ugo Basile, Milano, Italia) riempita con terreno di coltura e mantenuta a 37°C in presenza di 5% CO_2 tramite un bagno termostatico adeguatamente adattato. Deformazioni del substrato, differenti per percentuale di allungamento e frequenza, sono state applicate come stiramento uniassiale e confrontati con controlli non sottoposti a stiramento. L'intervallo delle deformazioni applicate al substrato va dall'1% al 25%, mentre le diverse frequenze applicate vanno da 0,25Hz a 3Hz.
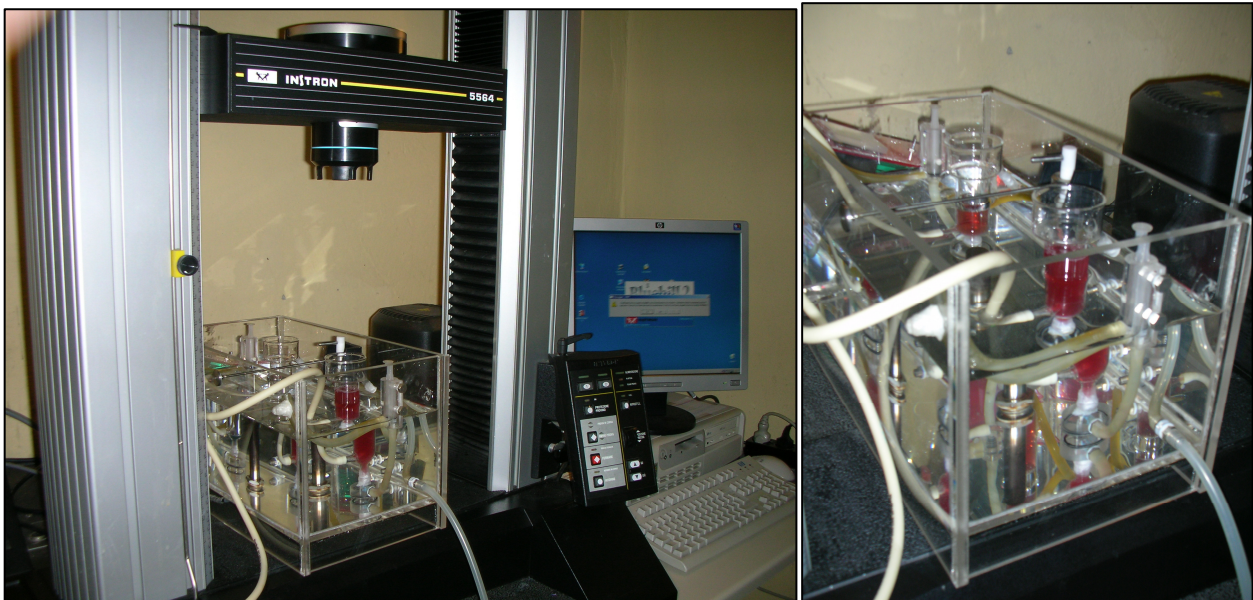

2.4 MTT test

L'MTT (3-[4,5-dimethylthiazol-2-yl]-2,5-diphenyltetrazolium bromide) è un composto chimico solubile in acqua. Le deidrogenasi mitocondriali attive convertono la soluzione gialla di MTT in sali di formazano insolubili e di colore porpora. Questa conversione non avviene nelle

cellule morte o fortemente danneggiate. I sali di formazano insolubili in acqua possono essere solubilizzati in dimetilsolfossido (DMSO), e l'intensità colorimetrica del soluto può essere misurata spettrofotometricamente. Dopo aver applicato gli stress meccanici ai substrati, le cellule sono state incubate per 3 ore con una soluzione di MTT 50μg/ml concentrazione finale in DMEM. I campioni sono stati successivamente lavati in PBS e in fine i sali di formazano formati sono stati dissolti in DMSO. L'assorbanza è stata letta alla frequenza di 570nm. I dati ottenuti sono espressi come media percentuale rispetto ai controlli ± la deviazione standard.

2.5 Orientamento cellulare

L'orientamento cellulare è stato misurato considerando l'asse maggiore delle cellule. Per valutare la percentuale di cellule orientate, i campioni sono stati fissati in formaldeide al 3,7% per 30 minuti e colorate per 10 minuti con blu di toluidina allo 0,01% in acqua. Per ogni campione sono state acquisite 7 immagini e i test sono stati ripetuti in triplicato per ogni condizione di stress meccanico considerata (n=21). Una griglia con diversi angoli di orientamento (0-30°; 30-60° e 60-90°) è stata applicata ad ogni immagine ed è stato misurato l'orientamento cellulare riportando in grafico la percentuale di cellule orientate per ognuno dei tre angoli di orientamento considerati. La direzione di deformazione uniassiale è stata considerata come 0°. La figura sottostante rappresenta un esempio del metodo usato per definire e misurare l'orientamento cellulare.
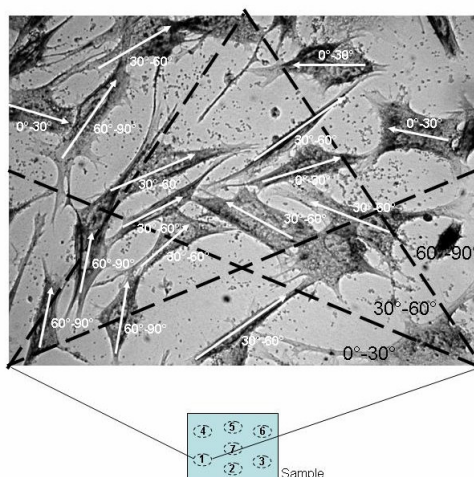
2.6 Microscopia a fluorescenza

Al fine di valutare l'espressione e la localizzazione della vinculina, le cellule sono state fissate in formaldeide 3,7% per 30 minuti a 4°C e poi incubate con anticorpo anti-vinculina (Oncogene, Italia) coniugato Texas red (Santa Cruz, Italia). Per la colorazione dei microtubuli, le cellule sono state incubate con un anticorpo primario anti-tubulina (Sigma, Italia) successivamente coniugato con fluoresceinaisotiocianato (FITC) (Santa Cruz, Italia). I nuclei sono stati individuati tramite colorazione con DAPI. I contatti focali vinculina-positivi delle cellule fissate sono stati osservati al microscopio a fluorescenza (Leica, DM 2500) ad un ingrandimento di 40x. I contatti focali sono stati analizzati quantitativamente utilizzando 10 immagini per ogni campione e ripetendo gli esperimenti in triplicato (n=30). Il sistema di analisi d'immagine si compone di un microscopio a fluorescenza connesso con un computer dotato di un software di analisi di immagine (Leica Q-Win) calibrato all'ingrandimento 40x. Sono stati misurati vari parametri incluso il numero di contatti vinculina-positivi per cellula, la lunghezza e l'area media degli stessi. I risultati ottenuti dai campioni di controllo sono stati paragonati con quelli ottenuti dai campioni sottoposti a stress meccanico.

2.7 Western blot

Al fine di quantificare l'espressione e l'eventuale attivazione di alcune proteine (vinculina, tubulina, pAkt, Akt, Rho e pRho) sono stati condotte delle analisi in western blot. Le cellule sono state lisate in buffer RIPA (25mM Tris, pH 7.5, 150mM NaCl, 1% sodium deossicolato, 1mM Na_3Vo_3, 0,1% SDS, 50mM sodio fluoruro, 1% Triton, 0,5M EDTA, 10μg/ml aprotinina, 1μg/ml leupeptina, 1μg/ml pepstatina, 1mM PMSF) per 30 minuti in ghiaccio. La concentrazione delle proteine totali dei campioni lisati è stata determinata con il saggio dell'acido bicinconinico (Pierce, Rockford, IL). 10μg di proteine totali sono state dissolte in Leamli buffer (62.5mM Tris-HCl, pH 6.8, 20% glycerol, 2% SDS, 5% β-mercaptoethanol, 0.5% bromophenol blue) e utilizzate per l'elettroforesi in SDS-PAGE e successivamente trasferite su membrane di nitrocellulosa

(Amersham Biosciences, Buckinghamshire, England). Le proteine trasferite su membrana sono state immerse per 1 ora a temperatura ambiente in una soluzione al 5% di latte in PBS al fine di bloccare i siti aspecifici di legame delle proteine e incubate per 12 ore a 4°C con l'anticorpo primario d'interesse (anti-vinculina, anti-tubulina, anti-pAkt, anti-Akt, anti-pRho ed anti-pRho a seconda delle condizioni sperimentali presentate). Dopo alcuni lavaggi in PBS 0,1% Tween 20, le membrane sono state incubate con l'anticorpo secondario coniugato a perossidasi (Amersham Biosciences, Buckinghamshire, England) per un'ora a temperatura ambiente. Le bande positive sono state visualizzate tramite i reagenti ECL (Amersham Biosciences, Buckinghamshire, England) utilizzando un visualizzatore chemisensitivo (VersaDoc, BioRad, Italy). I risultati sono stati inoltre quantificati e normalizzati utilizzando un software per l'analisi densitometrica QuantityOne (Bio-Rad Laboratories, CA, USA).

2.8 RT-PCR

L'RNA totale è stato isolato dale cellule e misurato utilizzando il RediPlate™ 96 RiboGreen® RNA Quantitation Kit (Molecular Probes Inc, Eugene, OR). 1 μg di RNA è stato retrotrascritto in cDNA (Enhanced Avian RT First Strand Synthesis Kit (Sigma) e amplificato in 50 μl di reazione PCR. Per l'amplificazione sono stati i seguenti primer: per la vinculina (senso, 5'-AAA CAC AgT TAC ACT TgT gCA CCC-3'; antisenso, 5'-AAC AgA ggg AAg TgT CCC CT-3') e per la β-actina (senso, 5'-ACA CTG TGC CCA TCTA CGA GGG G-3'; antisenso, 5'-ATG ATG GAG TTG AAG GTA GTT TCG TGG AT-3'). L'avvenuta amplificazione è stata controllata su gel di agaroso per la presenza di frammenti di cDNA generati dalla reazione di PCR a 360 pb e 125 pb rispettivamente per la β-actina e la vinculina. Anche in questo caso l'analisi densitometrica è stata determinata utilizzando il software QuantityOne (BioRad Laboratories, CA, USA).

RISULTATI

La figura 1 rappresenta i risultati ottenuti dei test di vitalità cellulare. Gli stress meccanici non interferiscono con la vitalità cellulare fino al raggiungimento del 20% di deformazione del substrato, come mostrano le medie dei risultati ottenuti dagli esperimenti tutte prossime al 100% di vitalità. Nel caso della deformazione del substrato al 25% invece la vitalità cellulare diminuisce raggiungendo una media statisticamente significativa di circa 60%. In questo caso la diminuzione del valore di vitalità è dovuto sia ad un rilevante distacco delle cellule dal substrato sia ad un effettivo danno alle strutture cellulari come confermato dai dati morfologici in seguito riportati.
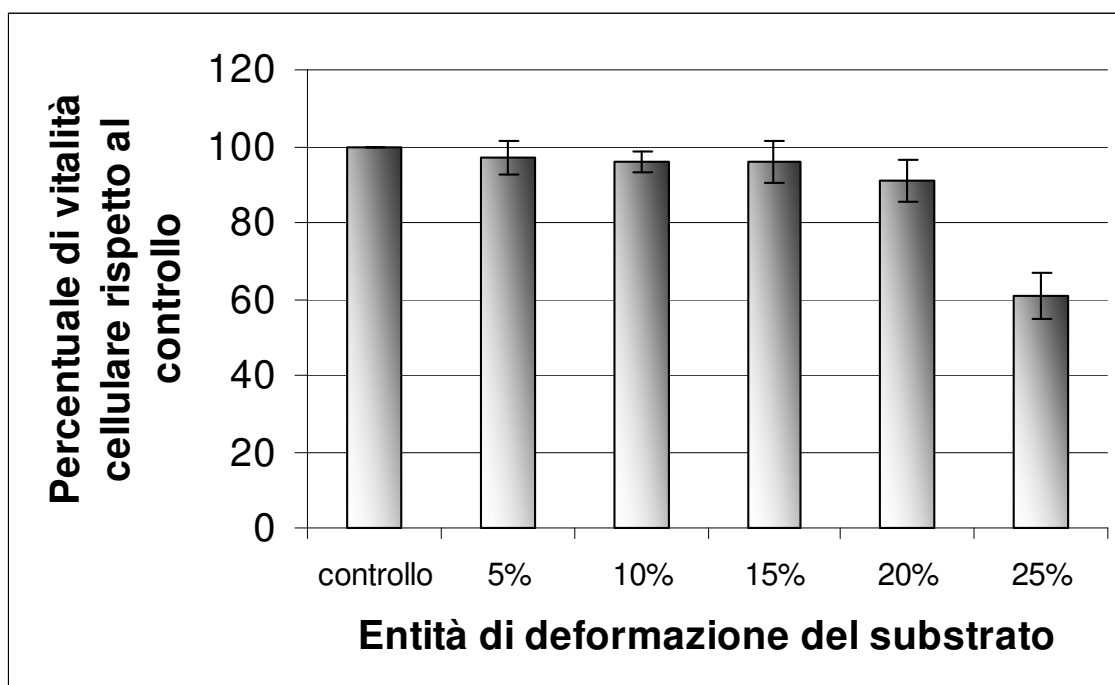

Figura 1. Vitalità cellulare ottenuta tramite MTT test delle cellule sottoposte a stress meccanici da stiramento (5%-25%) a confronto con le cellule di controllo in ambiente statico.

Le immagini in figura 2 sono rappresentative della morfologia e dell'allineamento delle cellule in seguito alle diverse deformazioni del substrato paragonate al controllo statico. Le cellule sono distribuite in maniera casuale sui controlli non sottoposti a stress meccanico, mentre una deformazione ≥2% orienta le cellule perpendicolarmente alla direzione dello stress. Nessuna modificazione significativa della morfologia risulta in seguito alla deformazione dal 2% al 20%

mentre le cellule sottoposte ad uno stress meccanico pari al 25% di deformazione presentano una

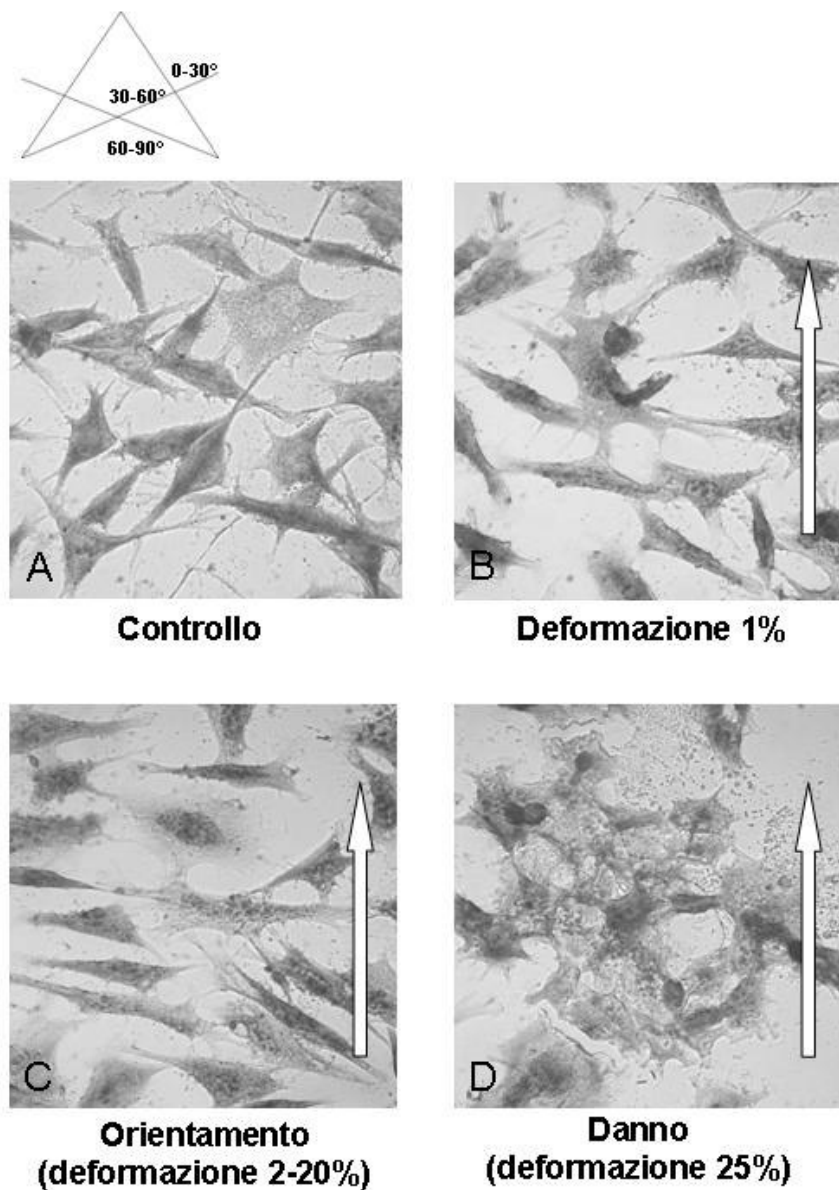morfologia profondamente alterata in seguito anche ad una non adeguata adesione.

Figura 2. Fotografie in microscopia ottica delle cellule di controllo e sottoposte a stress meccanici da stiramento con deformazioni del substrato dallo 0% al 25%.

Il grafico in figura 3 rappresenta la percentuale di cellule allineate nei tre angoli di orientamento in

seguito all'applicazione per tre ore delle diverse grandezze di deformazione del substrato alla

frequenza di 1Hz. A partire dal 2% di deformazione, il 60% dei fibroblasti si allinea

perpendicolarmente alla direzione dello stress, come indicato dai valori significativamente più alti

di cellule nell'intervallo di orientamento 60°-90° e da una percentuale minore di cellule negli intervalli 0°-30° e 30°-60°. Non ci sono invece differenze statisticamente significative tra le cellule sottoposte a stress dal 2% al 20% di deformazione del substrato, mentre al 25% la morfologia cellulare è profondamente alterata (come già mostrato in figura 2) e l'orientamento cellulare in questo modo risulta tecnicamente difficile da valutare a causa della rilevante percentuale di cellule danneggiate o staccate.
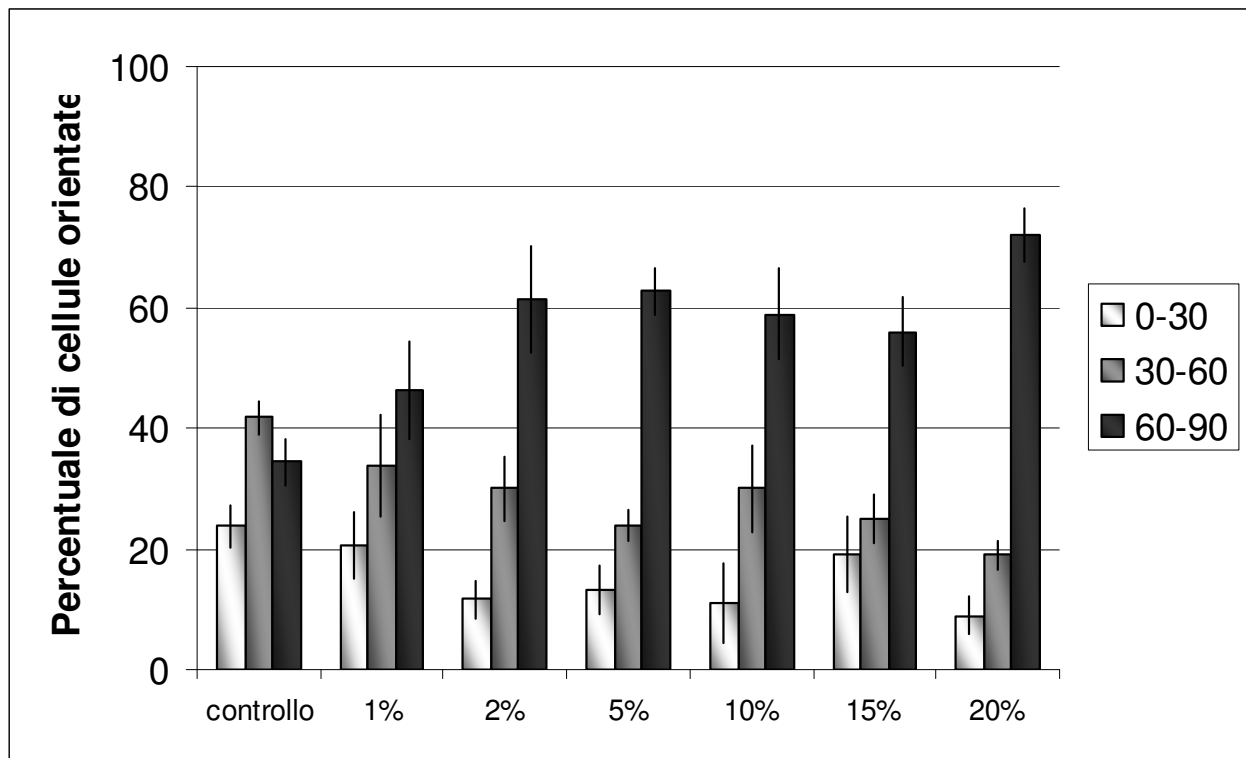

Figura 3. Misura dell'orientamento cellulare in seguito all'applicazione di deformazioni del substrato di diversa entità (0%-20%) per 3 ore alla frequenza di 1Hz.

E' stato valutato anche il comportamento delle cellule sottoposte per 3 ore ad uno stiramento del substrato di adesione pari al 2% modificando la frequenza da 0.25Hz a 3Hz. Come mostrato in figura 4 non si evidenzia alcun incremento o decremento delle percentuali di cellule allineate nei 3 angoli di orientamento considerati e i risultati ottenuti sono confrontabili fra loro senza differenze statisticamente significative.
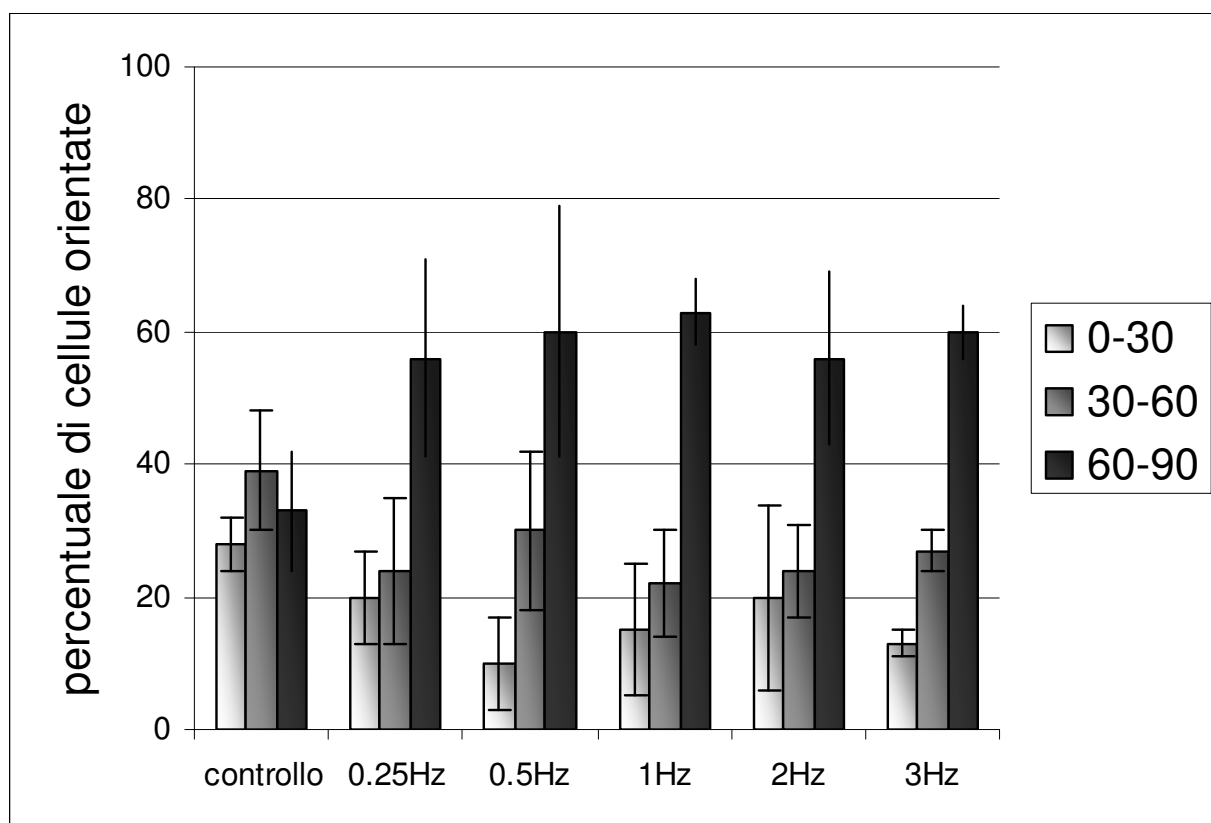
Figura 4. Misura dell'orientamento cellulare in seguito all'applicazione della deformazione del substrato al 2% per 3 ore a diverse frequenze (0Hz-3Hz).

La figura 5A è rappresentativa delle immagini in fluorescenza ottenute dagli esperimenti di applicazione degli stress meccanici. Le adesioni focali positive alla vinculina presenti sulla membrana delle cellule di controllo hanno forma tonda e sono distribuite in punti definiti mentre i contatti focali presenti sulle cellule sottoposte a stress meccanici hanno forma allungata e sono distribuiti su tutta la membrana cellulare in modo da seguire la direzione dell'orientamento cellulare. I grafici in figura 5B,C e D mostrano i dati morfometrici ottenuti dall'osservazione al microscopio a fluorescenza dei contatti focali positivi alla vinculina. Il grafico 5B riporta i risultati ottenuti dalla conta del numero di contatti focali per cellula. Quando le cellule sono sottoposte a stress meccanico il numero dei contatti focali per cellula è statisticamente maggiore rispetto alle cellule coltivate su substrati statici. Nei controlli la media delle adesioni focali positive alla vinculina per cellula è 7±3; questo numero aumenta raggiungendo una media di 10±4 contatti focali

per cellula in seguito ad una deformazione ciclica del substrato pari al 2% alla frequenza di 1Hz. La figura 5C riporta la lunghezza dei siti di adesione positivi alla vinculina ottenuti da misure morfometriche sulle immagini in fluorescenza. Si evince che i siti di adesione risultano statisticamente di lunghezza maggiore sulle cellule adese ai substrati deformati meccanicamente rispetto alle cellule di controllo statici. Infatti, la lunghezza delle adesioni focali nei controlli è in media di 3,6±0,2μm mentre la deformazione meccanica del substrato provoca un profondo cambiamento raggiungendo un lunghezza media di 7,7±0,3μm. La figura 5D dimostra che la stress meccanico influenza anche l'area dei contatti focali. Le misure morfometriche delle aree dei contatti focali positivi alla vinculina evidenziano un incremento dei valori nel caso in cui le cellule siano coltivate su substrati deformati meccanicamente.
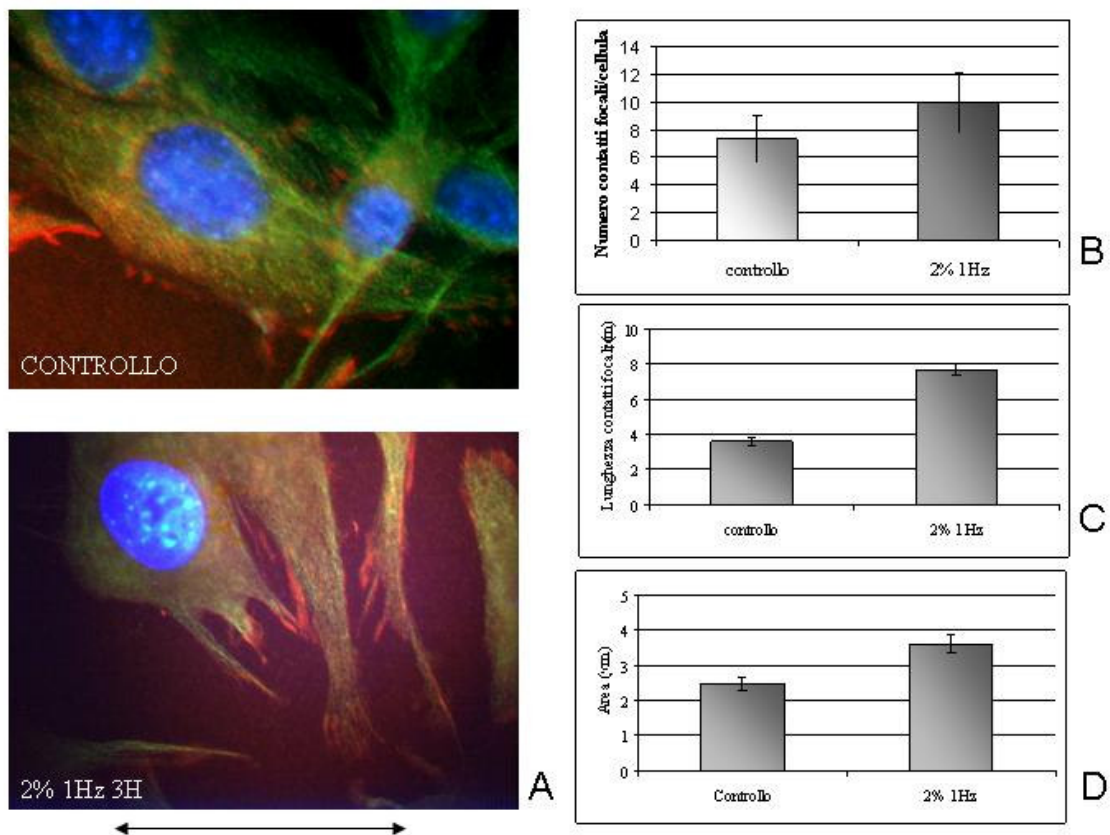

Figura 5. Immagini in fluorescenza dei contatti focali positivi alla vinculina e morfometria degli stessi in presenza e in assenza di deformazione del substrato.

Al fine di valutare l'ipotesi che la diversa morfologia dei contatti focali fosse dovuta alla presenza di vinculina neosintetizzata in seguito all'applicazione degli stress meccanici al substrato, sono state condotte analisi di western blot e RT-PCR. Come mostrato in figura 6, la sintesi e l'espressione della vinculina non vengono alterate in seguito all'applicazione dello stress meccanico. Infatti, la quantità di vinculina espressa sui controlli e sulle cellule sottoposte a stress ha la stessa intensità di segnale, come confermato anche dalla densitometria eseguita normalizzando i segnali in base all'espressione della tubulina sui campioni stessi. Dunque, dopo tre ore, lo stress meccanico sembra non interferire con la sintesi e l'espressione della vinculina.
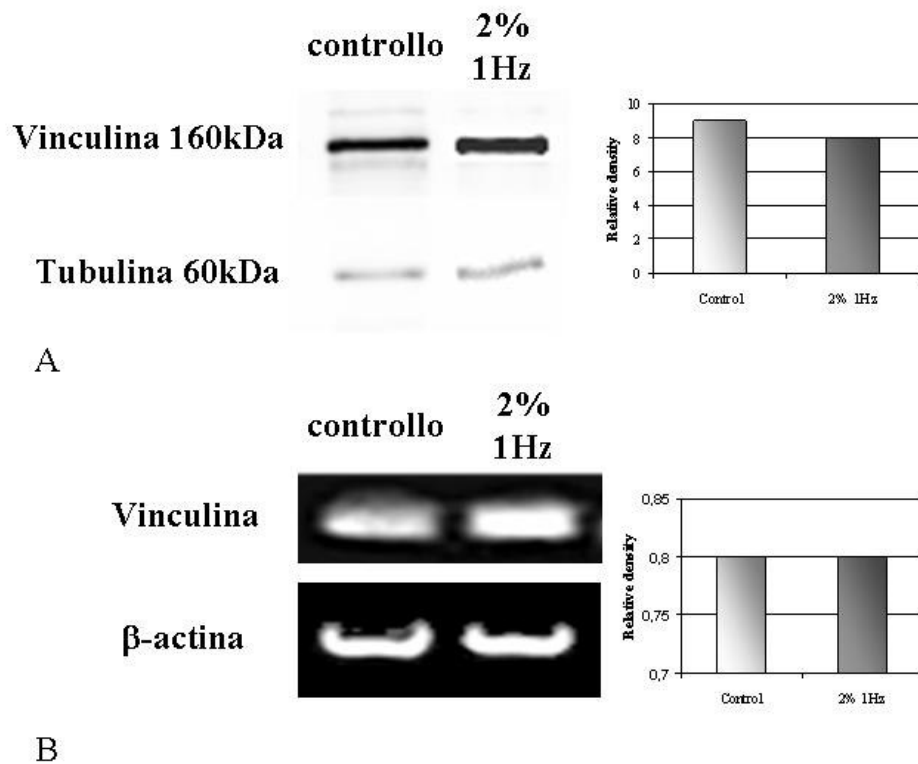

Figura 6. Analisi dell'espressione (western blot) e della sintesi (RT-PCR) della proteina vinculina in ambiente statico e in presenza di stress meccanici da stiramento.

La figura 7 mostra le immagini in fluorescenza ottenute applicando lo stress meccanico da stiramento in presenza dell'inibitore wortmannina (10µM) che interferisce sull'attività di Akt. Le immagini mostrano la presenza di contatti focali nei controlli in presenza e in assenza di

wortmannina. I contatti focali positivi alla vinculina sono distribuiti sulla membrana cellulare ed hanno una morfologia ben definita e allungata a seguire le parti terminali dei filamenti di actina citoscheletrici (fig 7A e B). In presenza di wortmannina l'applicazione degli stress meccanici, che i dati precedenti hanno dimostrato avere un effetto sulla morfologia delle adesioni vinculina positive, aumentandone il numero per cellula, la lunghezza e l'area, ha un effetto inibente sull'adesione stessa. Infatti, la positività alla vinculina diviene diffusa senza evidenziare punti definiti in membrana (fig 7C).
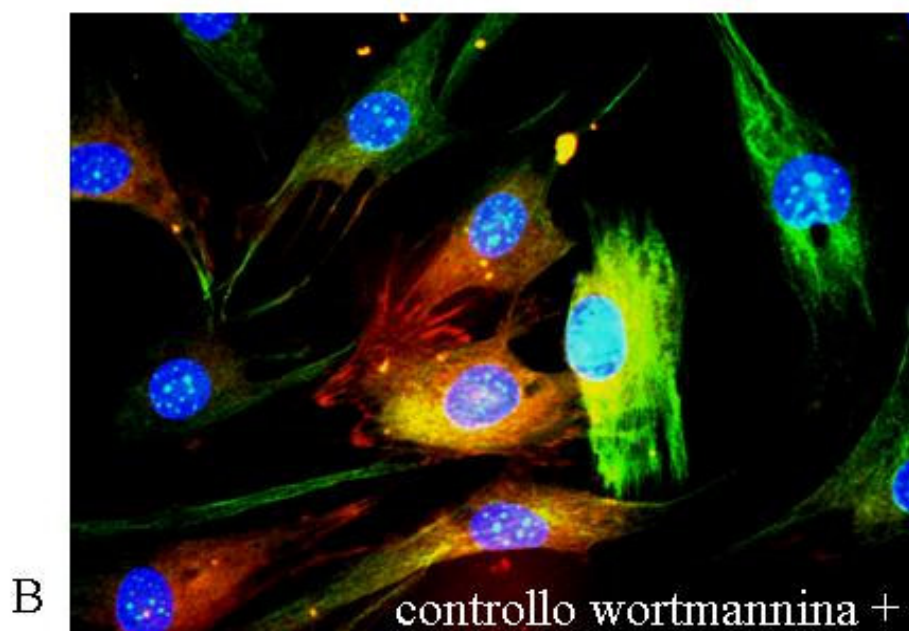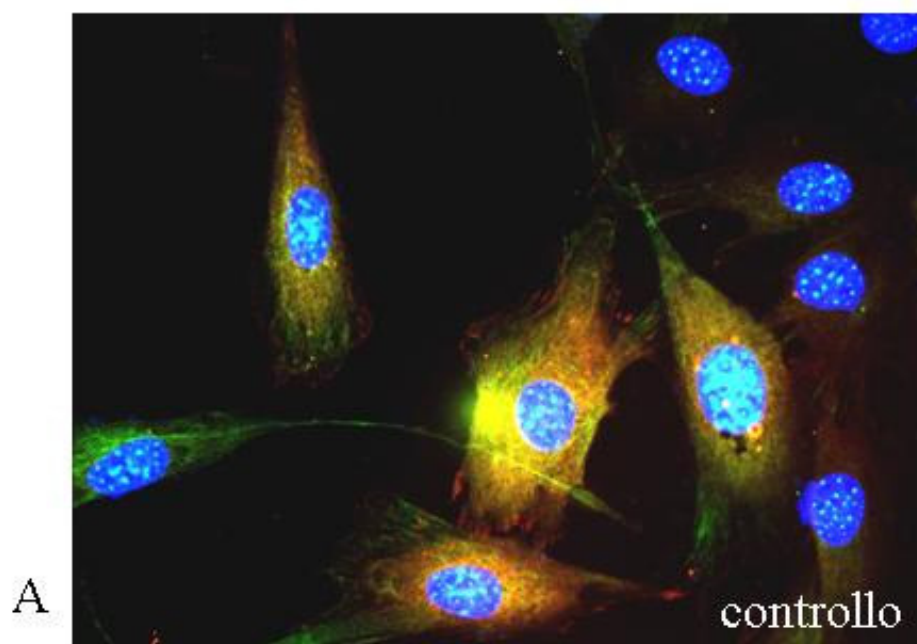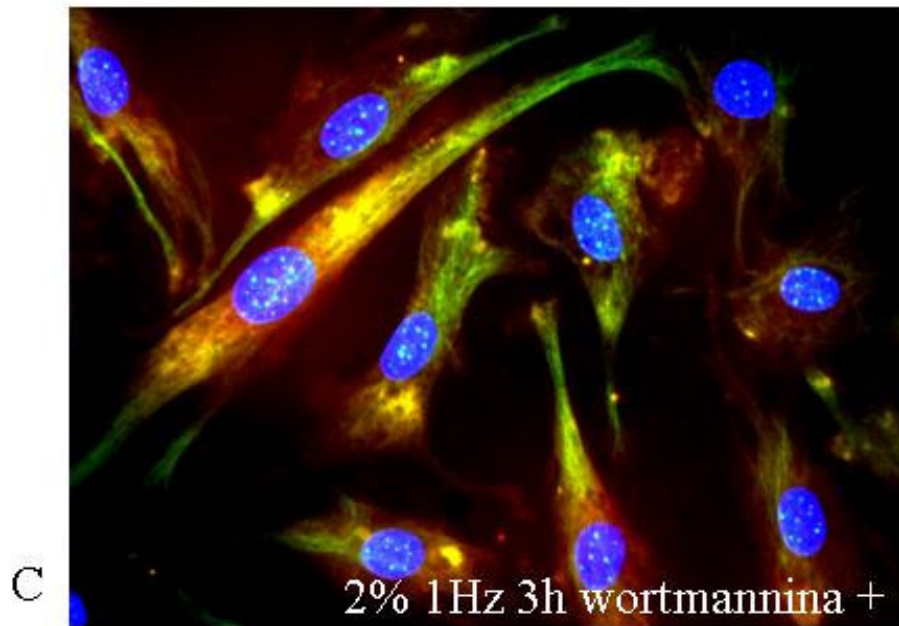
Figura 7. Immagini in fluorescenza delle adesioni focali positive alla vinculina in presenza di wortmannina (10μM) in ambiente statico e dinamico (stress meccanico da stiramento 2% 3h 1Hz).

La figura 8 mostra l'attivazione di Akt in seguito a stress meccanici da stiramento in presenza ed in assenza di wortmannina (wt). L'attivazione dovuta alla fosforilazione della proteina inizia nei primi 10 minuti di deformazione del substrato e raggiunge il picco massimo a 30 minuti. Viceversa in presenza di inibitore il livello di attivazione rimane invariato rispetto al controllo, confermando l'efficacia dell'inibizione della fosforilazione.
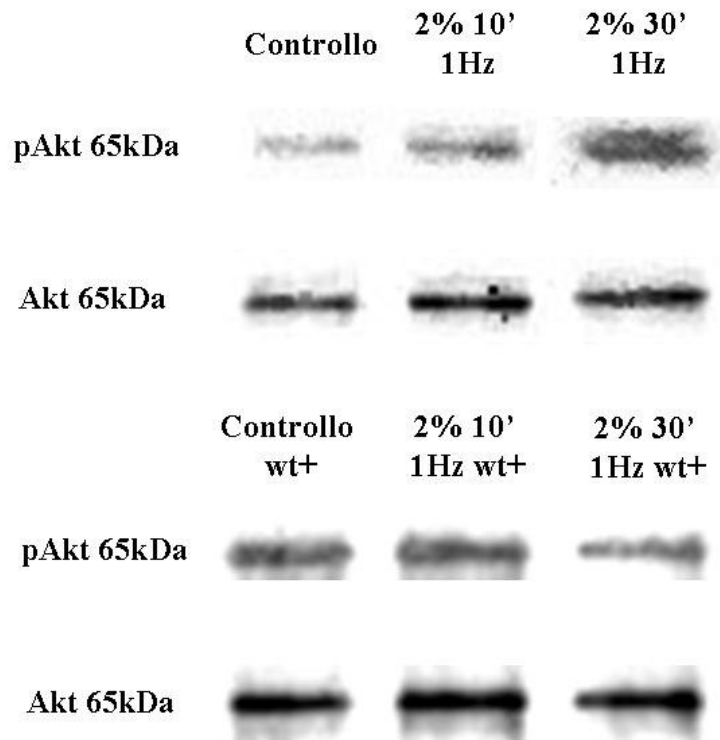
Figura 8. Western blot sui lisati cellulari d controllo in presenza ed assenza di inibitore di Akt a confronto con i lisati cellulari delle cellule sottoposte a stress meccanico da stiramento (2% 1Hz 10min e 30min).

La figura 9 mostra i risultati ottenuti dall'analisi in western blot dei lisati cellulari ottenuti dai controlli in presenza ed in assenza di wortmannina, e dai campioni sottoposti a stress meccanico (2% 3h 1Hz) in presenza ed in assenza dello stesso inibitore. L'espressione della proteina pRho aumenta solo nel caso dell'applicazione dello stiramento del substrato in assenza di wortmannina, mentre in tutti gli altri casi rimane invariata e paragonabile al controllo statico in assenza inibizione.
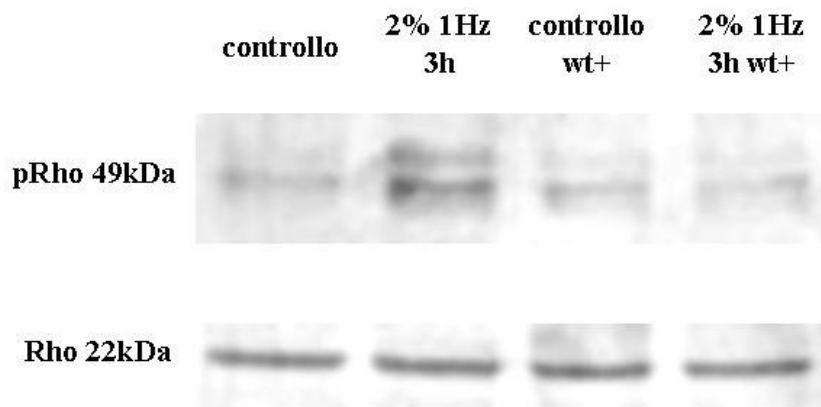
Figura 9. Western blot anti pRho e anti Rho sui lisati cellulari delle cellule di controllo e sottoposte a stress meccanici da stiramento in presenza e in assenza di inibitore di Akt, wortmannina (10µM).

4. DISCUSSIONE

Gli stress meccanici sono presenti nei tessuti durante le varie fasi della vita, sia a livello embrionale sia nel caso di organismi adulti, e conseguentemente sulle cellule nel corpo umano. Il tipo, l'entità, la frequenza e la durata degli stress variano in maniera significativa a seconda della funzione del tessuto e del distretto anatomico interessato. Le deformazioni tessutali da stiramento, per esempio, variano in un intervallo fisiologico che va dall'1% (piccoli vasi sanguigni) al 25% (tendini) con frequenze dagli 0Hz, nel caso di uno stiramento prolungato e fisso (tendini), fino a circa 1Hz (vasi sanguigni). Queste forze, generate da tensioni esterne o dalle proprietà di contrazione delle cellule stesse, condizionano la forma cellulare e l'orientamento in conseguenza ad una riorganizzazione del citoplasma che risulta da processi molecolari intracellulari.

Le integrine sono implicate in maniera altamente significative nella trasduzione degli stimoli meccanici [Katsumi et al., 2004] e le adesioni focali risultano essere strutture altamente dinamiche, fortemente influenzate dalle condizioni esterne. Infatti, l'area e la presenza di quest'ultime è stato verificato essere linearmente dipendenti dalla forza di adesione applicata dalla cellula [Balaban et al., 2001].

I risultati riportati in questo lavoro evidenziano come l'entità e la frequenza degli stress meccanici da stiramento di breve durata non influenzino il comportamento cellulare in maniera differente nel caso di deformazione del substrato pari a o superiore al 2% e frequenze fino ai 3Hz. Tutti gli stress applicati infatti allineano il monostrato cellulare in direzione perpendicolare allo stress. L'ipotesi a spiegazione di tale comportamento è che le cellule modifichino la loro posizione in modo da contrastare e minimizzare le forze dirette contro la cellula. A sostegno di tale ipotesi ci siamo occupati dell'adesione cellulare e della modificazione della morfologia dei siti di adesione nelle cellule sottoposte a stress meccanici da stiramento di breve durata (3ore). L'orientamento cellulare ha dato risultati statisticamente significativi a partire dal 2% di deformazione del substrato e pertanto abbiamo mantenuto questo valore come utile allo studio delle modificazioni dell'adesione.

Per quanto riguarda la frequenza la scelta è caduta su 1Hz in quanto è un'intensità ampiamente rappresentata a livello fisiologico ad esempio a livello cardiovascolare.

I dati ottenuti, pertanto, confortano l'ipotesi dell'orientamento dovuto ad una difesa delle cellule stesse. Infatti, i siti di adesione aumentano in numero e risultano coprire un'area maggiore rispetto alle cellule di controllo. Inoltre, la morfologia estremamente allungata degli stessi siti di adesione indicano che la vinculina si distribuisce in maniera più specifica lungo i filamenti di actina. Il dati ottenuti dimostrano che gli stress meccanici applicati per brevi tempi non hanno alcuna influenza sulla sintesi e sull'espressione della vinculina. Pertanto si può ipotizzare che essi provochino un cambiamento conformazionale della proteina vinculina dalla conformazione inattiva (chiusa) a quella attiva (aperta) nella quale vengono esposti i siti di legame per le proteine citoscheletriche (actina) e coinvolte nell'adesione (talina, paxillina, etc.) [Geiger et al., 2001]. Dunque, la vinculina in conformazione attiva lega specificamente proteine strutturali e di adesione modificando l'aspetto delle adesioni focali e conseguentemente la morfologia cellulare. Il fosfatidilinositolo bifosfato gioca un ruolo chiave nel cambiamento conformazionale della vinculina e più in generale nell'assemblaggio delle siti di adesione. Verosimilmente, gli stress meccanici inducono un'interazione tra vinculina e fosfatidilinositolo con la conseguente attivazione della prima e l'esposizione dei siti di legame per le proteine strutturali (actina) e di adesione. Tuttavia, ulteriori esperimenti sono necessari al fine di provare questa ipotesi di meccanismo.

Dunque, anche gli evidenti cambiamenti morfologici dei contatti focali vinculina positivi indicano una maturazione degli stessi e una maggiore organizzazione a vantaggio di una migliore adesione al substrato. In questo modo, una migliorata e più efficiente adesione al substrato può risultare anch'essa come una difesa cellulare ad una perturbazione meccanica recepita evidentemente da meccanorecettori specifici.

In letteratura, altri gruppi si sono occupati dei cambiamenti morfologici dei contatti focali indotti biochimicamente, individuando nelle GTPasi Rho, Rac e Cdc42 gli elementi maggiormente implicati a livello molecolare in tali processi [Rottner et al., 1999; Nobes et al., 1995]. In

particolare, Nobes e colleghi hanno individuato nella proteina Rho l'*upstream* comune tra la via di polimerizzazione dell'actina e l'assemblamento delle adesioni focali. Anche nel nostro studio Rho rivela avere un ruolo chiave nell'individuazione di una morfologia "matura" dei siti di adesione. E' riportato in letteratura che Rho regola l'attività della fosfatidilinositolo 4-fosfato 5-chinasi e di conseguenza regola la formazione di fosfatidilinositolo-2fosfato che abbiamo visto essere direttamente coinvolto nell'attivazione della proteina vinculina e nell'organizzazione definitiva delle adesioni focali.

E' interessante però constatare come in realtà le vie Akt-Rho si incrocino in questo caso. La mancata formazione delle adesioni focali avviene in presenza di wortmannina solo nel caso in cui gli stress meccanici inducano il coinvolgimento di Rho, come risulta dalla fosforilazione di questo in seguito all'applicazione degli stress meccanici. Infatti, anche l'attività di Akt è dimostrato dipendere dalla fosfatidilinositolo 3-chinasi [Clark et al., 1998]. Nel nostro caso il blocco del pathway di Akt ha effetti sulla maturazione dei contatti focali, provocandone il disassemblamento. Risulta evidente un *crosstalk* tra le vie molecolari intracellulari di Rho e Akt, entrambe coinvolte ed attivate in seguito all'applicazione di stress meccanici da stiramento alle colture cellulari.

In futuro sarà necessario approfondire il ruolo delle chinasi coinvolte nel metabolismo del fosfatidilinositolo e le interazioni dei loro prodotti con Akt e altri pathway intracelluari ad ulteriore chiarimento dei meccanismi molecolari coinvolti nell'adesione in presenza di stress meccanici.

5. BIBLIOGRAFIA

1. Chiquet M., Tunç-Civelek V., Sarasa-Renedo A. "Gene regulation by mechanotransduction in fibroblasts." Appl Physiol Nutr Metab 2007; 32: 967-973.

2. Helderman F., Segers D., de Crom R., Hierck B.P., Poelmann R.E., Evans P.C., Krams R. "Effect of shear stress on vascular inflammation and plaque development." Curr Opin Lipidol 2007; 18: 527-533

3. Marotti G., Palumbo C. "The mechanism of transduction of mechanical strain into biological signals at the bone cellular level." Eur J Histochem 2007; 51: 15-19.

4. Kreplak L., Fudge D. "Biomechanical properties of intermediate filaments: from tissues to single filaments and back". Bioessays 2007; 29: 26-35.

5. Wang J.H., Thampatty B.P. "An introductory review of cell mechanobiology" Biomech Model Mechanobiol 2006; 5: 1-16.

6. Shikata Y., Rios A., Kawkitinarong K., DePaola N., Garcia J.G.N., Birukov K.G. "Differential effects of shear stress and cyclic stretch on focal adhesion remodelling, site-specific FAK phosphorylation, and small GTPases in human lung endothelial cells". Exp Cell Res 2005; 304: 40-49.

7. Gautam M., Gojona A., Barakat A.I. "Flow-activated ion channels in vascular endothelium". Cell Biochem Biophys 2006; 26: 277-284.

8. Li C., Xu Q. "Mechanical stress-initiated signal transduction in vascular smooth muscle cells *in vitro* and *in vivo*". Cell Signal 2007; in press.

9. Greiger B., Bershadsky A. "Assembly and mechanosensory function of focal contacts" Curr Op Cell Biol 2001; 13: 584-592.

10. Katsumi A., Orr A.W., Tzima E., SchwartzM.A. "Integrins as mechanosensors" J Biol Chem 2004; 279: 12001-12004.

11. Balaban N.Q., Schwartz U.S., Riveline D., Goichberg P., Tzur G., Sabanay I., Mahalu D., Safran S., Bershadsky A., Addadi L., Geiger B. "Force and focal adhesion assembly: a close relationship studied using elastic micropatterned substrates". Nat Cell Biol 2001; 3: 466-472.

12. Rottner K., Hall A., Small J.V. "Interplay between Rac and Rho in the control of substrate contact dynamics". Curr Biol 1999; 9: 640-648.

13. Nobes C.D., Hall A. "Rho, rac, and cdc42 GTPases regulate the assembly of multimolecular focal complexes associated with actin stress fibers, lamellipodia, and filopodia". Cell 1995; 81: 53-62.

14. Clark E.A., King W.G., Brugge J.S., Symons M., Hynes R.O. "Integrin-mediated signals regulated by members of the Rho family of GTPases". J Cell Biol 1998; 142: 573-586.

Thoughts and Progress

Design of a Perfusion Bioreactor Specific to the Regeneration of Vascular Tissues Under Mechanical Stresses

*Katia Bilodeau, Frédéric Couet,
Francesca Boccafoschi, and Diego Mantovani
Laboratory for Biomaterials and Bioengineering,
Department of Materials Engineering, Laval
University, Quebec City, Canada*

Abstract: The objective of this work was to design a bioreactor to stimulate the three-dimensional regeneration of arterial tissue on a cylindrical scaffold with a methodological approach. Once seeded, the scaffold is perfused internally and the externally with culture medium with two independent perfusion systems at different flow rates. The horizontal position and the rotation of the construct ensure the uniformity of the arterial growth and of the endothelial cell spreading. During cell culture, the parameters, such as internal flow and stretching of the vessel, can evolve gradually from the fetal stage to the adult stage. The bioreactor will also be useful for investigating the influence of mechanical stresses and strains on the properties of mature arteries (rigidity, burst strength, adhesion of endothelial cells, etc.). **Key Words:** Tissue regeneration—Bioreactor—Design—Mechanical stresses—Three-dimensional cell culture.

Tissue engineering provides a new insight to the current problem of organ shortage and biomaterials failure after implantation. Despite the fact that several efforts in the last years have lead to the regeneration of two-dimensional tissues in a static environment the regeneration of a three-dimensional organized tissue (or organ), such as an artery, represents a great challenge. Appropriate bioreactors are required in order to reproduce and maintain the suitable environment essential for the three-dimensional cell regeneration (1).

In 1986, Weinberg et al. (2) first reproduced the three-layered arterial structure; after a period of static culture, they showed that the construct had a burst strength of 90 mm Hg, which is lower than the normal systolic blood pressure. The main limitation was the lack of adequate mechanical, electrical, and chemical stimulations during the growth that leads to dedifferentiation, low cohesion, and even the death of cells. Mechanical stresses during the culture period are known to be beneficial, even essential, mainly because cells adapt to surrounding functional demands (3). Once growing constructs are exposed to adequate pseudo-physiological mechanical stimuli, an improvement in the mechanical properties occurs. In 1999, Niklason et al. (4) seeded a biodegradable scaffold with smooth muscle cells (SMCs), and cultivated it under a pulsatile radial stress of 165 beats/min during 8 weeks, and finally measured a burst strength higher than 2000 instead of 300 mm Hg for the same construct cultured under static flow. This unequivocally shows that cell culture under mechanical stresses, including pulsating flow, is essential to obtain highly cohesive regenerated tissues.

The objective of this work was to design a bioreactor to mechanically stimulate arterial tissues during regeneration. Besides, the bioreactor should also allow the study of the influence of culture parameters, such as mechanical stress and strain, on the properties of mature arteries (rigidity, burst strength, adhesion of endothelial cells, etc.).

THE STRATEGY BEHIND BIOREACTORS AND MECHANICAL STRESSES

Bioreactors are too often presented like homemade bench tests, for which considerations regarding the design and the validation are often omitted. For example, in the scientific literature search engine Medline from 1970 to 2003, there are 153 indexed references containing the keywords "bioreactor" and "tissue engineering," but only a few focus on the complete design of the bioreactor, including the full list of requirements, and specifications to which the construct has to be submitted during the culture period in the bioreactor. Thus, the objective of this work was not only to design a bioreactor, but also to present and discuss the methodology behind this design.

Physiological mechanical constraints in an artery could be divided into five classes: internal pressure,

TABLE 1. *Mechanical effects on vascular tissue regeneration*

Flow rate in the lumen	Axial stress or strain on the seeded scaffold	Expected mechanical properties of the regenerated tissues
(a) None	None	Burst strength inferior to normal systolic pressure (4)
(b) Continuous	None	Higher than (a), but lower than native arteries (4)
(c) Pulsatile	None	Mechanical properties similar to native arteries (4)
(d) Pulsatile	Constant strain	Cells adapt to surrounding functional demands (3), so a higher rigidity or strength would be expected in the axial direction.
(e) Pulsatile	Pulsatile	The pressure wave in phase with pulsatile flow pressure in arteries could be reproduced to study the impact on mechanical properties. An interesting question to investigate would be to assess if the physiological pressure wave in the arterial wall would be better approximated by stress or strain.
(f) Continuous	Pulsatile stress equal or higher than stresses induced by the flow	SMCs orientation is usually circumferential to provide maximal rigidity in the maximal stress direction (29). It would be interesting to investigate the effect of a higher axial stress on the orientation of SMCs which would probably be more axial than circumferential, considering that culture conditions can change the structure of regenerated vessels.

SMCs, smooth muscle cells.

internal flow, axial strain, axial stress, and torsion. The first two, both being induced by blood flow, are isolated because it is possible to apply an internal pressure without a flow and vice versa. Axial stress and strain represent the constraints applied in the artery section in tension. Torsion, generally induced by the beats of the heart, is specific to coronary arteries. Thus, considering femoral artery conditions, the main goal was to design a multitask apparatus capable of mimicking various combinations of flow rate and axial stress/strain on the seeded scaffold, as shown in Table 1. Because internal pressure has not been isolated yet, this constraint is combined here with the flow in the lumen. Even if it could be logical to try reproducing all gradients constantly applied in the biological environment (concentration, chemical, electric, etc.), in this work we decided to focus only on the mechanical environment. In fact, although mass transport is also important, effects of the complex mechanical environment on the cells, known as the mechano-transduction, are essential, and very often neglected.

Mechano-transduction

A blood vessel substitute should possess the functional attributes of the native vessel it will replace. To reduce thrombogenicity, an "endothelial-like" lining, responsive to its mechanical environment, similar to that of the normal vascular endothelium, is required. If vaso-activity is a requirement, then this lining must also serve as a signal transduction interface, thereby communicating with the underlying smooth muscle cells having contractile phenotype in order to carry out their biomechanical functions resulting therefore in vessel contraction and expansion. In each of these cases, mechanics plays a key role. Vascular endothelial cells, which constitute the lumen of all blood vessels, serve as a barrier between perfused tissues and flowing blood. They act as sensors, detecting local changes in blood flow (5,6). In vivo studies indicate that endothelial cells are sensitive to the intensity of applied shear stresses and respond by changing their morphology and function (5). In fact, it has already been demonstrated that shear stresses induce morphological changes in cell orientation, reflecting the direction of flow in the immediate vicinity of the arterial wall (7). In vitro studies also showed that cell shape (8), and actin filament localization and alignment (9) are strongly dependent on hemodynamics. Besides the structural modifications incurred, mechanical forces can also initiate complex intracellular signals leading to functional changes within the cell. In fact, cell–matrix and cell–cell junction molecules are able to convert mechanical stimuli into biochemical signals (10). Studies with cultured cells have demonstrated that integrins, membrane proteins involved in cells attachment and inside-out and outside-in signaling (11), as well as G-protein coupled receptor (12), tyrosine-kinase receptors (13) and ion channels (14) play a key role in the activation of intracellular pathways by shear stresses (15). Shear stress responsive genes are involved in cell proliferation, cell differentiation, maintenance of vascular tone, thrombosis, cell–matrix, and cell–cell adhesion, and modulation of the inflammatory/immune system (16). In conclusion, mechanical stresses influence in vitro and in vivo cell behavior during the growth and the regeneration of cellular tissue. From this point of view, designing a bioreactor capable of mimicking the dynamic physiological cell environment is of main importance in tissue engineering and regeneration.

MATERIALS AND METHODS

Numerical modeling of the stresses in the arterial wall

A numerical simulation was used to approximate specific mechanical parameters, such as those induced in the arterial wall by the flow, with significant confidence level. Finite element analysis was carried out in order to model the stresses in the arterial wall, thus to have a better understanding of the intensity of the constraints that must be applied on the seeded scaffold to reproduce physiological conditions. The problem was mathematically treated with the finite elements software Ansys 6.1 (Ansys, Canonsburg, PA, U.S.A.) using FLEXlm v 8.0d and dynamically analyzed with a time step of 0.02 s.

The arterial wall was modeled as a perfect 10-mm-long cylinder with an average radius of 3 mm at rest and a wall thickness of 1 mm (Fig. 1a). These parameters approach those of the human femoral artery (17). The arterial wall properties were separated into two regions, the media and the adventitia, with the same thickness but distinct physical properties (18). The intima contribution was considered as negligible (18). The model was composed of two-dimensional axis symmetric elements, as done by Mosora et al. (19), to generate a two-wall cylindrical geometry (Fig. 1a).

Starting from this geometry, physical properties were assigned to the model. The arterial wall density was assumed to be of 1100 kg/m^3 and considered as incompressible (17). The longitudinal elastic modulus of the media and the adventitia was considered similar around 978 kPa (20). The circumferential elastic modulus of arteries varied from 1300 to 1700 kPa (21) with the media being three or four times stiffer than the adventitia (22). Finally, in the radial direction, the artery had an elastic modulus of about 118 kPa, as proposed by Blondel et al. (23). It has to be underlined that in arterial walls, stress–strain relation is nonlinear. However, for small deformations occurring in physiological conditions, a linear approximation can be accepted, thus considering the incremental elastic modulus (24).
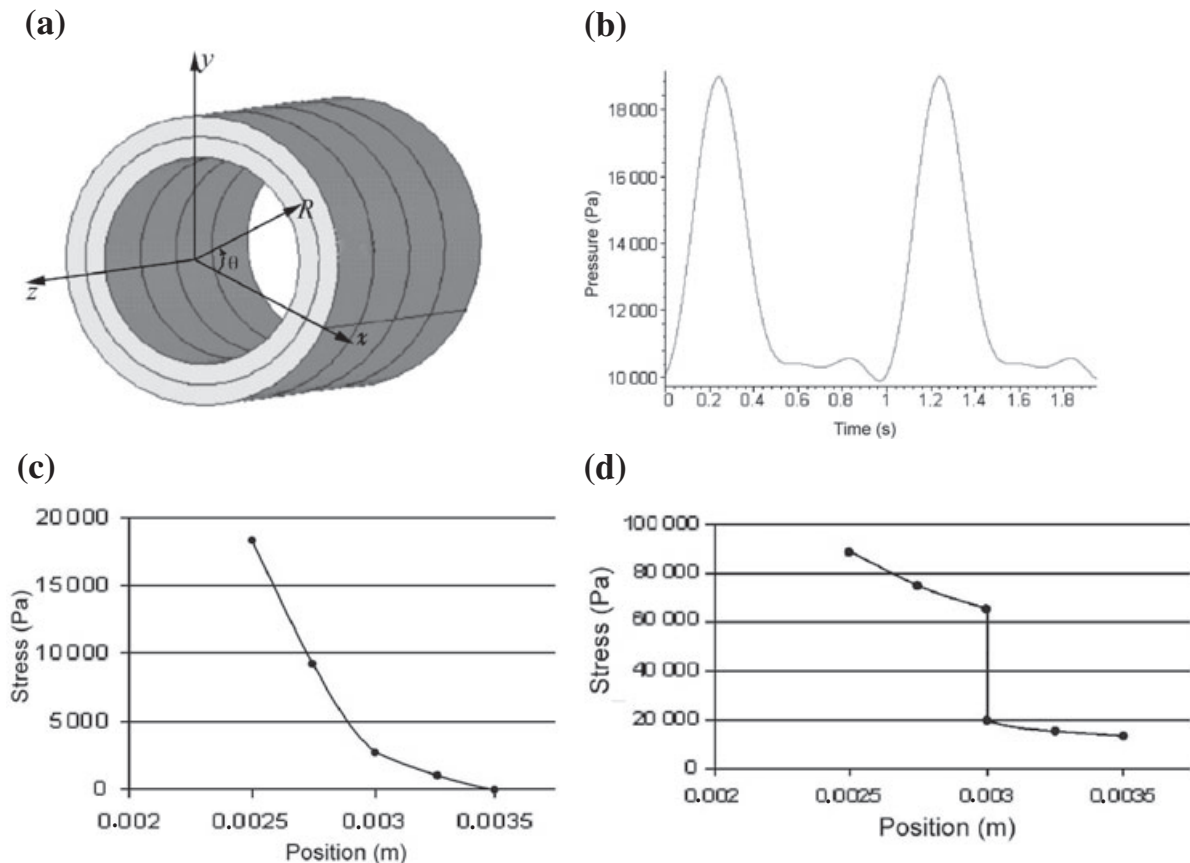

FIG. 1. Modeling the mechanical stresses in the arterial wall. (a) Axi-symmetric elements producing a two-layered arterial model; (b) Pressure profile applied on the model; (c) Radial stress distribution; (d) Circumferential stress distribution.

The numerical model was subjected to the following constraints in order to estimate stresses sustained by arteries under physiological conditions. The arterial wall was longitudinally stretched to approach its natural length as described by Blondel et al. (23). Then, a blood pressure profile varying from 80 (diastole) to 140 mm Hg (systole) with frequency of 1 Hz, as in a normal femoral artery, was applied to the numerical model. The pressure profile was approximated using a Fourier series with a frequency of 1 Hz (Fig. 1b).

Bioreactor design

The design focused on the identification of the requirements of the bioreactor, such as the main parameters to which cells should be exposed in order to proliferate and to regenerate tissue efficiently. These needs were converted into specifications that the model has to respect. The bioreactor was designed for in vitro culture of vessels with dimensions similar to a femoral artery (average radius of 3 mm, wall thickness of 1 mm [17]). A 5-cm length was chosen in order to have a sufficiently long vessels to reproduce physiological movements and to allow an eventual in vivo implantation, while minimizing the required quantity of cells at the same time. The bioreactor was designed using Pro/Engineer Wildfire software (PTC, Needham, MA, U.S.A.). A prototype of the bioreactor chamber was built and preliminary tests assessing the functionality were performed.

RESULTS AND DISCUSSION

Numerical modeling of the stresses in the arterial wall

An analysis was carried out to evaluate the order of intensity of the shear stress caused by a blood flow of around 200 mL/min in the femoral artery (25). Simulating a laminar, fully developed and pulsated flow inside the artery model, shear stresses varying from 0 to 2.48 Pa were calculated using a viscosity of 0.0035 Pa s and a density of 1050 kg/m^3, as suggested by Ghalichi (26). These results are in agreement with estimations of around 10 dynes/cm^2 (1 Pa) made by Fung (27). Considering that shear stresses are significantly lower than tensile stresses in the arterial wall, they might be neglected in the arterial wall (28).

Besides, the stress distribution inside the arterial wall was approximated. In the radial direction, the maximal stress appears to be around 18 kPa during systole and is located on the internal arterial surface, as seen in Fig. 1c. On the external side of the arterial wall, the level of radial stress tends toward zero. In the longitudinal direction, the stress level is roughly uniform around 65 kPa. These values are in agreement with experimental measurements made by Blondel et al. (23) which vary from 46 kPa to 67 kPa.

Finally, we observed that the stress distribution is not uniform in the circumferential direction, because there is a discontinuity at the media-adventitia interface as observed by Xie et al. (22). Numerical results presented in Fig. 1d show that the maximal stress is about 90 kPa near the arterial lumen, which is in agreement with stress distribution described by Fung (27). Finally, the strongest stresses are obtained in the circumferential direction inside the media, mostly because of the blood pressure. This is in agreement with the circumferential orientation of the smooth muscle cells that have to resist to this stress (29).

Bioreactor design

Even if an entirely biological approach is possible for the regeneration of an implantable vessel, as shown by L'Heureux et al. (30), a structural support, better known as scaffold, has the benefit of providing mechanical support to fragile young tissues while allowing cell proliferation and tissue regeneration (31). Besides, mechanical constraints, especially the axial stretching, cannot be applied directly to cells.

The design focused on the application of native-like mechanical stresses and strains on cultivated tissues utilizing different flows, pressures, and mechanical stretching. Normal strains in the axial direction are around 25–40% (32) and corresponding axial stresses are around 65 kPa, as obtained by numerical modeling. Normal pressure in the lumen is around 80–140 mm Hg and induced stresses in the arterial wall are pulsatile because of the pulsation of blood flow.

Culture chamber

The culture chamber was fabricated in acrylic (see Fig. 2b). The scaffold is inserted and mounted between stainless steel tubing, and sealed with FDA-compatible polymeric seals (#3, Swagelok, Québec, Canada). A longitudinal force could be applied to the scaffold/construct during its growth with a variable load pulley device (not shown). Otherwise, an oscillatory/constant strain could be applied with a pneumatic cylinder controlled by a microcontroller. The bellow side rotary union (#4, McMaster Carr, Atlanta, GA, U.S.A.) is placed on an open v-groove track roller guide block (#6, Cole-Parmer, Vernon Hills, IL, U.S.A.), which sits on a flanged ball spline (#5, ND Linear System, Wood Dale, IL, U.S.A.) allowing translation of the bellow side tube. The bel-
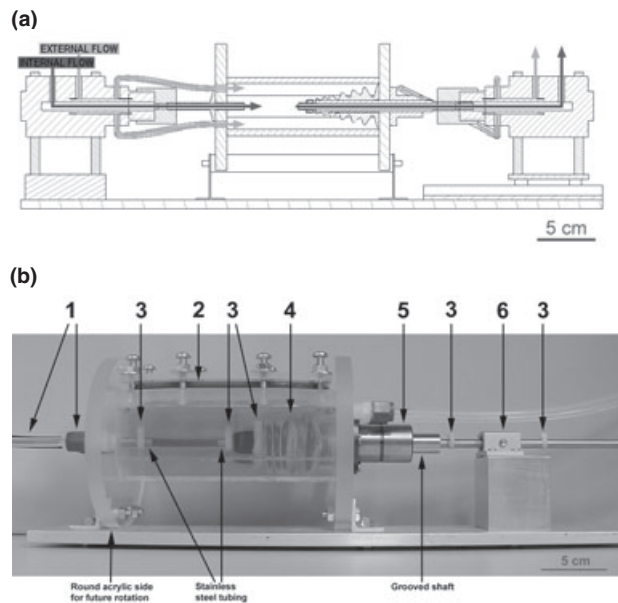
(a)

(b)

FIG. 2. (a) Section of the culture chamber showing the two double-flow rotary unions (at the extremities); and (b) the prototype of the culture cell (front views).

low side rotary union is essential to avoid any torsion on the growing construct that would occur during its rotation or its stretching. This could be interesting to mimic heart beating effects on coronary arteries, as previously studied by Vorp et al. (33).

A thin latex membrane was chosen to isolate the cell medium from the bellow side rotary union (#4) while allowing translation of the stainless steel tube. The latex membrane resisted to the standard autoclave sterilization process (20 min at 121°C in wet environment). A critical point of the design was the watertight nature of this membrane (#4) because it is directly linked to the sterile culture chamber. Tests were made to verify the water tightness of the latex membrane O-ring seal. The seal resisted to a 140 cm water column (13.7 kPa, 103 mm Hg) without any leakage. Thus, even if subdued to negligible external pressures, it would be able to support the internal pressure if a breakage of the vessel occurs. All other tubing connections are FDA-compatible fittings (#1), and parts are sealed by FDA-compatible O-rings (#2). The chamber can be rotated by an electric motor (not shown) at about 1 rpm to decrease the influence of gravity and to encourage uniform growth of the artery and the spreading of endothelial cells (2). The rotating components are essential for further scaffold-based tissue regeneration in order to allow a uniform seeding of an endothelium which is essential for vessel hemocompatibility. Finally, the real-time diameter of the growing construct can be

monitored by an optical interferometer (not shown), the culture chamber being made of transparent material (acrylic).

Scaffold/construct perfusion

The internal and external parts of the seeded scaffold/constructs are surrounded by culture medium to feed cultivated cells. Both perfusions are kept separate to avoid contamination between different cell types. Thus, the bioreactor is designed to be a part of a double flow perfusion system maintained at a temperature of 37°C. A pump provides an adjustable flow that can be continuous or pulsatile with a frequency range of 50–200 beats/min to cover the range from fetal to adult cardiac frequencies. The external medium is perfused at a slow and continuous rate to minimize shear stress on the outside of the artery. The perfusion of the internal medium is laminar and pulsatile in order to reproduce the physiological flow. Two double-flow rotary unions (9300 Rotary Union, Stainless steel series, Talco), allow the separation of the perfusions and the rotation of the culture chamber (Fig. 2a).

Progressive application of mechanical constraints

All culture parameters can be customized. Some parameters, such as diameter and presence or absence of torsion, can be easily modified even between two consecutive cultures. The internal flow, the internal pressure, the axial force, and the stretching of the vessel can evolve during the culture process. For example, at the beginning of the culture period, the pulsation frequency could be similar to a fetal cardiac frequency, and the flow rate and the stretching could be in the fetal range. These parameters could gradually progress toward adult requirements during the culture period. It has to be underlined that the design process was inspired by the phenomena occurring during the prenatal development of the fetus in order to reproduce the organogenesis process in the uterus. Niklason et al. (4) already regenerated a vessel under vertical flow and pressure in the fetal range. Here, the fetal inspiration was extended to the horizontal position of the vessel and the evolution of the magnitude of axial stretching. This evolution is crucial because beneficial stresses on a mature tissue can have dramatic effects on a newly seeded construct. Also, after a few weeks of maturation in an unvarying environment, the properties of the tissue stop improving, remain constant for a while and then begin to decrease, as observed by Hoerstrup et al. (34). The culture parameter evolution could help to overcome this plateau phenomenon.

CONCLUSION

A multitask, flexible, and polyvalent bioreactor was designed with a rational approach in order to apply various combinations of constraints such as internal flow, internal pressure, axial stress, axial strain, and torsion during the three-dimensional culture of cells onto and into a cylindrical construct. Physiological stresses in the arterial wall were approximated using finite element analysis, the bioreactor was specifically designed in order to apply similar stresses to the construct during the maturation period of the three-dimensional cell culture. Focus was addressed on mechanical constraints because they are essential for cell differentiation, tissue cohesion, and growing construct strength. Further studies will be carried out on the effects of mechanical stresses during the maturation on the properties of regenerated arteries (such as rigidity, burst strength, and adhesion of endothelial cells) in order to determine the optimal constraints at each stage of maturation.

REFERENCES

1. Lalan S, Pomerantseva I, Vacanti JP. Tissue engineering and its potential impact on surgery. *World J Surg* 2001;25:1458–66.
2. Weinberg CB, Bell E. A Blood vessel model constructed from collagen and cultured vascular cells. *Science* 1986;231:397–400.
3. Gray ML, Pizzanelli AM, Grodzinsky AJ, Lee RC. Mechanical and physiochemical determinants of the chondrocyte biosynthetic response. *J Orthop Res* 1988;6:777–92.
4. Niklason LE, Gao J, Abbott WM, et al. Functional arteries grown in vitro. *Science* 1999;284:489–93.
5. Davies PF. Flow-mediated endothelial mechanotransduction. *Physiol Rev* 1995;75:519–60.
6. Patrick CW Jr, McIntire LV. Shear stress and cyclic strain modulation of gene expression in vascular endothelial cells. *Blood Purif* 1995;13:112–24.
7. Nerem RM, Levesque MJ, Cornhill JF. Vascular endothelial morphology as an indicator of the pattern of blood flow. *J Biomech Eng* 1981;103:172–6.
8. Helmlinger G, Geiger RV, Schreck S, Nerem RM. Effects of pulsatile flow on cultured vascular endothelial cell morphology. *J Biomech Eng* 1991;113:123–31.
9. Yoshigi M, Clark EB, Yost HJ. Quantification of stretch-induced cytoskeletal remodeling in vascular endothelial cells by image processing. *Cytometry* 2003;55A:109–18.
10. Ingber D. In search of cellular control: signal transduction in context. *J Cell Biochem Suppl* 1998;30–31:232–7.
11. Coppolino MG, Dedhar S. Bi-directional signal transduction by integrin receptors. *Int J Biochem Cell Biol* 2000;32:171–88.
12. Hsieh HJ, Li NQ, Frangos JA. Shear-induced platelet-derived growth factor gene expression in human endothelial cells. *J Cell Physiol* 1992;150:552–8.
13. Iwasaki H, Eguchi S, Ueno H, Maruma F, Hirata F. Mechanical stress stimulates growth of vascular smooth muscle cells via epidermal growth factor receptor. *Am J Phys Heart Circul Phys* 2000;278:H521–9.
14. Sackin VP. Stretch-activated ion channels. *Kidney Int* 1995;48:1134–47.
15. Bhullar IS, Li YS, Miao H, et al. Fluid shear stress activation of IkappaB kinase is integrin-dependent. *J Biol Chem* 1998;273:30544–9.
16. McCormick SM, Eskin SG, et al. DNA microarray reveals changes in gene expression of shear stressed human umbilical vein endothelial cells. *Proc Natl Acad Sci USA* 2001;98:8955–60.
17. Megerman J, Abbott WM. Compliance in vascular grafts. In: Wright CB, ed. *Vascular Grafting: Clinical Applications and Techniques*. Boston, MA: John Wright PSG, 1983;344–64.
18. von Maltzahn WW, Warriyar RG, Keitzer WF. Experimental measurements of elastic properties of media and adventitia of bovine carotid arteries. *J Biomech* 1984;17:839–47.
19. Mosora F, Harmant A, Bernard C, et al. Modelling the arterial wall by finite elements. *Arch Int Phys Bioch Biophys* 1993;101:185–91.
20. Tsangaris S, Drikakis D. Pulsating blood flow in an initially stressed, anisotropic elastic tube: linear approximation of pressure waves. *Med Biol Eng Comput* 1989;27:82–8.
21. Lee JM, Wilson GJ. Anisotropic tensile viscoelastic properties of vascular graft materials tested at low strain rates. *Biomaterials* 1986;7:423–31.
22. Xie J, Zhou J, Fung YC. Bending of blood vessel wall: stress–strain laws of the intima-media and adventitial layers. *J Biomech Eng* 1995;117:136–45.
23. Blondel WCPM, Lehalle B, Maurice G, Wang X, Stoltz JF. Rheological properties of fresh and cryopreserved human arteries tested in vitro. *Rheol Acta* 2000;39:461–8.
24. Hayashi K, Stergiopulos N, Meister J-J, Greenwald SE, Rachev A. Techniques in the determination of the mechanical properties and constitutive laws of arterial walls. In: Leondes CT, ed. *Cardiovascular Techniques. Biomechanical Systems: Techniques and Applications*, Vol. 6. Boca Raton, FL: CRC Press LLC, 2001;1–61.
25. Hussain ST, Smith RE, Wood RF, Bland M. Observer variability in volume tric blood flow measurements in leg arteries using duplex ultrasound. *Ultrasound Med Biol* 1996;22:287–91.
26. Ghalichi F. *Pulsatile laminar and turbulent blood flow simulation in large stenosed arteries and stenosed carotid artery bifurcation*. (PhD Thesis). Mechanical Engineering, Université Laval, Sainte-Foy, Québec, Canada, 1998.
27. Fung YC. *Biomechanics: Motion, Flow, Stress, and Growth*. New York: Springer-Verlag, 1990.
28. Manak JJ. The two-dimensional in vitro passive stress–strain elasticity relationships for the steer thoracic aorta blood vessel tissue. *J Biomech* 1980;13:637–46.
29. Vorp DA, Rajagopal KR, Smolinsk PJ, Borovetz HS. Identification of elastic properties of homogeneous, orthotropic vascular segments in distension. *J Biomech* 1994;28:501–12.
30. L'Heureux N, Paquet S, Labbe R, Germain L, Auger FA. A completely biological tissue-engineered human blood vessel. *Faseb J* 1998;12:47–56.
31. Ratcliffe A. Tissue engineering of vascular grafts. *Matrix Biol* 2000;19:353–7.

32. Li J. *The Arterial Circulation: Physical Principles and Clinical Applications*. NJ: Humana Press, 2000.
33. Vorp DA, Severyn DA, Steed DL, Webster MW. A device for the application of cyclic twist and extension on perfused vascular segments. *Am J Physiol* 1996;270:H787–95.
34. Hoerstrup SP, Sodian R, Daebritz S, et al. Functional living trileaflet heart valves grown in vitro. *Circulation* 2000;102 (19 Suppl. 3):III44–9.

Development of the Pulsation Device for Rotary Blood Pumps

*Tomoyuki Yambe, *Yasuyuki Shiraishi,
*Kazumitsu Sekine, *Mune-ichi Shibata,
*Tasuku Yamaguchi, *Liu Hong Jian,
†Makoto Yoshizawa, ‡Akira Tanaka,
‡Hidetoshi Matsuki, ‡Fumihiro Sato,
‡You-ichi Haga, ‡Masayoshi Esashi,
§Kouichi Tabayashi, ¶Yoshinori Mitamura,
**Hiroshi Sasada, and *Shin-ichi Nitta
*Department of Medical Engineering and Cardiology,
Institute of Development, Aging and Cancer, Tohoku
University, Sendai; †Information Synergy Center,
Tohoku University, Sendai; ‡Graduate School of
Engineering, Tohoku University, Sendai; §Graduate
School of Medicine, Tohoku University, Sendai;
¶Graduate School of Engineering, Hokkaido
University, Hokkaido; and **Graduate School of
Agriculture, Tohoku University, Sendai, Japan

Abstract: A rotary blood pump (RP) is desirable as a small ventricular assist device (VAD). However, an RP is non-pulsatile. We tried to develop a device that attaches a pulse to the RP. We also tried to develop a pulse-generating equipment that was not air-pressure driven. The ball screw motor was considered a candidate. The application of a small-sized shape memory alloy was also attempted. An electrohydraulic system was adopted, and actuator power was connected to the diaphragm. The diaphragm was placed on the outer side of the ventricle. Most RPs that have been developed all over the world drain blood from the ventricle. The wave of a pulse should be generated if a pulse is added by the drawn part. The output assistance from the outer side of the ventricle was attempted in animal experiments, and the device operated effectively. This device can be used during implantable operation of RP. This may serve as an effective device in patients experiencing problems in peripheral circulation and in the function of internal organs. **Key Words:** Pulsation device—Rotary blood pump—Electrohydraulic—Ball screw—Artificial myocardium.

The Japanese are small in stature as compared to Europeans (1–4). The ventricular assist devices (VADs) presently available are designed in accordance with the physique of Europeans and Americans and are too large and heavy for the Japanese (5–9). Therefore, implantation of such VADs is difficult, and smaller-sized artificial hearts are needed.

The development of the rotary blood pump (RP) has gained momentum globally (10–14). Clinical applications of Micromed (Houston, TX, U.S.A.), Jarvik2000 (New York, NY, U.S.A.), HeartMate2 (Pleasanton, CA, U.S.A.), and the INCOR (Berlin, Germany) have already been carried out (12–14). The results of the clinical application of axial flow pump have attracted attention, and the clinical applications of the centrifugal blood pump have also advanced. Because an RP is small in size, it may be implanted effectively in the Japanese.

Unfortunately, because an RP is not a capacity-type pump, pulsating is difficult. The human heart has a blood chamber that generates a natural pulse. If chambers are made instead of a natural heart ventricle, then a mechanical actuator to work the chambers must be developed. Thus, a small-sized artificial heart cannot be structured because of the chamber and actuator.

Because of these factors, a vibrating flow pump (VFP) was developed in Tohoku University (15–17). In this system, a small chamber with a central tube is responsible for the vibrating blood flow that generates a pulse. The pulse can be generated provided the system is of a capacity rotation type, which is similar to the undulation pump (UP) developed at the University of Tokyo (18–20). These systems are alike with respect to the small pumping chamber.

However, there is no pumping chamber in a classic RP; therefore, the generation of a pulse is difficult. Furthermore, irrespective of this fact, many reports showing physiological disadvantage in circulation in animal experiments and clinical situations have also been encountered. In circulation using VADs, the generation of a natural pulse is expected. However, patients for whom a VAD is adopted have lower contraction power. A RP may not easily generate a pulse for a patient whose circulation depends on a VAD. Tohoku University has developed the artificial myocardium in the 80s. Consequently, in this study,
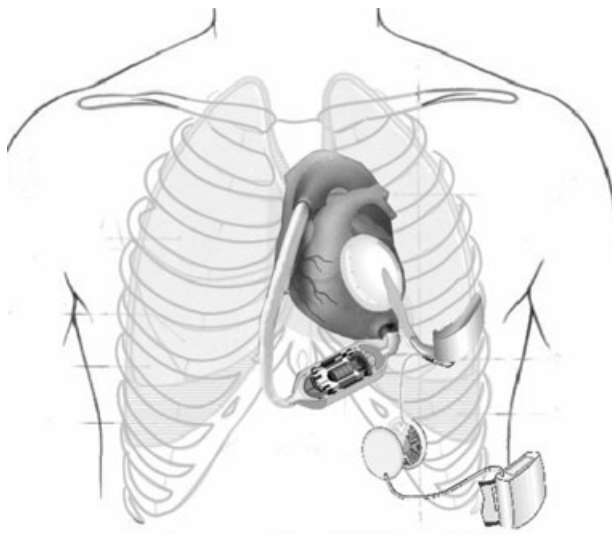
FIG. 1. Concept design of a pulsation device.

the development of a pulsation device by using an artificial myocardium was initiated.

PULSATION DEVICES

The left ventricular approach is used widely in RPs. The left ventricle (LV) generates a big pulse; thus, a pulse is generated in the VAD flow by LV power. However, a patient using a VAD has a weak heart; therefore, pulse generation becomes dependent solely on the VAD. We have developed the artificial myocardium (21), a system that helps contraction. The artificial myocardium and RP were used in combination in this study.

The concept of this system is shown in Fig. 1. In this system, the blood flows into the RP from the LV. To generate the pulse in the inflow wave, the diaphragm attached to the LV directly pushes the heart, as in a cardiac massage, which can generate a pulse. Therefore, in this system, a pulse is formed even when the heart is weak. This pulsation device is driven by an electrohydraulic power. Silicone oil is driven by the actuator designed to be implanted between ribs.

Energy is provided through the skin. The transcutaneous energy transmission system of Tohoku University raises the efficiency of the process by magnetic shielding.

ANIMAL EXPERIMENT

In Tohoku University, the axial flow pump was developed in cooperation with Hokkaido University and Keio University. This pump is to be implanted in place of the aortic valve; hence, this axial flow pump

is named Valvo pump. In this study, the Valvo pump was used in an animal experiment that was conducted using an adult goat. We approached the left chest cavity by resecting the left fourth rib. Inflow cannulae were inserted into the LV from the left appendage through the mitral valve. Outflow cannulae were sutured to the descending aorta. Experiments on left heart bypass were then performed. Subsequently, the newly developed pulsation device was attached to the LV to generate a pulse. Electrohydraulic power directly pushed the diaphragm and the left ventricular wall. Electrocardiogram, pump flow, arterial blood pressure, left ventricular pressure, and cardiac output measured at the pulmonary artery were recorded in the digital data recorder. Off-line analyses were then performed by using an AD convertor with a personal computer system.

RESULTS

Hemodynamic parameters were maintained within the normal range and the satisfactory pump output was easily obtained by using the Valvo pump axial flow assist device in the experiment conducted on a goat. Satisfactory supporting effect was also obtained. However, the pulse width of the arterial blood pressure tended to decrease while using the device.

Hemodynamic parameters during left ventricular assistance with the Valvo pump and the pulsation device are shown in Fig. 2. In the animal experi-
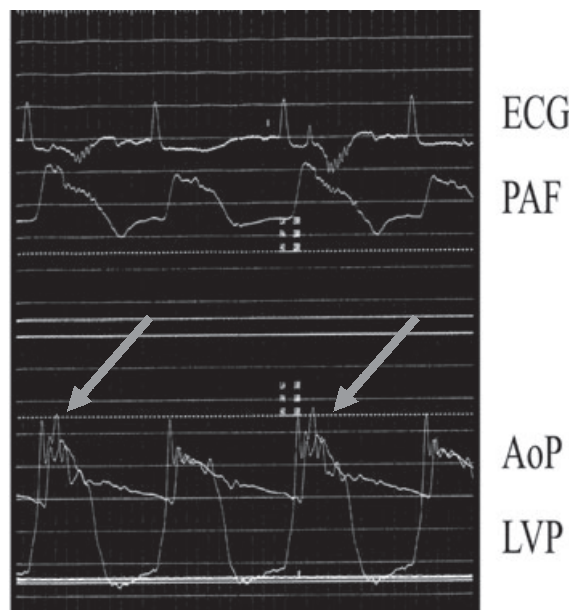

FIG. 2. Time series data of the hemodynamic parameters during left ventricular assistance with a Valvo pump and a pulsation device.

ments, 1/2 assist of the pulsation device was performed. The pulsation device was assisted in one beat and was not assisted in the next beat. Thus, we could compare the hemodynamic parameters with and without the pulsation device assist during Valvo pump-left ventricular bypass. When the pulsation device assisted the hemodynamics with the Valvo pump assist, the left ventricular pressure and arterial pressure tended to increase, thereby suggesting the pulsation effect.

Subsequently, ventricular fibrillation was induced by electric current. The assistance effect of the Valvo pump and the pulsation device was examined in the experiment. However, under the condition of ventricular fibrillation, the pump flow of the Valvo pump was not very satisfactory. Hemodynamics could not be maintained with only the left ventricular bypass; hence, the pulsation device was assisted. However, it could only generate a weak pulse in the left ventricular pressure and arterial pressure. The effect was not very satisfactory in the case of a cardiac arrest.

DISCUSSION

Many researchers have investigated the effect of pulse, and many reports have considered the meaning of pulse. In 1982, Nosé et al. reported that a nonpulsatile pump could maintain the circulation in chronic animal experiments. Recent clinical reports concerning the percutaneous cardiopulmonary support system (PCPS) showed that continuous flow circulation could maintain viability even in clinical cases. Recent progress in clinical reports of axial flow pumps was obviously important. However, nonpulsatile assist differed from nonpulsatile circulation. The effect of continuous flow circulation must be studied extensively for further development of RP.

In this article, a pulsation device was developed to generate a pulse during RP assist. A discussion regarding pulsation device may be needed because several researchers reported that nonpulse circulation was satisfactory and that a small pump was preferred.

In this study, pulsatile support by our newly developed pulsation device was confirmed during axial flow pump assist. However, the supporting effect was not very satisfactory in the case of a cardiac arrest. We must redesign the profile of the pulsation device while considering the condition of vital arrhythmia in the clinical stage.

Many investigators suggested that the pulsatile support might be desirable for organ circulation. Multiple organ failure (MOF) is critical when we consider the clinical use of a VAD. Hence, the pulsation device may be desirable for patients with MOF.

Recent reports concerning the weaning from a VAD in dilated cardiomyopathy are important. If the weaning from an implantable RP will be considered in clinical situations, our pulsation device may become an important device. As this device will be sutured on the outer side of the ventricle, we will not consider the antithrombogenicity of this implantable device. Furthermore, this device need not be driven continuously; it can be driven only when required. Hence, the durability of the device will be satisfactory. From this point of view, the pulsation device is completely different from conventional assist pumps.

In conclusion, pulsatile support was observed in the animal experiments. This device may be useful in the treatment of MOF. However, the supporting effect of the pulsation device was not very satisfactory under the condition of ventricular fibrillation (VF). We must redesign the profile of the device while considering vital arrhythmia in clinical situations. The pulsation device is attached to the outer side of the ventricle; hence, thrombus formation need not be considered. It may become a useful device in the future.

REFERENCES

1. Pantalos GM, Chaing BY, Bishop DN, et al. Development of smaller artificial ventricles and valves made by vacuum forming. *Int J Artif Organs* 1988;11:373–80.
2. Nakazawa T, Makinouchi K, Ohara Y, et al. Development of a pivot bearing supported sealless centrifugal pump for ventricular assist. *Artif Organs* 1996;20:485–90.

3. Yambe T, Owada N, Kobayashi SI, et al. Totally implantable ventricular assist system that can increase brain blood flow. *Artif Organs* 2000;24:644–7.
4. Mitamura Y, Yozu R, Tanaka T, Yamazaki K. The valvopump. An axial, nonpulsatile blood pump. *ASAIO Trans* 1991;37:M510–2.
5. Saito S, Westaby S, Piggot D, et al. End-organ function during chronic nonpulsatile circulation. *Ann Thorac Surg* 2002;74:1080–5.
6. Yambe T, Kawano S, Nanka S, et al. Peripheral vascular resistances during total left heart bypass with an oscillated blood flow. *Artif Organs* 1999;23:747–50.
7. Mitamura Y, Nakamura H, Okamoto E, Yozu R, Kawada S, Kim DW. Development of the Valvo pump: an axial flow pump implanted at the heart valve position. *Artif Organs* 1999;23:566–71.
8. Kihara S, Yamazaki K, Litwak KN, et al. In vivo evaluation of a MPC polymer coated continuous flow left ventricular assist system. *Artif Organs* 2003;27:188–92.
9. Yambe T, Owada N, Kobayashi S, et al. Left heart bypass using the oscillated blood flow with totally implantable vibrating flow pump. *Artif Organs* 1998;22:426–9.
10. Margreiter R, Schwab W, Klima G, et al. Rotacor: a new rotary blood pump. *ASAIO Trans* 1990;36:M281–4.
11. Schima H, Honigschnabel J, Trubel W, Thoma H. Computer simulation of the circulatory system during support with a rotary blood pump. *ASAIO Trans* 1990;36:M252–4.
12. Wieselthaler GM, Schima H, Hiesmayr M, et al. First clinical experience with the DeBakey VAD continuous-axial-flow pump for bridge to transplantation. *Circulation* 2000;101:356–9.
13. Song X, Throckmorton AL, Untaroiu A, et al. Axial flow blood pumps. *ASAIO J* 2003;49:355–64.
14. Myers TJ, Robertson K, Pool T, Shah N, Gregoric I, Frazier OH. Continuous flow pumps and total artificial hearts: management issues. *Ann Thorac Surg* 2003;75(6 Suppl.):S79–85.
15. Yambe T, Sonobe T, Naganuma S, et al. Fractal dimension analysis of the oscillated blood flow with a vibrating flow pump. *Artif Organs* 1995;19:729–33.
16. Kobayashi S, Nitta S, Yambe T, et al. Experimental study of physiological advantages of assist circulation using oscillated blood flow. *Artif Organs* 1995;19:704–7.
17. Yambe T, Nitta S, Sonobe T, et al. Chaotic hemodynamics during oscillated blood flow. *Artif Organs* 1994;18:633–7.
18. Abe Y, Chinzei T, Isoyama T, et al. Basic study to develop the undulation pump for practical use: antithrombogenicity, hemolysis, and flow patterns inside the pump. *Artif Organs* 1995;19:691–3.
19. Yambe T, Abe Y, Isoyama T, et al. Non-linear dynamic analysis of hemodynamic parameters in an undulation type artificial heart system. *Biomed Pharmacother* 2002;56(Suppl. 2):364s–366s.
20. Dobsak P, Vaskuo J, Baba A, et al. Microvessels of bulbar conjunctiva in UPTAH goats. *Artif Organs* 2003;27:114–8.
21. Yambe T, Yoshizawa M, Tanaka A, et al. Recent progress in artificial organ research at Tohoku University. *Artif Organs* 2003;27:2–7.

Hepatocyte Function in a Radial-flow Bioreactor Using a Perfluorocarbon Oxygen Carrier

*†Martin J. Nieuwoudt, ‡Sean F. Moolman, §Kobus J. Van Wyk, †Elke Kreft, †Brenda Olivier, ¶J.B. Laurens, **Frik G. Stegman, ††Joanne Vosloo, †,‡‡Robert Bond, and †,‡‡Schalk W. van der Merwe
*Department of Bioengineering, University of Pretoria; †Hepatology and Gastrointestinal Research Laboratory, University of Pretoria; ‡Centre for Polymer Technology, M & Mtek, CSIR; Departments of §Mechanical Engineering, ¶Chemical Pathology, **Anesthesia, Onderstepoort Veterinary Hospital, ††Surgery and ‡‡Internal Medicine and Gastroenterology, University of Pretoria, Pretoria, South Africa*

Abstract: The aims of this study were, first, to indicate the metabolic activity of hepatocytes in a radial-flow polyurethane foam matrix bioreactor relative to monocultures, and second, to evaluate the effect on the hepatocytes of including a synthetic perfluorocarbon (PFC) oxygen carrier to the recirculating medium. The efficient O_2-carrying ability of PFCs may be beneficial to bioreactors employed in stressed cellular environments. Thus, they may also be useful in the treatment of an acute liver failure patient with a bioartificial liver support system (BALSS). Data on the function of three-dimensional (3-D) hepatocyte cultures exposed to emulsified PFCs are lacking. Results: the metabolic functions of the 3-D hepatocyte cultures were improved relative to monocultures. Three-dimensional cultures with and without PFC behaved similarly, and no adverse effects could be detected when PFC was included in the recirculating medium. The addition of PFC significantly improved lidocaine clearance possibly due to the presence of higher O_2 tension in the medium. Imaging indicated that large aggregates formed and that seeding had followed flow through the matrix. Simulations indicated first, that the cell numbers used in this study had been insufficient to challenge the bioreactor O_2 supply explaining the similarity in performance of the 3-D cultures, and second, that the benefit of adding PFC would be more pronounced at the cell densities likely to be used in a BALSS bioreactor. **Key Words:** Bioartificial liver—In vitro hepatocyte metabolism—Perfluorocarbon oxygen carrier.

The aim of this study was to determine the effect of bioreactor design and the inclusion of a circulating oxygen carrier on the in vitro metabolic activity of hepatocytes in a simplified bioartificial liver support system (BALSS) circuit. The BALSS under

development in our laboratory (1,2) incorporates a direct hepatocyte-plasma contact, radial-flow bioreactor with a polyurethane foam (PUF) matrix. The open-cell pore size of the PUF matrix is on average 500 μm, each of which may incorporate an aggregate with 15 000 or more hepatocytes. The internal volume of the PUF matrix is 250 mL, thus, a total of 6×10^{10} cells or 300 g may be seeded, accounting for 20% of a normal liver's hepatocyte mass. This should be sufficient to maintain the estimated minimal requirements for liver support (3,4). An ongoing concern among investigators is the presence of domains of low O_2 tension and hypometabolism in their bioreactors (3,5). To overcome potential mass transfer limited domains within our bioreactor, we developed a perfluorocarbon (PFC) oxygen carrier that is incorporated in the bioreactor subcirculation. Perfluoro-octyl bromide (PFOB) is a synthetic polymer with a very high gas solubility. It is chemically and biologically inert and tends to be both hydrophobic and lipophobic. Thus, it requires emulsification prior to use in a recirculating aqueous environment (1,2). In this study, we investigate the metabolic activity of hepatocytes seeded into the PUF matrix of the radial-flow bioreactor using established indicators of liver function, and we compare the performance of our bioreactor with and without PFC to monocultures.

MATERIALS AND METHODS

The University of Pretoria Animal Use and Care Ethics committee granted approval for the protocol. Twenty-kilogram Landrace pigs were used. All media and chemicals used in the cell culturing, transport, and dissolution of the liver are as described by Nieuwoudt et al. (6). PFC-lecithin emulsions were prepared according to the method of Moolman et al. (1,2). The emulsions were mixed with double concentrated minimum essential medium (MEM) and sterile deionized water to achieve a 20% v/v PFC emulsion-MEM mixture. The mixture was pH adjusted and was used as a culturing medium. For liver perfusion and hepatocyte isolation, the method of Nieuwoudt et al. (6) was used throughout. This is a high-yield, sterile automated procedure.

Cell culture and evaluations

Cell count and viability were assessed with trypan blue (T-0776, Sigma, Johannesburg, South Africa). The suspension was then seeded into a sealed recirculating system in an incubator, representing a sim-

plified dynamic model of the BALSS. To facilitate homogenous seeding throughout the matrix, the bioreactor was designed for even flow using computational fluid dynamics (CFD). A total of eight 7-day-long metabolic trials were conducted on the dynamic and static systems. Five studies employed ordinary MEM, (PFC[–]), while three used the supplemented PFC-MEM emulsion (PFC[+]).

Daily sampling investigated lactate dehydrogenase (LD), aspartate aminotransferase (AST), glucose, lactate, and pyruvate concentrations. These were measured using enzymatic kits. The pO_2, pCO_2, and pH were measured on a blood gas machine. The oxygen uptake rate (OUR) was calculated after sampling with the gas supply turned off.

Metabolic clearance/production studies were performed in both dynamic and static configurations as follows: on day 2 D(+) galactose elimination, using gas chromatography mass spectrometry for detection; on day 3 ammonia detoxification (NH_4Cl) with urea synthesis, using enzymatic methods for detection; on day 4 lidocaine clearance, using liquid chromatography mass spectrometry (LC-MS) for detection; and on day 5 albumin production, using a spectrophotometric method. Upon termination on day 7, imaging studies involved either scanning electron microscopy (SEM), to investigate the presence of cells in the foam, or isotopic scanning to investigate the seeded distribution of the cells in the foam. For hepatocyte labeling, the isotope used was ^{99m}Tc-labeled-DISIDA.

Statistics

Microsoft Excel was used for data processing while Statistix 8 (Tallahassee, FL, U.S.A.) was used for analysis. Values were presented as the mean ± standard deviation. Clearance/production rates were calculated by converting the raw data to absolute quantities and graphing according to time. The gradients of the linear fittings were taken to be the rates. Statistical significance was measured using the Student's *t*-test.

RESULTS

Cell counts ranged between 6×10^9 and 2×10^{10} for all studies, with viability 95.91 ± 3.0%.

Daily sampling

The pO_2, pCO_2, and pH values averaged 286.5 ± 25.5 mm Hg, 30.0 ± 1.4 mm Hg, and 7.45 ± 0.03 mm Hg, respectively, in both PFC(+) and PFC(–) cultures. Within the detection ability of the electrodes, no significant drop in pO_2 was measur-
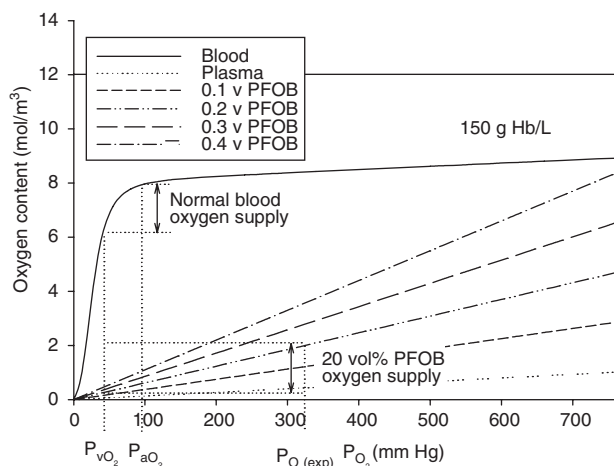
FIG. 1. Increased PFOB volume fraction increases the oxygen-carrying capacity of the emulsions. The oxygen solubility in the emulsions follows a linear relationship with partial oxygen pressure. The experimentally measured partial oxygen pressure in the UP-CSIR BALSS is indicated on the graph, showing similar potential oxygen delivery compared to blood (if exposed to normal venous partial oxygen pressure).

able when PFC was present. Thus, daily OUR determinations were only possible in PFC(–) cultures, average: 17.8 ± 4.0 nmol/h/10^6 cells. The gas-carrying ability of PFC is far greater than that of MEM or plasma (Fig. 1). Because majority of all other measurements of the PFC(–) and PFC(+) cultures were similar, OUR was assumed to be equivalent. Lactate values were similar in both cultures, while pyruvate values were slightly decreased in the PFC(+) cultures. Because an increase in the lactate-to-pyruvate ratio is generally due to an increase in anaerobic metabolism, it seems likely that the difference was caused by the interference of PFC with pyruvate measurement, rather than by an anaerobic state. AST and LD concentrations decreased exponentially in the first 3 days of culturing, with initial levels of 217.9 ± 60.7 and 98.4 ± 50.8 IU/L, respectively, descending to 23.0 ± 19.5 and 48.2 ± 22.4 IU/L by day 5. This would indicate the progressive stabilization of the cell culture.

Metabolic clearance/production studies

D(+) galactose elimination on day 2 revealed that PFC(+) and PFC(–) cultures cleared similar amounts, 1.6 ± 0.1 and 1.7 ± 0.1 μg galactose/h/10^6 cells, respectively. Monocultures cleared 0.35 ± 0.2 μg/h/10^6 cells. Urea production on day 3 revealed that PFC(+) cultures produced 42.34 ± 14.5 μg urea/h/10^9 cells, PFC(–) cultures produced 148.93 ± 20.1 μg/h/10^9 cells, and flasks produced 20.2 ± 8.2 μg/h/10^9 cells. The differences in production may reflect

interference with the measurement of urea in PFC(+) cultures. The clearance of ammonia was similar in the three-dimensional (3-D) cultures; 8.2 ± 3.0 μg ammonia/h/10^9 cells for PFC(+) and 8.6 ± 4.4 μg/h/10^9 cells for PFC(–). The clearance of lidocaine on day 4 was 1.6 ± 0.1 μg lidocaine/h/10^6 cells for PFC(–) cultures. PFC(+) cultures cleared lidocaine at 2.8 ± 0.3 μg/h/10^6 cells, which was significantly better than PFC(–) cultures ($P < 0.05$). Monocultures cleared 0.6 ± 0.4 μg/h/10^6 cells. The production of albumin on day 5 was similar in the 3-D cultures; PFC(–) cultures produced 21.9 ± 0.9 μg albumin/h/10^6 cells, while PFC(+) cultures produced 21.9 ± 0.5 μg/h/10^6 cells.

Upon termination on day 7, SEM confirmed the presence of large hepatocyte aggregations in the open-cell matrix. Isotopic imaging demonstrated that the distribution of hepatocytes in the matrix was determined by the flow of the circulating medium through the foam. This was taken to be an indication that CFD had been useful for bioreactor design.

DISCUSSION

Our observations suggested that OUR tends to a limit determined by cell density and the pO_2 of the circulating medium. However, the usefulness of OUR as an indicator of the metabolic state of hepatocytes in a bioreactor is balanced by the challenge of its accurate determination in 3-D cultures. The assumption that the OUR measured for hepatocytes grown in monolayers is constant in 3-D culture configurations at high cell densities may be incorrect (5,7). Previous investigations of the OUR of a variety of types of hepatocytes have revealed that as cell density and the pO_2 of a perfusing culture medium increases, OUR per unit cell mass decreases (8). It has been proposed that the release of humoral factors controlling cell-cell communication may enable the cells to manage "crowding" by temporarily suppressing oxidative metabolism (9). Perhaps the decrease in OUR with increasing cell density follows an allometric relationship, such as that first described by Kleiber (10,11)? This relationship represents an evolutionary strategy whereby OUR is diminished with increasing body mass. There is utility in observing such a relationship: OUR may potentially be scaled to large cell numbers, enabling real-time functional quantification of a bioreactor.

In this study, ammonia clearance, albumin production, and galactose elimination were similar in
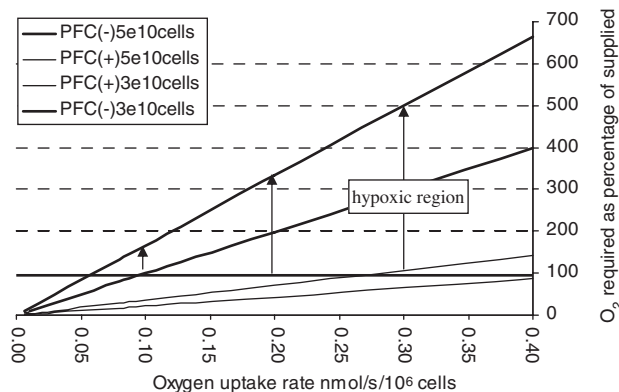
FIG. 2. Simulation of bioreactor O_2 requirements. PFC emulsions provide a significant advantage to high cell densities in a BALSS. The cell densities in this study were insufficient to challenge the O_2 supplied to the bioreactor. The flow rate was 300 mL/min.

the dynamic cultures and higher than in monocultures. Increased metabolic activity was therefore observed in dynamic compared to monolayer cultures. Urea production was increased in PFC(−) cultures relative to PFC(+) cultures, while lidocaine clearance was significantly higher in PFC(+) cultures. The increased lidocaine clearance in PFC(+) cultures may indicate that lidocaine metabolism (Cytochrome P450) is more dependent on oxidative metabolism and higher O_2 tension than the other metabolic variables studied. Several previous investigators using PFCs in production bioreactors have noted significantly improved metabolic functions (12–14). Our observation was that similar results were obtained for PFC(+) and PFC(−) cultures for most variables studied. It should be kept in mind that there is 0.5 times more CO_2 and 4.5 times more O_2 present in a 20% v/v PFC emulsion relative to normal medium (Fig. 1). Thus, the benefit of adding PFC may only be apparent when high cell densities are employed in a bioreactor. If the O_2-carrying ability of plasma is taken to be approximately equal to that of medium, it is clear that the emulsion would be far better at preventing hypoxia in high density, stressed cellular environments. Additionally, simulations of bioreactor O_2 requirements (refer to Moolman [1]) reveal that with increasing OUR, the demand relative to the supply of O_2 becomes severely limiting when PFC is not used (Fig. 2). It was also revealed that the present experiments were conducted at cell densities that were insufficient to challenge the O_2 supply of the bioreactor. This may explain why the metabolic performances were similar.

CONCLUSION

In this study, we observed that hepatocyte aggregation occurred in the PUF matrix of our bioreactor and metabolic functions were improved relative to flask cultures. The addition of PFC to the medium improved some hepatocyte functions such as lidocaine clearance, and no adverse effects were otherwise detectable. Simulations revealed that the cell densities employed were insufficient to challenge the O_2 supplied to the bioreactor, and this may explain the similarity in the results. The true benefits of PFCs are more likely to be found in preventing hypoxia when very high cell densities are employed in a bioreactor. Further studies are recommended.

REFERENCES

1. Moolman FS. Oxygen carriers for a novel bio-artificial liver support system. 2004 PhD Thesis, University of Pretoria. Available at: http://upetd.up.ac.za#etd-09092004-162043. Accessed June 2004.
2. Moolman FS, Rolfes H, van der Merwe SW, Focke WW. Optimization of perfluorocarbon emulsion properties for enhancing oxygen mass transfer in a bio-artificial liver support system. *Biochem Eng J* 2004;19:237–50.
3. Morsiani E, Brogli M, Galavotti D, Pazzi P, Puviani AC, Azzena GF. Biologic liver support: optimal cell source and mass. *Int J Artif Organs* 2002;25:985–93.
4. Tsiaoussis J, Newsome PN, Netson LJ, Hyes PC, Plevris JN. Which hepatocyte will it be? Hepatocyte choice for bioartificial liver support systems. *Liver Transpl Rev* 2001;7:2–10.
5. Hay PD, Veitch AR, Gaylor JDS. Oxygen transfer in a convection enhanced hollow fiber bioartificial liver. *Artif Organs* 2001;25:119–30.
6. Nieuwoudt M, Kreft E, Olivier B, et al. A large scale automated method for hepatocyte isolation: effects on proliferation in culture. *Cell Transplant* 2005;14:291–9.
7. McClelland RE, MacDonald J, Coger RN. Modeling O2 transport within engineered hepatic devices. *Biotechnol Bioeng* 2003;82:12–27.
8. Smith MD, Smirthwaite AD, Cairns DE, Cousins RB, Gaylor JD. Techniques for measurement of oxygen consumption rates of hepatocytes during attachment and post-attachment. *Int J Artif Organs* 1996;19:36–44.
9. Sand T, Condie R, Rosenberg A. Metabolic crowding effect in suspension of cultured lymphocytes. *Blood* 1977;50:337–46.
10. Kleiber M. Body size and metabolic rate. *Physiol Rev* 1947;27:511–41.
11. Wang Z, O'Connor TP, Heshka S, Heymsfield SB. The reconstruction of Kleiber's law at the organ-tissue level. *J Nutr* 2001;131:2967–70.
12. Ju LK, Lee JF, Armiger WB. Enhancing oxygen transfer in bioreactors by perfluorocarbon emulsions. *Biotechnol Prog* 1991;7:323–9.
13. McMillan JD, Wang DIC. Enhanced oxygen transfer using oil-in-water dispersions. *Ann N Y Acad Sci* 1987;506:569–82.
14. Elibol M, Mavituna F. Effect of perfluorodecalin as an oxygen carrier on actinorhodin production by Streptomyces coelicor. *Appl Microbiol Biotechnol* 1995;43:206–10.

Enhancement of the Transmesothelial Resistance of the Parietal Sheep Peritoneum by Epinephrine In Vitro: Ussing-type Chamber Experiments

*Ioannis Stefanidis, †Sotirios Zarogiannis,
†Chrissi Hatzoglou, *Vasilios Liakopoulos,
*Panagiota Kourti, *Antigoni Poultsidi,
*Peter R. Mertens, ‡Konstantinos Gourgoulianis,
and †Paschalis-Adam Molyvdas
*Division of Nephrology, University Hospital of
Larissa, Larissa; †Department of Physiology, Medical
School, University of Thessaly, Thessaly; and
‡Department of Respiratory Medicine, University
Hospital of Larissa, Larissa, Greece*

Abstract: The peritoneal mesothelium constitutes an ion transport barrier that is taken advantage of in peritoneal dialysis. The aim of this study was to investigate the effects of epinephrine on the electrical transmesothelial resistance (R_{TM}) of the isolated parietal sheep peritoneum by means of Ussing-type chamber experiments. Intact parietal (diaphragmatic) peritoneal samples were obtained from adult sheep immediately after sacrifice and transferred within 0.5 h to the laboratory in a cooled Krebs–Ringer bicarbonate solution (4°C, pH 7.5), bubbled with 95% O_2–5% CO_2. A parietal peritoneal planar sheet was mounted in a Ussing-type chamber. Epinephrine (10^{-7} M) was added to the apical and the basolateral side. The R_{TM} was measured before and serially after the addition of epinephrine for 30 min. As active ion transport is temperature-dependent, all measurements were performed at 37°C. The results were calculated as means with standard errors ($x \pm$ SE) of six independent experiments. The control R_{TM} was 20.05 ± 0.61 Ω·cm². The addition of epinephrine to the basolateral side within 1 min induced an increase of R_{TM} to 21.8 ± 0.45 Ω·cm², which decreased thereafter progressively to reach control values again after 15 min. A similar effect of epinephrine on the apical side was apparent with a rapid rise of R_{TM} to 22.5 ± 0.66 Ω·cm² and a subsequent decrease ($P < 0.05$). A clear association between the R_{TM} and active ion transport was established from previous studies. The results of our study indicate a rapid action of epinephrine on the parietal peritoneum permeability. **Key Words:** Epinephrine—Peritoneum—Permeability—Transmesothelial resistance—Ussing-type chamber.

The peritoneal mesothelium constitutes one of the main barriers for water and ion transport from the peritoneal cavity to the peritoneal capillary bed (1). The physiological solute transport across the perito-neal mesothelium is essential for effective peritoneal dialysis treatment. One of the major problems associated with peritoneal dialysis is ultrafiltration failure, which affects up to 50% of patients on peritoneal dialysis treated for more than 6 years (2,3). It has been proven, that the peritoneal permeability for small solutes increases over time in patients on peritoneal dialysis, a circumstance that eventually leads to ultrafiltration failure and practically obsoletes this treatment modality (2,3).

Since a pioneering study by Ussing and Zerahn (4,5), electrophysiological methodologies have become a valuable tool for the characterization of the ionic transport properties of epithelial membranes (6–8), especially of actively secreting and absorbing tissues (i.e., tubular and colonic epithelia). In recent years, Ussing-type chamber experiments have also been reported in certain serosal membranes such as the peritoneum (9–11) and the pleura (12–14) that utilize electrophysiological and pharmacological approaches. Alterations in the permeability of serosal membranes in relation to the action of certain substances, such as sexual hormones, insulin, channel blockers, NO inhibitors, and antibiotics and their metabolites, have been investigated hitherto.

The aims of the present study were to investigate the electrophysiological properties of the parietal sheep peritoneum and to determine the effect of epinephrine on the transmesothelial resistance (R_{TM}).

MATERIALS AND METHODS

Intact sheets of parietal sheep peritoneum were obtained from adult male and female animals. The samples were collected from a slaughterhouse immediately after the animals were sacrificed (time of warm ischemia was close to 0 min), and were transferred within 0.5 h to the laboratory in an oxygenated Krebs–Ringer solution at 4°C (time of cold ischemia was <30 min). The peritoneal tissue was removed and immediately placed in a Krebs–Ringer bicarbonate solution, which was bubbled with 95% O_2–5% CO_2. The pH was adjusted to 7.4, and the solution contained (in millimoles) 117.5 NaCl, 1.15 NaH_2PO_4, 24.99 $NaHCO_3$, 5.65 KCl, 1.18 $MgSO_4$, 2.52 $CaCl_2$, and 5.55 glucose.

Pieces of the parietal peritoneum were isolated from the diaphragmatic peritoneum and visually examined for holes and adherent tissue. Precautions were taken to avoid touching the surface. Additionally, after the end of the experiments, several peritoneal samples were examined by histology to ensure the lack of perforations and holes. The peritoneum was mounted as a planar sheet separating two

acrylic Ussing-type chambers filled with Krebs–Ringer bicarbonate solution. Each Ussing-type chamber was conical in shape and connected to a glass reservoir. The overall volume including the chamber was 20 mL. The cross-sectional area of exposed tissue between the reservoirs was 1.43 cm^2. Because temperature influences the active transport of ions, measurements of transmesothelial potential differences were performed at a constant temperature of 37°C.

The transmesothelial potential difference across the parietal peritoneum was measured by means of 3 M KCl 3% agar bridges placed 3 mm on either side of the membrane and connected to Ag/AgCl electrodes. The output was amplified by a preamplifier (DVC-3; World Precision Instruments, Berlin, Germany) with an input impedance of 10^{12} Ω. In order to determine the voltage response to an external current, direct current provided by a voltage-clamp apparatus (DVC-1000; World Precision Instruments) was applied to the tissue via 3 M KCl agar bridges placed in the reservoirs connected to each hemichamber.

The voltage responses to applied currents (range: from –400 to 400 μA) were measured. The R_{TM} was calculated according to Ohm's law from the voltage deflections produced in response to constant current pulses that were applied to the tissue with the resistance of the solution being deducted (Fig. 1).

The mesothelial cell membranes facing the peritoneal fluid or the blood side in vivo will be cited as the apical or the basolateral membranes, respectively. The experimental solution bathing the apical side is denoted *serosal solution*, while the solution bathing the basolateral side is denoted *mucosal solution*.

After the addition of epinephrine in each bathing solution (mucosal and serosal consecutively), measurements were held for 30 min (on the 1st, 3rd, 5th, 10th, 15th, 20th, 25th, and the 30th min). Preliminary
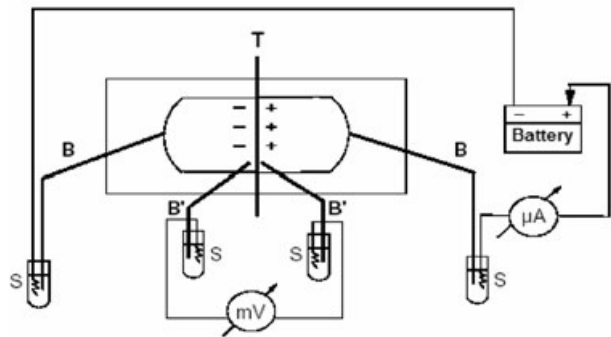

FIG. 2. Transmesothelial resistance values (R_{TM}; Ω·cm^2) of the parietal sheep peritoneum in control experiments (●) and after addition of epinephrine (10^{-7} M) to the apical side of the membrane (□). The data represent mean values and standard error ($x \pm$ SE) of six independent experiments. The * indicates $P < 0.05$ for comparison of R_{TM} after the addition of epinephrine compared with control R_{TM} values.

experiments with epinephrine were performed at various concentrations (10^{-5}–10^{-8} M). These indicated that the lowest concentration exerting an effect on the R_{TM} was 10^{-7} M. Thus, the concentration of epinephrine used was 10^{-7} M in all subsequent experiments. All solutions were freshly prepared before each experiment, equilibrated to 37°C, and continuously bubbled with a 95% O_2–5% CO_2 gas mixture.

The mean values were calculated from six independent experiments. The data were expressed as means with standard errors of mean ($x \pm$ SE). The probability of error for comparison of the mean values was calculated using the *t*-test for paired data. P values <0.05 were regarded as significant.

RESULTS

The spontaneous electrical potential difference across the parietal peritoneum was not significantly different from zero (0.5 ± 0.14 mV). The R_{TM} values of the parietal peritoneum in the control experiments and before the addition of epinephrine were 21.71 ± 0.53 Ω·cm^2.

In control experiments (n = 6), the R_{TM} remained unchanged throughout the whole 30-min observation period. The addition of epinephrine (10^{-7} M) to the apical side of the peritoneal membrane led to a significant rise of the R_{TM} within 1 min to 23.46 ± 0.45 Ω·cm^2 ($P < 0.05$). Thereafter, the R_{TM} decreased progressively but remained significantly higher than the R_{TM} values in the control experiments ($P < 0.05$)

FIG. 1. Schematic of the Ussing-type chamber. B and B′, agar bridges; M, tissue; T, silver-silver chloride electrodes.

Epinephrine on the basolateral peritoneal membrane side

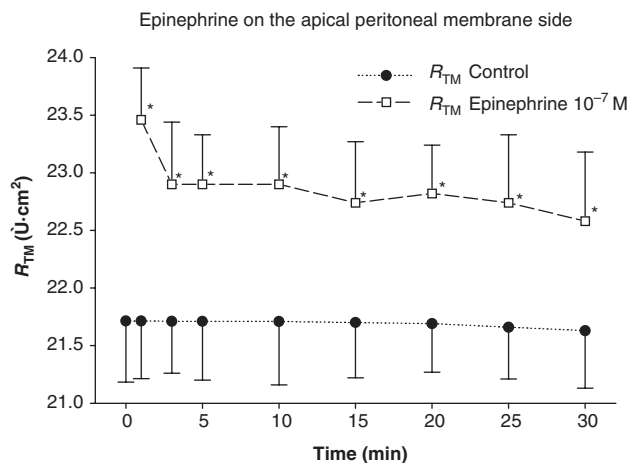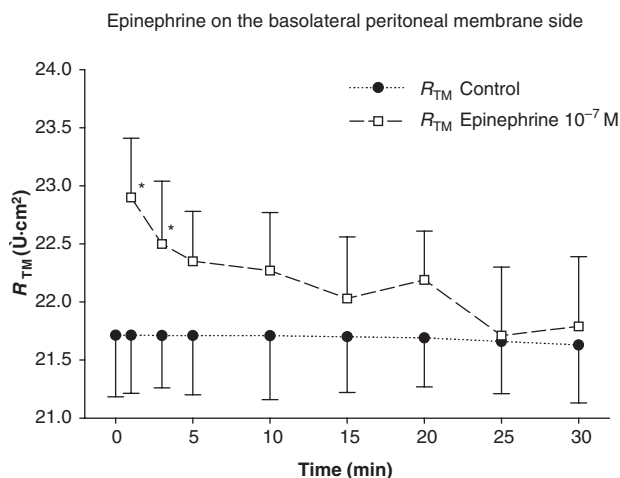**FIG. 3.** Transmesothelial resistance values (R_{TM}; $\Omega \cdot cm^2$) of the parietal sheep peritoneum in control experiments (●) and after the addition of epinephrine (10^{-7} M) to the basolateral side of the membrane (□). The data represent mean values and standard error ($x \pm SE$) of six independent experiments. The * indicates $P < 0.05$ for comparison of R_{TM} after the addition of epinephrine compared with control R_{TM} values.

throughout the chosen 30-min observation period (Fig. 2).

Similarly, after the addition of epinephrine (10^{-7} M) to the basolateral membrane side, the R_{TM} increased significantly to 22.9 ± 0.51 $\Omega \cdot cm^2$ ($P < 0.05$) within 1 min. The R_{TM} remained significantly higher compared with the R_{TM} value in the control experiment for 3 min ($P < 0.05$) and decreased thereafter progressively until it reached control values by the end of the experiments at 30 min (Fig. 3).

The resistance values measured after the addition of epinephrine were slightly different depending on the side of epinephrine administration (Figs. 2 and 3). However, these differences did not reach statistical significance ($P > 0.05$).

DISCUSSION

Our data indicate that across the parietal sheep peritoneum, there is no measurable spontaneous potential difference and that its ohmic resistance is very low. The R_{TM} values (21.71 ± 0.53 $\Omega \cdot cm^2$) determined are comparable to the ones previously reported for "leaky" epithelial tissues such as the proximal renal tubuli and the sheep pleura (13).

The ohmic resistance values of the parietal sheep peritoneum (R_{TM}) increased significantly within 1 min after the incubation with epinephrine at 10^{-7} M. This observation indicates the existence of an adrenergic influence on the ionic permeability of the peritoneal membrane, which becomes less perme-

able to ionic currents through the action of epinephrine. Similar data were obtained with isolated sheep pleura incubated with epinephrine (data not shown). The concentration of epinephrine at 10^{-7} M used in the present study is far below the one chosen in previous studies dealing with the adrenergic effects on epithelia, that is, 10^{-6}–5×10^{-5} M. We selected this epinephrine concentration because it is the lowest to exhibit an effect on the R_{TM} value. The epinephrine concentration of 10^{-7} M is close to blood levels observed in vivo during biologically stressful conditions (15). Furthermore, in patients on peritoneal dialysis, catecholamine levels are known to be significantly elevated compared with those in healthy controls (16).

The most likely physiological explanation for the R_{TM} elevation is an inhibition of the Na transport across the peritoneal mesothelium. In previous studies, adrenergic stimulation was found to either inhibit or stimulate Na transport. Active Na transport inhibition was observed as a consequence of epinephrine incubation in rat cortical collecting ducts (8) and with canine tracheal epithelium in vitro (6). Adrenergic stimulation of the Na transport was found in rabbit hydrothoraces (15), human tracheas (17,18), alveoli (19), mature fetal lungs of sheep (20,21), and rat alveolar epithelium in vivo (22).

The addition of epinephrine increased the R_{TM} of the parietal peritoneum within 1 min. The velocity of this increase indicates that the effect is mediated by adrenergic receptors. Notably, the changes in R_{TM} induced by the addition of epinephrine on the apical side of the parietal peritoneum were prolonged when compared to its influence on the basolateral side. This finding could be due to differences in the number of adrenergic receptors on both sides and the receptor subtype composition. However, data on this particular matter are still lacking in the literature.

Our results would lend support to the notion that infusion of epinephrine in patients on peritoneal dialysis leads to decreased peritoneal Na transport. However, apart from this direct action on the peritoneal mesothelium, intravenous epinephrine administration also results in constriction of mesenteric arteries. The resultant alteration of the mesenteric blood flow most likely favors a further decrease of peritoneal solute permeability. In line with this hypothesis, intravenous vasopressor doses of norepinephrine have been shown to reduce peritoneal clearances of creatinine and urea in rabbits (23).

In conclusion, our findings indicate that epinephrine exerts a rapid effect on the ionic permeability of the parietal peritoneum. The effect of epinephrine on the apical side of the mesothelial membrane is more

prolonged than that on the basolateral side. Therefore, the mechanisms of peritoneal ion transport are different from a "simple" passive transport. Future studies may confirm their significance for outcome of peritoneal dialysis treatment.

REFERENCES

1. Gotloib L, Shostak A. The functional anatomy of the peritoneum as a dialyzing membrane. In: Twardowski ZL, eds. *Peritoneal Dialysis. New Concepts and Application.* New York: Churchill Livingstone, 1990;1–27.
2. Krediet RT. The peritoneal membrane in chronic peritoneal dialysis. *Kidney Int* 1999;55:341–56.
3. Davies SJ, Phillips L, Griffiths AM, et al. What really happens to people on long-term peritoneal dialysis? *Kidney Int* 1998;54:2207–17.
4. Ussing HH, Zerahn K. Active transport of sodium as the source of electric current in the short-circuited isolated frog skin. *Acta Physiol Scand* 1951;23:110–27.
5. Ussing HH, Zerahn K. Active transport of sodium as the source of electric current in the short-circuited isolated frog skin. Reprinted from *Acta Physiol Scand* 1951;23:110–27. *J Am Soc Nephrol* 1999;10:2056–65.
6. Sugahara K, Kiyota T, Baba T, Nakamura M, Morioka T. Effects of autonomic agents and chemical mediators on ion transport by canine tracheal epithelium. *Jpn J Physiol* 1989;39:421–8.
7. Koefoed-Johnsen V, Ussing HH, Zerahn K. The origin of the short-circuit current in the adrenaline stimulated frog skin. *Acta Physiol Scand* 1952;27:38–48.
8. Hawk CT, Kudo LH, Rouch AJ, Schafer JA. Inhibition by epinephrine of AVP- and cAMP-stimulated Na^+ and water transport in Dahl rat CCD. *Am J Physiol* 1993;265:F449–60.
9. Li FK, To CH, Leung JK, Chan TM, Lai KN. Electrophysiology and glucose transport of human peritoneal mesothelial cells: implications for peritoneal dialysis. *Perit Dial Int* 2001;21:115–21.
10. Simon M. Peritoneal mesothelium in vitro: an electrophysiologic study. *Perit Dial Int* 1996;16:393–7.
11. Szary B, Czyzewska K. Diffusive permeability of rabbit peritoneum for small solutes in vitro: effect of gentamicin and insulin. *Int J Artif Organs* 2002;25:290–6.
12. Hatzoglou C, Gourgoulianis KI, Hatzoglou A, Castanas E, Molyvdas PA. Rapid effects of 17 beta-estradiol and progesterone on sheep visceral and parietal pleurae via a nitric oxide pathway. *J Appl Physiol* 2002;93:752–8.
13. Hatzoglou CH, Gourgoulianis KI, Molyvdas PA. Effects of SNP, ouabain, and amiloride on electrical potential profile of isolated sheep pleura. *J Appl Physiol* 2001;90:1565–9.
14. Sarkos S, Hatzoglou C, Dahabre J, Gourgoulianis KI, Molyvdas PA. Effect of amiloride in human and sheep parietal pleura. *Respir Physiol Neurobiol* 2002;132:233–7.
15. Zocchi L, Raffaini A, Agostoni E. Effect of adrenaline and alpha-agonists on net rate of liquid absorption from the pleural space of rabbits. *Exp Physiol* 1997;82:507–20.
16. Zabetakis PM, Kumar DN, Gleim GW, et al. Increased levels of plasma renin, aldosterone, catecholamines and vasopressin in chronic ambulatory peritoneal dialysis (CAPD) patients. *Clin Nephrol* 1987;28:147–51.
17. Liedtke CM. The role of protein kinase C in alpha-adrenergic regulation of NaCl(K) cotransport in human airway epithelial cells. *Am J Physiol* 1995;268:L414–23.
18. Liedtke CM. Alpha-adrenergic regulation of NaCl cotransport in human airway epithelium. *Am J Physiol* 1989;257:L125–9.
19. Berthiaume Y, Staub NC, Matthay MA. Beta-adrenergic agonists increase lung liquid clearance in anesthetized sheep. *J Clin Invest* 1987;79:335–43.
20. Brown MJ, Olver RE, Ramsden CA, Strang LB, Walters DV. Effects of adrenaline and of spontaneous labour on the secretion and absorption of lung liquid in the fetal lamb. *J Physiol* 1983;344:137–52.
21. Barker PM, Brown MJ, Ramsden CA, Strang LB, Walters DV. The effect of thyroidectomy in the fetal sheep on lung liquid reabsorption induced by adrenaline or cyclic AMP. *J Physiol* 1988;407:373–83.
22. Pittet JF, Wiener-Kronish JP, McElroy MC, Folkesson HG, Matthay MA. Stimulation of lung epithelial liquid clearance by endogenous release of catecholamines in septic shock in anesthetized rats. *J Clin Invest* 1994;94:663–71.
23. Hirszel P, Lasrich M, Maher JF. Divergent effects of catecholamines on peritoneal mass transport. *Trans Am Soc Artif Intern Organs* 1979;25:110–3.

ELSEVIER

Biological performances of collagen-based scaffolds for vascular tissue engineering

F. Boccafoschi[a,b], J. Habermehl[a], S. Vesentini[c], D. Mantovani[a,*]

[a]*Laboratory for Biomaterials and Bioengineering, Laval University, Québec City, G1K 7P4, Canada*
[b]*Human Anatomy Laboratory, Research Center for Biocompatibility, University of Eastern Piedmont "A. Avogadro", Novara, Italy*
[c]*Department of Bioengineering, Politecnico of Milan, Italy*

Abstract

Collagen is widely used for biomedical applications and it could represent a valid alternative scaffold material for vascular tissue engineering. In this work, reconstituted collagen films were prepared from neutralized acid-soluble solutions for subsequent haemocompatibility and cell viability performance assays. First, haemoglobin-free, thrombelastography and platelet adhesion tests were performed in order to investigate the blood contact performance. Secondly, specimens were seeded with endothelial cells and smooth muscle cells, and cell viability tests were carried out by MTT and SEM. Results show that neutralized acid-soluble type I collagen films do not enhance blood coagulation, do not alter normal viscoelastic properties of blood and slightly activate platelet adhesion and aggregation. Cell culture shows that the samples are adequate substrates to support the adhesion and proliferation of endothelial and smooth muscle cells.

Keywords: Collagen; Blood compatibility; Endothelial cells; Smooth muscle cells; Platelet adhesion

1. Introduction

According to the World Health Report (2003), 16.7 million people around the globe die of cardiovascular diseases each year, nearly one-third of total global deaths [1]. Cardiovascular diseases are often caused by atherosclerosis, which could lead to evolutive arterial diseases like thrombosis and aneurysms [2]. When the substitution of a diseased vessel is necessary, artificial prostheses, made of natural or synthetic material, are therefore required. Different materials are currently used as synthetic vascular substitutes; for instance, Teflon is used for prostheses of medium diameter (around 6 mm) vessels [3]. However, no biomaterial has yet shown satisfactory performances when in contact with blood for long time periods. This leads to clinical complications, such as aneurysms, thrombosis or restenosis [4,5]. Moreover, no appropriate biomaterial has yet been developed for small diameter vessel replacement.

Tissue engineering has already shown a strong potential for regenerating and repairing chronic wounds [6], burns [7] and, at the experimental level, cartilage defects [8] and represents a promising field in vascular reconstruction. The overall goal of vascular tissue engineering is to obtain the same mechanical and biological properties as a native vessel. Different approaches have been taken using collagen as a main scaffold constituent. In 1986, Weinberg and Bell [9] performed their groundbreaking study using a scaffold based on collagen for blood vessel reconstruction. They used an in vitro model generated using multiple layers of collagen integrated with a Dacron mesh to provide the necessary tensile strength. Smooth muscle cells were cultured in the graft and endothelial cells were used to line the inner lumen. Various polymeric materials have

*Corresponding author. Tel.: +418 656 2131 #6270; fax: +418 656 5343.

E-mail address: diego.mantovani@gmn.ulaval.ca (D. Mantovani).

also been used for mechanical support in addition to collagen such as PGA and PLGA. Moreover, cells have been grown under dynamic conditions in particular bioreactors to closely mimic in vivo conditions [10]. Research has also been done using decellularized vein as a potential scaffold for vascular tissue engineering. This process preserves the extracellular matrix, the basement membrane structure and sufficient strength for vascular grafting [11]. It is clear that collagen plays a crucial role in all these studies, and that it could represent a suitable candidate to scaffold tissue regeneration.

Finally, collagen is one of the main proteins forming the vascular extracellular matrix. It is primarily produced by the smooth muscle cells of the media and the fibroblasts of the adventitia. Functionally, collagen fibres impose constraints on the elongation of large vessels under pressure, limiting the distension of the vessel. It also provides attachment to smooth muscle cells, transmitting force around the circumference of the vessel [12]. Collagen has low antigenicity, low inflammatory and cytotoxic responses [13] and is also biodegradable [14]. However, there exists a lack of knowledge about the biological performance of collagen-based scaffolds when in contact with blood and cells. Therefore, the aim of this work was to investigate neutralized collagens' impact when in contact with blood and cells.

2. Materials and method

2.1. Sample preparation

Specimens consist of flat sheets of collagen type I, which was extracted from rat tail collagen. Briefly, rat tail tendons were dissolved in acetic acid for 48 h; then the gel-like mass was mixed in a blender, frozen and lyophilized. The lyophilized sponge was mixed again with 0.02 N acetic acid at a dry weight to a solution ratio of 4 mg/ml. The resulting solution was centrifuged, degassed in vacuum and sterilized. Sterilization was performed in dialysis bags (Spectra/Por 1, MWCO:6–8000, Spectrum Laboratories Inc., California, USA) and soaked in 0.02 N acetic acid for 1 h followed by 1 h in 1% chloroform in water. Dialysis was continued in 0.02 N sterile acetic acid for 4–5 days. The resulting sterile solution was neutralized to a pH of 6.8 with 1% NaOH immediately prior to use. Samples were prepared in the form of thin films by solvent evaporation from neutral collagen solutions poured onto glass coverslips.

2.2. Blood performances

2.2.1. Reference materials

Teflon, which is a commonly employed material for vascular prostheses [15], was used as a reference material for clotting time measurement and thrombelastography. Glass, although not used for surgical purposes but due to its negative reaction when in contact with blood [16], was considered as a negative control.

2.3. Blood

Native whole blood was collected from 11 healthy male donors having taken no medication for at least 10 days prior to donation. 40 ml of blood, collected in tubes containing sodium citrate, was used for thrombelastograph assays and platelet extraction. 10 ml of blood without anticoagulants was used for clotting time assessment.

2.4. Clotting time

The haemoglobin free method for clotting time measurement is described elsewhere [17]. Briefly, 0.1 ml of untreated blood was immediately dropped onto the specimens. After 10, 20, 30, 40 and 50 min, 5 ml of distilled water was added to each specimen and incubated for 5 min. Red blood cells not entrapped in a thrombus were haemolysed and free haemoglobin molecules in the water were colorimetrically measured by monitoring the absorbance at 570 nm using a spectrophotometer ELISA reader (BioRad mod.450, Mississauga, Ontario, Canada). Absorbance values were converted into a percentage of the maximum amount of free haemoglobin present in the water. Statistical significance was determined by the Student's *t*-test.

2.5. Thrombelastograph (TEG)

Blood (400 μl) was exposed to the surface of collagen and controls for 30 min at 37 °C. Then, 300 μl of this blood was placed in TEG stainless-steel cups and 60 μl of 1.29% isotonic $CaCl_2$ solution were added for recalcification. TEG traces were obtained with a Thrombelastograph D (Hellige GMBH, Germany) and analyses were conducted following manufacturer's instructions. Briefly, the cylindrical cup containing blood oscillates through an angle of 4°45′ and is heated to a temperature of 37 °C. Each rotation cycle of the cup lasts 10 s. A stainless-steel cylindrical piston is suspended from a torsion wire and immersed in the cup. The torque of the cup is transmitted to the piston through the fibrin fibres that gradually form between the piston and the wall of the cup; the rotation of the piston becomes increasingly stronger as the clot becomes more solid.

Thrombelastography measures the elastic properties of blood clots as they form. The strength of the clot is graphically represented over time as a characteristic cigar-shaped figure. There are three main parameters of the TEG trace which are used in this study: *r*, *k* and MA. The time for the initial fibrin formation is given by *r*. The time from the beginning of clot formation until 20 mm of amplitude (*k*) is characteristic of the dynamics of clot formation. The maximum amplitude (MA) represents the strength of the clot, which is dependent on the number and function of platelets and their interaction with fibrin [18]. Combining *k* and MA leads to the thrombogenicity index. Statistical significance was determined by the Student's *t*-test.

2.6. Platelet adhesion

In vitro testing was performed to investigate the morphology, aggregation and pseudopodium of the adherent platelets.

After centrifuging, platelet-rich plasma was obtained and a suspension of 3×10^5 platelets was placed on the samples and incubated for 30 min at 37 °C. Samples were then prepared for SEM analysis as described later. Images are representative of all results obtained.

2.7. Biological performances

2.7.1. Cell culture

Endothelial cells and smooth muscle cells were isolated from porcine aorta as described elsewhere [19,20]. Briefly, after removing the external adventitia, the aorta was incubated for 25 min at 37 °C with collagenase type IA 130 U/ml (Gibco, Invitrogen Corporation, Burlington, Ontario, Canada). Endothelial cells were isolated and seeded on Petri dishes coated with 0.2% porcine gelatine. DMEM growth medium was supplemented with 10% porcine serum, glutamine (2 mM), penicillin (100 U/ml), streptomycin (100 μg/ml), fungizone (0.25 μg/ml) and heparin (0.09 g/l) (all from Sigma Aldrich, Milwaukee, USA). As already reported in the literature, a fluorescent die labelling acetylated low-density lipoprotein (Dil-Ac-LDL, Biomedical Technologies Inc., Stoughton, Massachusetts, USA) was used to confirm the sole presence of endothelial cells [21].

Following the first digestion, the aorta was incubated overnight with collagenase type II 270 U/ml (Worthington Biochemical Corporation, Lakewood, New Jersey, USA). Smooth muscle cells were subsequently extracted and seeded in tissue-culture flasks coated with porcine gelatine 0.2%. DMEM growth medium was supplemented with 15% porcine serum, 10% foetal bovine serum, glutamine (2 mM), penicillin (100 U/ml), streptomycin (100 μg/ml) and fungizone (0.25 μg/ ml) (all from Sigma Aldrich, Milwaukee, USA). Positive staining using an anti α-smooth muscle actin-specific antibody was used to confirm the smooth muscle phenotype of the extracted cells (Boehringer Mannheim, Mannheim, Germany) [22].

Cells were maintained at 37 °C in 5% CO_2-humified atmosphere and harvested by trypsinization when a monolayer was reached. All experiments were performed using cells between the 4th and 8th passage and 2×10^5 cells were seeded on each sample. Cells used as controls were seeded on Petri dishes or cover slides previously treated with porcine gelatine 0.2% (Sigma Aldrich, Milwaukee, USA).

2.8. Scanning electron microscopy (SEM)

Cell morphology after adhesion and growth on collagen was investigated by SEM. The medium was removed, samples were washed twice in 0.15 M cacodylate buffer and fixed for 30 min at 4 °C with Karnowsky solution (2% paraformaldehyde and 2.5% glutaraldehyde in 0.15 M cacodylate buffer, pH 7.2–7.4). Following fixation, samples were treated for 30 min with 1% osmium tetroxide in 0.15 M cacodylate buffer solution. Samples were then dehydrated with graded ethanol (from 50% to 100%), soaked for 30 min in hexamethyldisilazane, dried and sputter-coated with gold–palladium. Images were collected using an SEM (JSM-35CF, JEOL, Tokyo, Japan).

2.9. Cytotoxicity assay

After three growth periods (24, 48 and 72 h) the cell viability was assessed using the MTT colorimetric assay (Sigma Chemical Co., St. Louis, MO). Briefly, [3-(4, 5 dimethylthiazol-2-yl)-2, 5-diphenyl-2*H*-tetrazolium bromide] (MTT) is reduced to purple formazan by mitochondrial dehydrogenase in cells indicating normal metabolism. After each time point, MTT (1 mg/ml in PBS) was added to the medium (1:10) and samples were further incubated for 4 h. The medium was removed and purple formazan crystals were solubilized with 200 μl acidic isopropanol (0.04 M HCl in isopropanol) at room temperature. The optical density at a wavelength of 570 nm was determined using an ELISA reader (BioRad mod.450, Mississauga, Ontario, Canada). All tests were performed in triplicate. Results are expressed as mean ± standard deviation. Statistical significance was determined by the Student's *t*-test.

3. Results

3.1. Clotting time

During clot formation, the quantity of haemoglobin entrapped by fibrin increases with time as the clot forms. Therefore, the amount of free haemoglobin available for haemolysis decreases. This can be used as a significant indicator for evaluating the potential of a substrate to not induce immediate clotting. In fact, the longer the clotting time, the better the compatibility between the substrate and blood. The blood clotting profiles for collagen, Teflon and glass are presented in Fig. 1. As collagen consistently failed to initiate fibrin clotting after 10 min, the maximum absorbance value was taken as 100% for comparison purposes. The clot formation was found to be complete at approximately 25%.

Results show significant differences between collagen and Teflon after 20 min of contact. In fact, free haemoglobin in water remains higher for collagen until 50 min after contact, at which time the clot is completely formed. Teflon forms a stable clot 20 min after contact. Glass, as expected, forms a stable clot within the first 10 min after contact.

3.1.1. Fibrin formation

The parameter *r* obtained from the thrombelastograph profile indicates the time, in minutes, from the beginning of the test to initial fibrin formation. Fibrin formation times are shown in Fig. 2. In this respect, blood in contact with collagen behaves identically to that of blood having had no contact with control surfaces. Teflon and glass initiate coagulation significantly faster than collagen.

3.2. Thrombogenicity index

The thrombogenicity index informs about the dynamics of blood coagulation as well as the strength of
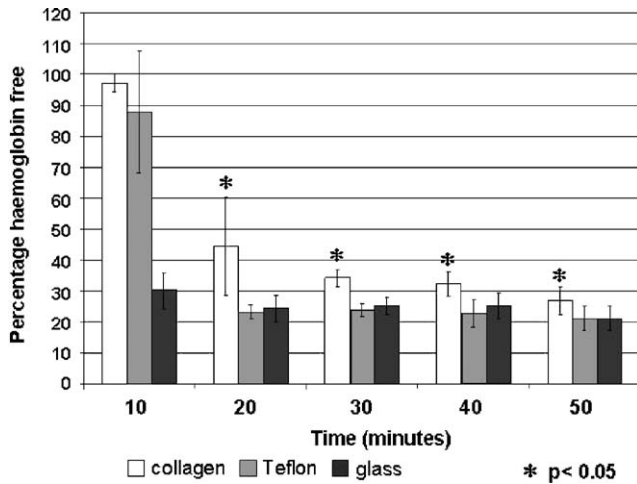
Fig. 1. Haemoglobin free test on collagen, Teflon and glass. * indicates that results of collagen with respect to both reference materials are statistically significant.
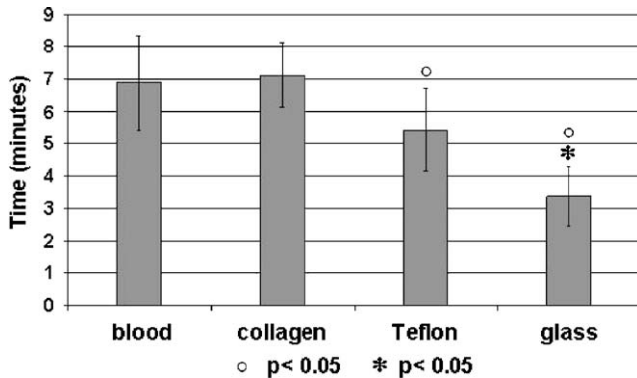

Fig. 2. Fibrin formation. * indicates statistically significant results with respect to blood. ° indicates statistically significant results with respect to collagen.
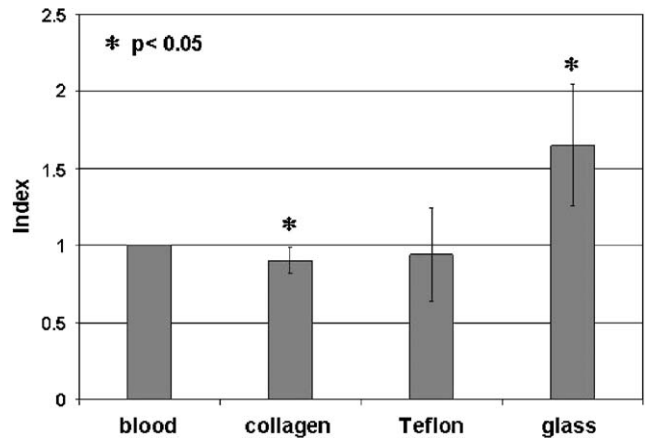

Fig. 3. Thrombogenicity index. * indicates that results are statically significant with respect to ones obtained for blood.

completely free of platelets (data not shown). Figs. 4b and c show platelet morphologies after adhesion to collagen. In Fig. 4b cells express a rounded morphology with no pseudopodium. Small aggregates were also observed on the surface, and they are shown in Fig. 4c. It is interesting to note that large aggregates as well as long pseudopodia are entirely absent, showing low activation.

3.4. Cell morphology

As observed by SEM, endothelial cells (Fig. 5a) and smooth muscle cells (Fig. 5b) were well attached and spread after 24 h. Both cell types exhibited solid and numerous focal contacts to the collagen substrate. The cobblestone morphology, typical of endothelial cells, as well as the spindle morphology of smooth muscle cells, are well-defined. After 72 h of proliferation on collagen, a complete monolayer was reached for both cell types (data not shown).

3.5. Cytotoxicity assay

MTT results obtained with endothelial cells and smooth muscle cells seeded on collagen film are presented in Fig. 6a and b , respectively. Endothelial cells are proliferating, as demonstrated by the increased absorbance with time. However, cell growth is significantly slower on collagen than on controls. Smooth muscle cells, on the other hand, exhibit significantly lower proliferation than on the control after 72 h, once a complete monolayer has been formed.

the final clot. This index is significantly lower for blood after contact with collagen, thus showing that platelets and fibrin weakly interact in blood after contact with collagen. The index for Teflon displays a similar trend but it is highly affected by inter-donor variability, and therefore the variance is important. Glass shows strong and stable clot formation, which indicates activation of the coagulation cascade (Fig. 3).

3.3. Platelet adhesion

Although SEM does not allow quantification of adhered platelets, it is possible to visually compare surfaces after platelet adhesion and gain insight into platelet activation and aggregation. A SEM image of a representative zone of the highest platelet density for collagen is shown in Fig. 4a. It is important to note that platelets adhere in a non-homogeneous way on collagen substrates, and several parts of the specimens were

4. Discussion

It is well known that, in native blood vessels, the endothelium possesses natural anticoagulant and
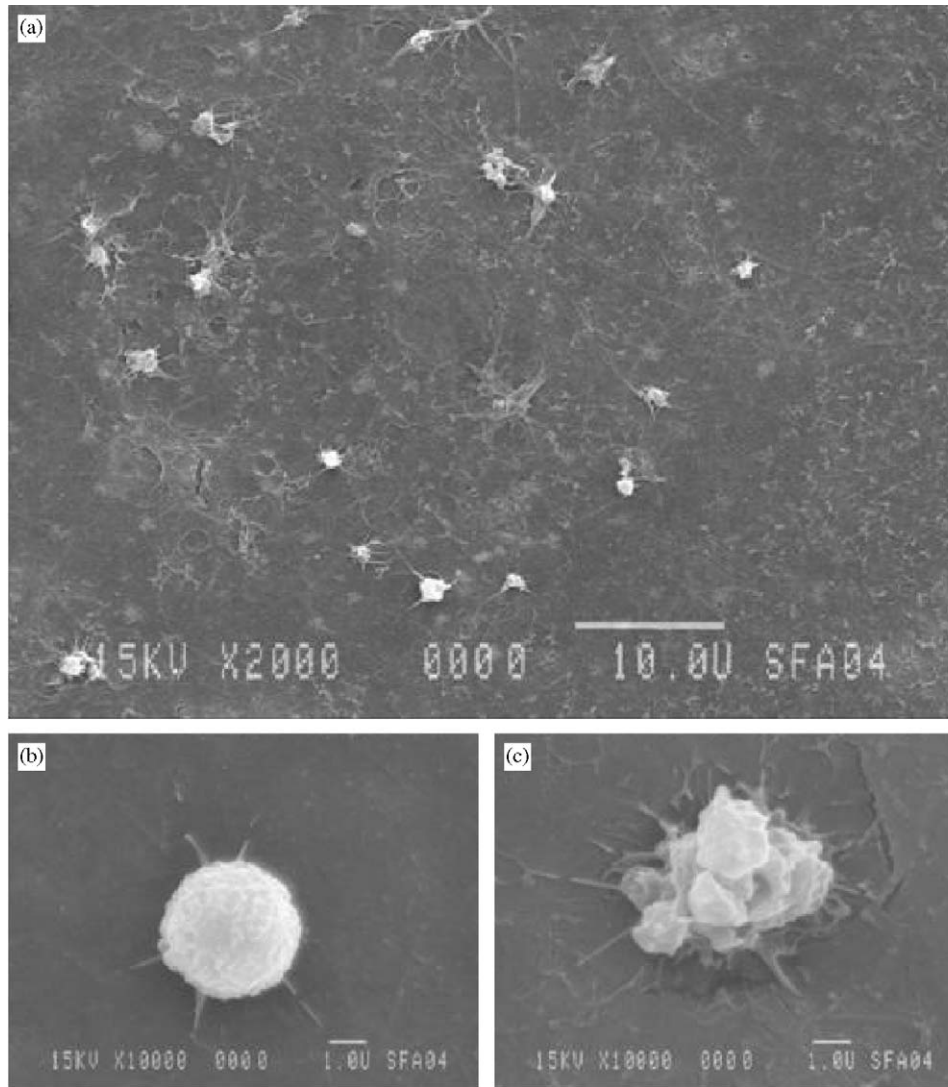
Fig. 4. (a)–(c) SEM analyses of platelets on collagen film.

antithrombotic properties [23]. One of the major downfalls of prosthetic vascular grafts is the inability to obtain a confluent endothelium on the luminal surface. To improve antithrombotic performances of vascular replacements, tissue-engineering attempts to mimic as close as possible the behaviour of a native vessel. A successful tissue-engineered arterial replacement, apart from adequate mechanical properties, requires two fundamental biological qualities: thromboresistance and adequate cell presence and functionality. In this study we investigated blood–material and cell–material interactions in order to evaluate the potential of an acid-soluble type I collagen from rat tail tendon to be considered as a natural scaffold for vascular regeneration. Teflon, due to its current satisfactory use for medium diameter vascular prostheses, and due to its demonstrated low capacity for platelet activation compared to other polymeric prosthetic materials, was considered as a positive control [24].

Thrombelastography is the only test that evaluates the entire dynamics of clot formation. By measuring the viscoelastic properties of blood that characterize the strength of the clot over time, it gives information about several steps in the coagulation process. An important indicator of coagulant activity is the parameter r, which indicates the time required for fibrin formation. Blood having had no contact with control materials has a variability between 5 and 8 min for the initiation of fibrin formation. This variability does not allow to conclude that significant differences in fibrin formation time exist when compared with collagen and Teflon. However, it is notable that collagen has an r value significantly higher than Teflon, with a small variability indicating constant positive performances. Glass, in terms of fibrin formation, enhances clot formation in a shorter time when compared to all other materials. The thrombogenicity index takes into account the dynamics
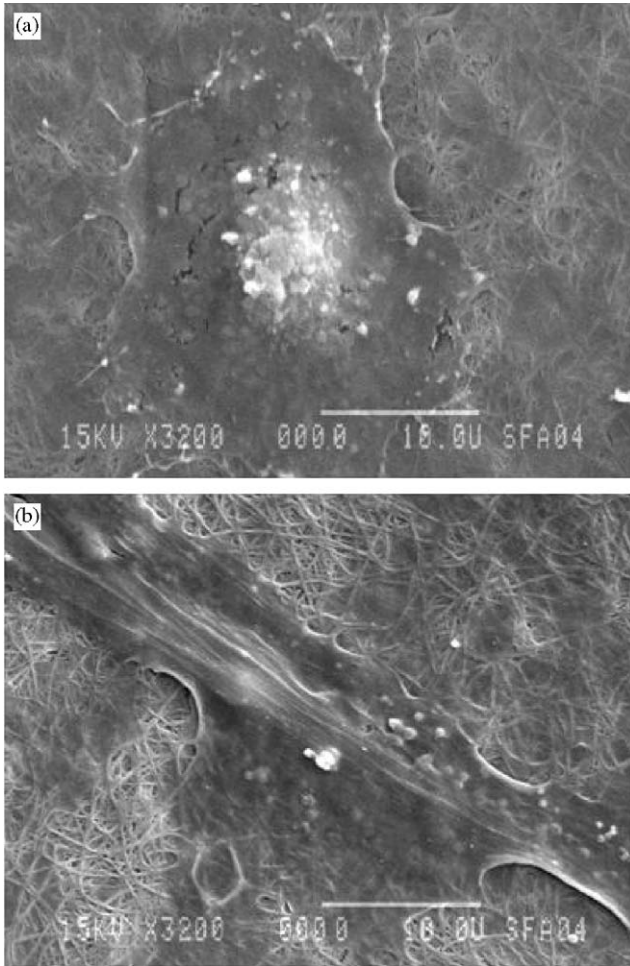
Fig. 5. SEM analyses of (a) endothelial cell and (b) smooth muscle cell morphology after 24 h of contact with collagen films.

Fig. 6. MTT results on (a) endothelial cells and (b) smooth muscle cells. * indicates significant results with respect to control.

of clot formation as well as the strength of the interactions between platelets and fibrin. A low index indicates a low thrombogenic potential. This is the case for blood after contact with collagen, which demonstrates a weak interaction between platelets and fibrin, meaning that platelets are not activated to enhance the coagulation cascade. As with fibrin formation time, the low standard deviation indicates that all assays with collagen have the same trend. Clotting time, measured by the haemoglobin free test, confirms that collagen is less efficient than Teflon in enhancing clot formation. Moreover, morphological analyses show a low percentage of platelet adhesion and the absence of aggregates, proving that good performances obtained concerning blood reactions are due to the modest activation of platelets on collagen.

Collagen in the body is a natural coagulant and plays an important role in haemostasis and thrombogenesis [25]. However, in this study, neutral collagen films have demonstrated good performances in not enhancing clo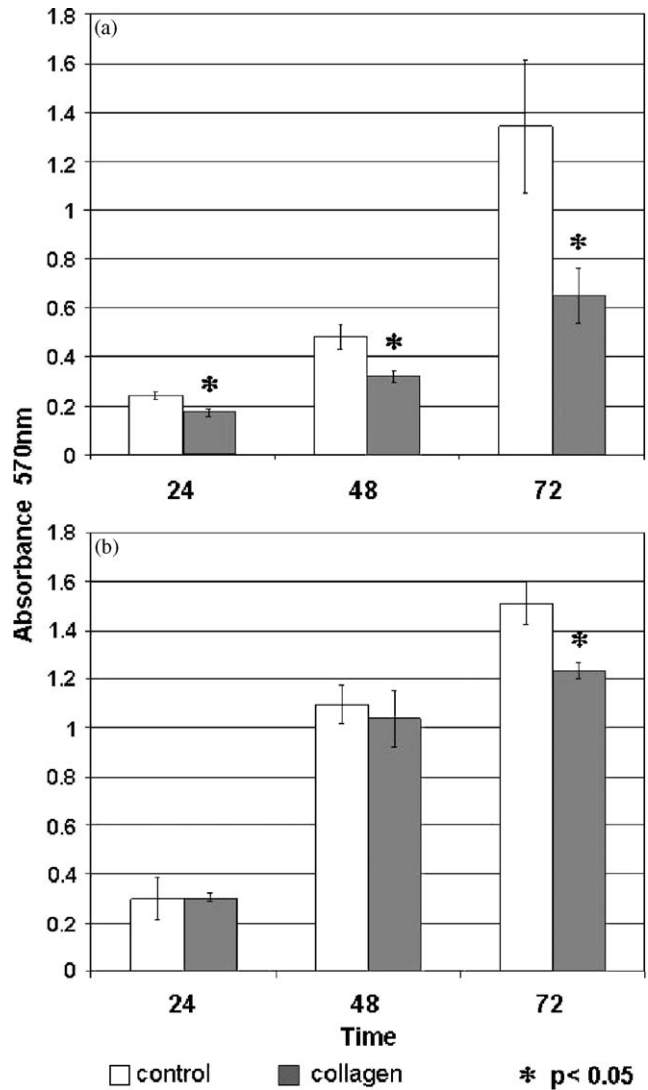t formation. This discrepancy might be due to the structure of the collagen substrate and the absence of the von Willebrand factor. In fact, it has been shown that different collagen preparations vary in their ability to aggregate platelets and support their adhesion. Fibrillar collagen is much more potent in inducing platelet activation than the same collagen type in acid-soluble form [26]. It was concluded that the quaternary structure of collagen is important in inducing platelet activation [25]. Although structural aspects of fibrils mediate platelet adhesion and aggregation, biochemical factors may also play a dominating role. Recently, the von Willebrand factor, which constitutes a major difference between acid-soluble and fibrillar collagen, acts synergistically with collagen fibrils in the activation of the coagulation cascade [27]. This protein, not present in acid-soluble collagen, has been purposed as the main mediator for the initial capture of platelets to the site of vascular injury [28]. An enzymatic test (Asserachrom

vWF; Boehringer-Mannheim, Mannheim, Germany) was performed (data not shown) to insure that our acid-soluble collagen was absolutely free of the von Willebrand factor. In fact, it is widely known that the first step in platelet–collagen interactions is the binding of platelet glycoprotein Ib (GPIb) to the von Willebrand factor. Only subsequently will platelets adhere to collagen with specific cell surface receptors [29]. It has also been reported that an enhanced level of the von Willebrand factor increases platelet adhesion and aggregation on collagen surfaces [30]. This may explain why collagen, which naturally has exceptional haemostatic properties, in this particular context, does not enhance the activation of the coagulation cascade.

The use of collagen as a substrate for endothelial and smooth muscle cells is not an innovative strategy [31,32]. However, we considered this test with the aim to prove that acid-soluble collagen, extracted from rat tails followed by lyophilization, constitutes an acceptable substrate for cell growth. We previously performed preliminary tests demonstrating the adequate biological performance of the substrate for fibroblasts (data not shown). This study continues in this direction using two primary cell lines, which will potentially be used for vascular regeneration. Morphological analyses show good cell spreading and, even if cell growth is slightly slower than on the control, cells are proliferating on the surface. A possible explanation for this difference in the dynamics of cell growth could be due to the different stimuli induced by collagen on cellular metabolism, which may increase extracellular matrix production at the expense of proliferation. Moreover, the good performances shown by this collagen solution as a substrate for various cell cultures allows us to speculate as to its suitability for different tissue engineering applications, involving, for example, myocytes or hepatocytes and eventually growth in a three-dimensional environment.

The results obtained indicate that collagen films present low thrombogenicity and that they support cell spreading. Therefore, this could be promising and this type of collagen can represent an adequate substrate to successfully scaffold vascular tissue during regeneration or engineering.

Acknowledgements

References

[1] World Health Organization. World Health Report. 2003.

[2] Ross R. Atherosclerosis—An inflammatory disease. New Engl J Med 1999;340:115–26.

[3] Xue L, Greisler HP. Biomaterials in the development and future of vascular grafts. J Vasc Surg 2003;37:472–80.

[4] Callow AD. Problems in the construction of a small diameter graft. Int Angiol 1988;7:246–53.

[5] Bruck SD. Problems and challenges of biomaterials in cardiovascular applications: A status report. Biomater Med Devices Artif Organs 1983–84;11:271–80.

[6] Naughton GK, Mansbridge JN. Human-based tissue-engineered implants for plastic and reconstructive surgery. Clin Plast Surg 1999;26:579–86.

[7] Kopp J, Jeschke MG, Bach AD, Kneser U, Horch RE. Applied tissue engineering in the closure of severe burns and chronic wounds using cultured human autologous keratinocytes in a natural fibrin matrix. Cell Tissue Bank 2004;5:81–7.

[8] Angele P, Abke J, Kujat R, Faltermeier H, Schumann D, Nerlich M, Kinner B, Englert C, Ruszczak Z, Mehrl R, Mueller R. Influence of different collagen species on physico–chemical properties of crosslinked collagen matrices. Biomaterials 2004; 25:2831–41.

[9] Weinberg CB, Bell E. A blood vessel model constructed from collagen and cultured vascular cells. Science 1986;231:397–400.

[10] Niklason LE, Langer RS. Advances in tissue engineering of blood vessels and other tissues. Transplant Immunol 1997;5:303–6.

[11] Schaner PJ, Martin ND, Tulenko TN, Shapiro IM, Tarola NA, Leichter RF, Carabasi RA, DiMuzio PJ. Decellularized vein as a potential scaffold for vascular tissue engineering. J Vasc Surg 2004;40:146–53.

[12] Bou-Gharios G, Ponticos M, Rajkumar V, Abraham D. Extracellular matrix in vascular networks. Cell Prolif 2004;37:207–20.

[13] Nicolas FL, Gagnieu CH. Denatured thiolated collagen II. Crosslinking by oxidation. Biomaterials 1997;18:815–21.

[14] Goissis G, Marcantonio EJ, Marcantonio RA, Lia RC, Cancian DC, de Carvalho WM. Biocompatibility studies of anionic collagen membranes with different degree of glutaraldehyde cross-linking. Biomaterials 1999;20:27–34.

[15] Bos GW, Poot AA, Beugeling T, van Aken WG, Feijen J. Small-diameter vascular graft prostheses: current status. Arch Physiol Biochem 1998;106:100–15.

[16] Umemura Y, Huskey RA, Anderson JM. Human platelet interactions with surfaces of type I collagen, chondroitin-4-sulphate, and chondroitin-6-sulphate in vitro. Biomaterials 1988; 9:133–7.

[17] Huang N, Yang P, Leng YX, Chen JY, Sun H, Wang J, Wang GJ, Ding PD, Xi TF, Leng Y. Hemocompatibility of titanium oxide films. Biomaterials 2003;24:2177–87.

[18] Vig S, Chitolie A, Bevan DH, Halliday A, Dormandy J. Thromboelastography: A reliable test? Blood Coagulat Fibrinolys 2001;12:555–61.

[19] Carrillo A, Chamorro S, Rogríguez-Gago M, Álvarez B, Molina MJ, Rodríguez-Barbosa JI, Sanchez A, Ramírez P, Muñoz A, Domínguez J, Parrilla P, Yélamos J. Isolation and characterization of immortalized porcine aortic endothelial cell lines. Vet Immunol Immunopathol 2002;89:91–8.

[20] Varela O, Martínez-Gonzalez J, Badimon L. The response of smooth muscle cells to a-thrombin depends on its arterial origin: Comparison among different species. Eur J Clin Investig 1998;28:313–23.

[21] Voyta JC, Via DP, Butterfield CE, Zetter BR. Identification and isolation of endothelial cells based on their increased uptake of acetylated-low density lipoprotein. J Cell Biol 1984;99:2034–40.

[22] Skalli O, Ropraz P, Trzeciak A, Benzonana G, Gillessen D, Gabbiani G. A monoclonal antibody against a-smooth muscle actin: a new probe for smooth muscle differentiation. J Cell Biol 1986;103:2787–96.

[23] Michiels C. Endothelial cell functions. J Cell Physiol 2003; 196:430–43.

[24] Kottke-Marchant K, Anderson JM, Rabinovitch A. The platelet reactivity of vascular graft prostheses: an in vitro model to test the effect of preclotting. Biomaterials 1986;7:441–8.

[25] Kawamoto Y, Kaibara M. Procoagulant activity of collagen. Effect of difference in type and structure of collagen. Biochim Biophys Acta 1990;1035:361–8.

[26] Savage B, Ginsberg MH, Ruggeri ZM. Influence of fibrillar collagen structure on the mechanisms of platelet thrombus formation under flow. Blood 1999;94:2704–15.

[27] Bernardo A, Bergeron AL, Sun CW, Guchhait P, Cruz MA, López JA, Dong J- F. Von Willebrand factor present in fibrillar collagen enhances platelet adhesion to collagen and collagen-induced platelet aggregation. J Thromb Haemost 2004; 2:660–9.

[28] Sixma JJ, Hindriks G, Van Breugel H, Hantgan R, Groot PG. Vessel wall proteins adhesive for platelets. J Biomater Sci Polym Ed 1991;3:17–26.

[29] Kahn ML. Platelet–collagen responses: Molecular basis and therapeutic promise. Sem Thromb Hemost 2004;30:419–25.

[30] Tomokiyo K, Kamikubo Y, Hanada T, Araki T, Nakatomi Y, Ogata Y, Jung SM, Nakagaki T, Moroi M. VWF stimulates platelet deposition in platelet-reduced blood. *Blood First Edition Paper* 2004; in press.

[31] Kanda K, Matsuda T, Oka T. In vitro reconstruction of hybrid vascular tissue. ASAIO J 1993;39:M561–5.

[32] Song J, Rolfe B, Hayward IP, Campbell G, Campbell J. Effects of collagen gel configuration on behavior of vascular smooth muscle cells in vitro: Association with vascular morphogenesis. In vitro Cell Dev Biol Anim 2000;36:600–10.

Preparation and Characterization of a Scaffold for Vascular Tissue Engineering by Direct-Assembling of Collagen and Cells in a Cylindrical Geometry

Francesca Boccafoschi, Navneeta Rajan,
Jason Habermehl, Diego Mantovani*

In the past 25 years, several efforts have been focused on developing vascular substitutes showing long-term patency when implanted in humans. In this study, we present our last findings in an ongoing project aiming to develop a tissue-regenerated blood vessel from collagen-based scaffolds. A collagen-based scaffold with adequate biological properties was developed by directly assembling collagen and cells in a cylindrical geometry. The technique mainly involves the use of a ventilated rotating tube allowing smooth muscle cells to grow in a cylindrical collagen matrix. Scanning electron microscopy (SEM), histology, and cell cycle analyses were carried out in order to assess the biological potential of the cell-based scaffold for further maturation. Compliance results showed that this technique allows cells to assemble in the collagen matrix, thus providing enough rigidity to the structure to be handled and mounted in a perfusion bioreactor for further growth and maturation.
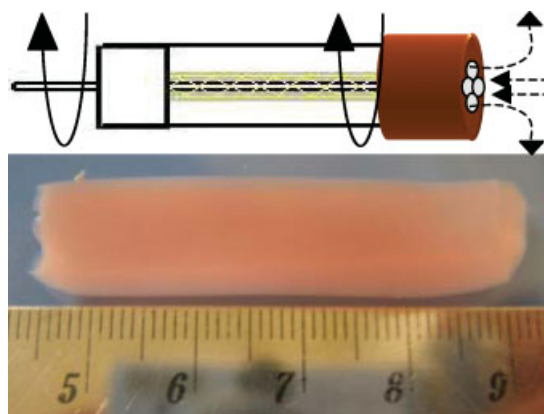
Introduction

Tissue engineering applies the principles of engineering and life sciences toward the development of biological substitutes that restore, maintain, or improve tissue function. Developing vascular substitutes with biological and mechanical properties as close as possible to a native vessel is one of the main goals of vascular tissue engineering.[1] In the past two decades, several groups have focused on the in vitro construction of blood vessels using a collagen matrix. In 1986, Weinberg and Bell were pioneers in this field, casting collagen and bovine aortic smooth muscle cells together to create an annular mould. A Dacron mesh sleeve was added after 1 week and then the inner surface was seeded with bovine endothelial cells. An outer layer was formed with bovine adventitial fibroblasts. Maturation of the structure was then performed for

F. Boccafoschi, N. Rajan, J. Habermehl, D. Mantovani
Laboratory for Biomaterials and Bioengineering, Department of Materials Engineering and Research Centre, Quebec University Hospital, Laval University, Quebec City, G1K 7P4, Canada
Fax: (+1) 418 656 5343; E-mail: diego.mantovani@gmn.ulaval.ca
F. Boccafoschi
Human Anatomy Laboratory, University of Eastern Piedmont "A. Avogadro", Novara, Italy

WILEY
InterScience®
DISCOVER SOMETHING GREAT

2 weeks outside the mould.[2] About 10 years later, L'Heureux and colleagues developed a different technique for a completely biological tissue-engineered human blood vessel. Smooth muscle cells and fibroblasts were cultured to form sheets, comprising cells and extracellular matrix that could be manually peeled off from the culture flask after a period of 30 d and wrapped around a tubular support to produce a cylinder composed of concentric layers. The adventitia was subsequently added in a similar manner followed by a maturation period. This protocol involved a total culture period of 3 months, with multiple and complexes steps to reach the final three-dimensional tubular structure.[3] Recently, Berglund and colleagues published an interesting work on a biological hybrid model for collagen-based tissue engineered vascular constructs. They used a sleeve-hybrid construct which utilizes a temporary crosslinked collagen support to impart the necessary mechanical integrity while the extracellular matrix was synthesized by the cells.[4]

The use of natural materials as scaffold for the support of cell culture is particularly well-suited for the development of vascular substitutes. In particular, due to its low antigenicity, low inflammatory, and cytotoxic responses, collagen type I represents a valid alternative material for tissue engineering.[5] As already shown in literature, it is easily stockable,[6,7] it possesses desirable biological and hematological properties,[8] and it can be remodeled by the host and integrated into existing tissues.[4] Although its presence in biological structures is mainly responsible for their high mechanical resistance, hydrated collagen prepared under the form of sheets or structures are also known to be very difficult to handle. This represents a dramatic limitation for its further use and development in tissue engineering, mainly because the scaffold needs to be manipulated and mounted in a bioreactor in order to be subdued to a wide range of gradients, including mechanical ones, after seeding with cells and for the entire maturation period. Therefore, the aim of this study was to develop a method leading to a collagen-based cylindrical scaffold strong enough to be handled while being suitable for vascular tissue engineering. This work represents the first step toward a tissue-engineered blood vessel which will be obtained by

inserting the tubular scaffold in a perfusion bioreactor stimulating cell-growth and the final maturation period under mechanical stresses.[9]

Materials and Methods

Scaffold Fabrication

Rotating Device for the Tubular Scaffold

In order to allow the horizontal rotation of the gel (and the cells) while in the tubular mould for extended time periods, a tube-mandrel setup was designed and it is presented in Figure 1. This setup is constituted of a 15 ml polypropylene tube (Corning, Montreal, Canada) with the bottom cutoff and replaced by a rubber stopper pierced with a plastic mandrel (VWR International, Montreal, Canada). Gas-exchange caps from 25 cm^2 cell culture flasks (Corning) were used to seal the top of the tubes. The mandrel was coated with neutralized collagen (pH 7) in order to avoid the contraction of the gel, carried out by the cells in the matrix, in its longitudinal direction. Once the gel was formed, the tube-mandrel setup was inserted horizontally and fixed at both ends in the custom-made rotation device. An electrical motor permitted continuous rotation at 4 rpm. The rotating device was then placed in an ordinary cell culture incubator.

Cell Isolation

Two different cell lines were used: (1) smooth muscle cells were directly seeded in the collagen cylindrical matrix,
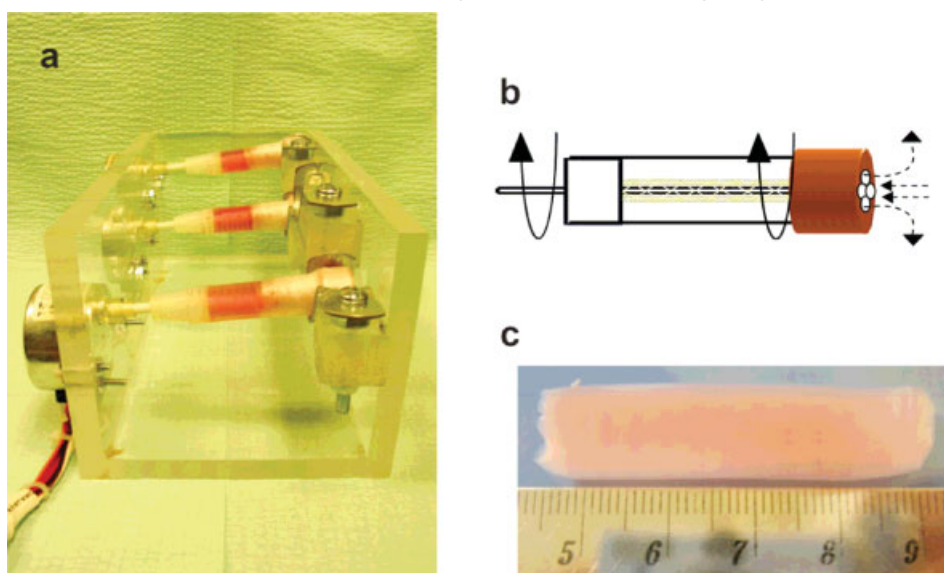

Figure 1. Macrophotograph (a) and schematic representation (b) of the rotating device used for the culture of the tubular collagen and smooth muscle cells-based scaffold, shown in the picture after 1 week of culture in an ordinary cell culture incubator (c). The arrows to the left in (b) indicate the direction of rotation while the small arrows indicate the gas exchanges through the ventilated cap. Each division of the scale indicated in (c) is in millimeter.

Preparation and Characterization of a Scaffold for Vascular Tissue Engineering...

Macromolecular
Bioscience

thus obtaining a composite cells/collagen construct (hereafter named "the construct") and (2) endothelial cells were seeded onto the luminal surface of the construct and used for hematological tests. Cell lines were isolated from porcine aorta as described elsewhere.[10,11] Briefly, after removing the external adventitia, the aorta was incubated for 25 min at 37 °C with collagenase type IA 130 U·ml^{-1} (Gibco, Invitrogen Corporation, Burlington, Ontario, Canada). Endothelial cells were isolated and seeded on Petri dishes coated with 0.2% porcine gelatin. Dulbecco's modified eagles medium (DMEM) was supplemented with 10% porcine serum, glutamine (2×10^{-3} M), penicillin (100 U·ml^{-1}), streptomycin (100 µg·ml^{-1}), fungizone (0.25 µg·ml^{-1}), and heparin (0.09 g·L^{-1}) (all from Sigma-Aldrich, Milwaukee, USA). A fluorescent dye-labeled acetylated low-density lipoprotein (Dil-Ac-LDL, Biomedical Technologies Inc., Stoughton, Massachusetts, USA) was used to confirm the sole presence of endothelial cells.[12]

Following the first digestion, the aorta was incubated overnight with collagenase type II 270 U·ml^{-1} (Worthington Biochemical Corporation, Lakewood, New Jersey, USA). Smooth muscle cells were subsequently extracted and seeded in tissue-culture flasks coated with porcine gelatin 0.2%. DMEM growth medium was supplemented with 15% porcine serum, 10% fetal bovine serum, glutamine (2×10^{-3} M), penicillin (100 U·ml^{-1}), streptomycin (100 µg·ml^{-1}), and fungizone (0.25 µg·ml^{-1}) (all from Sigma-Aldrich). Positive staining with an anti-α-smooth muscle actin-specific antibody was used to confirm the smooth muscle phenotype of the isolated cells (Boehringer Mannheim, Mannheim, Germany).[13] Cells were maintained at 37 °C in 5% CO_2 humidified atmosphere and harvested by trypsinization when a monolayer was reached. All the experiments were performed using cells between the forth and eighth passage.

Scaffold Preparation

Collagen type I was extracted from rat tails and processed as previously described in details.[6,7] Briefly, rat tail tendons were dissolved in acetic acid for 48 h, then the gel-like mass was mixed in a blender, frozen, and lyophilized. The resulting sponge was mixed again with 0.02 N acetic acid at a dry weight to solution ratio of 4 mg·ml^{-1}. The resulting solution was centrifuged, degassed in vacuum and sterilized as follows. The collagen solutions were placed in dialysis bags (Spectra/Por 1, MWCO: 6 000–8 000) and soaked in acetic acid 0.02 N for 1 h followed by 1 h in a mixture of chloroform and water (1:99, v/v). Dialysis was continued in sterile 0.02 N acetic acid for 4–5 d. This solution was changed daily. Collagen gels were then processed by mixing the sterile solution with a suspension of smooth muscle cells in DMEM (Gibco, Invitrogen Corporation) which lead to a final concentration

of 2 million cells per ml. This solution was then poured into the above mentioned tube-mandrel system. After 1 h at 37 °C, the gel was solidified and an adequate amount of medium was placed in the tube as a nutrient supplement for cells. The tubes were then placed on the rotating device and cultured for up to 1 week. The medium was replaced every 2 d. To avoid misunderstanding, we should bring to the reader attention that this 1 week-long culture has not to be confused with the maturation period. In fact, this latter is expected to be carried out in the perfusion bioreactor, after to the 1 week-long culture, and is mainly expected to lead to the development of a functional vascular tissue. Therefore, the 1 week-long culture in the tube-mandrel system is required to allow the cells to grow into the gel, thus conferring to the construct (cell-colonized scaffold) enough mechanical strength to be manipulated and mounted in the bioreactor.

Biological and Hematological Performances

Histological Procedure (Masson's Trichrome)

In order to evaluate the cell distribution and eventual cell/matrix alignment, histology was performed. Appropriate samples were cut from the construct and carefully rinsed with PBS and fixed in 3.7% formaldehyde for 72 h, then embedded in paraffin and 4 µm thick sections were sliced and stained with a modified Masson's trichrome. Briefly, sections were deparaffinized with toluene and rehydrated with graded alcohol. Three different dyes were used in order to differentiate between cells and extracellular matrix: (1) celestine blue solution was used for cell staining (dark blue-black); (2) acid fuchsin solution was used for elastin (pink); and 3) methyl blue solution for collagen (blue).

Cell Cycle Analysis

In order to evaluate the evolution of the cells and the proliferation rate, cell cycle analyses were performed. The activity of cells grown in the tubular moulds was compared to that of cells grown in a conventional Petri culture dish (control). Briefly, after collagen digestion with collagenase type I (0.25 mg·ml^{-1} in DMEM) for 3 h at 37 °C, cells were rinsed with PBS and fixed with ethanol 70% at −20 °C. Before the analyses, cells were labeled with a solution of 50 µg·ml^{-1} propidium iodide and 40 U·ml^{-1} RNase A in PBS. Cell cycle analyses were performed using a BD FACSCalibur flow cytometer (Becton Dickinson, Mississauga, Canada). Histograms were then analyzed using WinMDI software (Scripps Research Institute, La Jolla, USA).

Scanning Electron Microscopy (SEM)

To evaluate the adhesion of platelets, SEM was performed according to the following procedure: samples were rinsed twice with PBS and fixed in Karnowsky solution (2% paraformaldehyde and 2.5% glutaraldehyde in 0.15 M cacodylate buffer, pH 7.2–7.4) for 48 h. Following fixation, samples were treated for 30 min with 1% osmium tetroxide in 0.15 M cacodylate buffer solution. Samples were then dehydrated with graded ethanol (from 50 to 100%), soaked for 30 min in hexamethyldisilazane, dried, and sputter-coated with gold–palladium. Images were collected using a SEM (JSM-35CF, JEOL, Tokyo, Japan) at different magnifications.

After removing the scaffold from the mould, endothelial cells were seeded on the luminal surface of the structure and allowed to grow in a Petri dish for 1 week. In vitro testing was performed to investigate the morphology, aggregation, and philopodia of the adherent platelets on collagen scaffolds with and without the endothelial layer. Native whole blood was collected from five healthy male donors having taken no medication for at least 10 d prior to donation. Blood was collected in tubes containing sodium citrate and used for platelet extraction. After centrifuging, platelet-rich plasma was obtained and a suspension of 3×10^5 platelets was placed on the samples and incubated for 30 min at 37 °C. SEM Images are representative of all the results obtained. Platelet counting was performed on five different areas on each sample.

Compliance Measurement

In order to evaluate appropriately the mechanical properties (burst pressure) of the cylindrical scaffold, a testing apparatus capable to measure the compliance was developed. Briefly, this consists in recording the external diameter when increasing the pressure. The pressure was applied using a 50 ml syringe and highly rigid-tubing both filled with deionized water. A laser scan interferometer (Serie 183 B, LaserMike inc., Dayton, Ohio) was used to measure the external scaffold diameter. A pressure transducer (PX136 Series, Omega, Laval, Canada) monitored the pressure with precision of 1 mmHg.

After 1 week of culture in the rotating device, the compliance was measured. The samples were mounted on supports transmitting an axial tension of 0.4 N. The pressure and diameter data obtained from the measurements were further used to calculate the diameter compliance as:

$$C = \frac{\Delta D}{D \Delta P}$$

where C is the compliance (% · mmHg^{-1}), ΔP is the pressure gradient, ΔD is the difference in the diameter when the pressure is applied, and D is the initial diameter.[14] Experiments were performed in triplicate.

Statistics

Results were expressed as mean ± standard deviation. Statistical significance was determined by variance analysis (ANOVA test).

Results

Biological and Hematological Performances

Histology

Figure 2(a) and 2(b) shows the Masson's trichrome staining used for both smooth muscle cells and extracellular matrix detection (collagen and elastin). Observation at low magnification shows several areas with a darker blue coloration revealing a higher collagen concentration. These
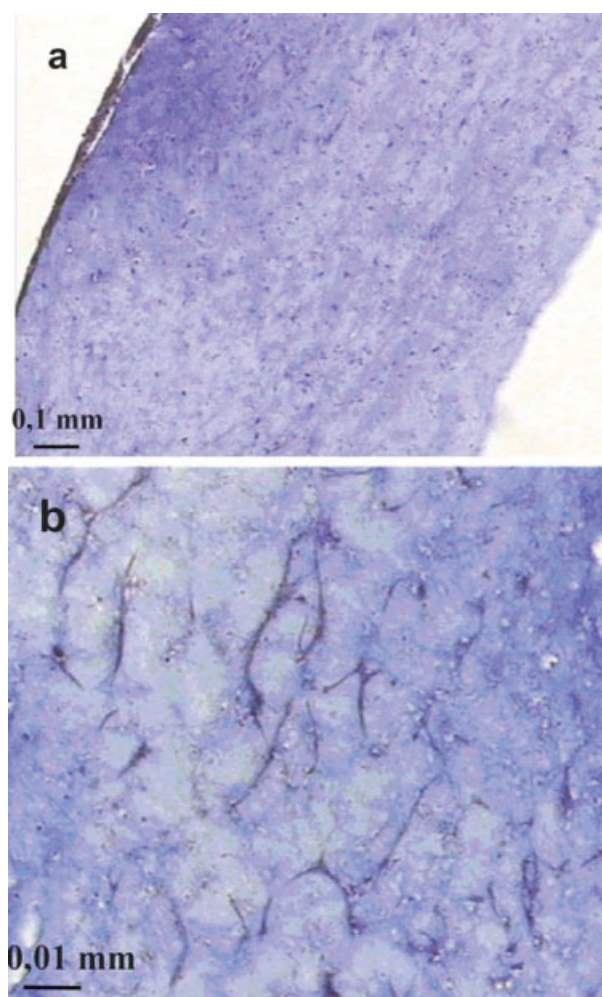

Figure 2. Masson's trichrome on a transversal (a) and longitudinal (b) session of the tubular collagen gel scaffold seeded with smooth muscle cells after 1 week of culture. Collagen is colored in blue, while the cells are colored in dark blue-black, and elastin is colored in pink, but no evident traces of elastin are present.

Preparation and Characterization of a Scaffold for Vascular Tissue Engineering...

Macromolecular
Bioscience

zones are mainly located in the proximity of cells, which are observed in black, thereby suggesting a cell-mediated reorganization of the extracellular matrix. Figure 2(b) shows smooth muscle cells spread in the collagen gel. Elastin was not detected in any of the samples.

Cell Cycle

Cell cycle analyses showed that cells are constantly progressing through the various phases of the cell cycle. The G_1 and G_2 phases are characteristic of protein and RNA synthesis, while the S phase involves DNA synthesis and the M phase is when the cell divides. G_0 is a quiescent stage with cells not fully active. The timing of the cell cycle and the relative lengths of the various stages depend on the specific type of cell and on the growth conditions. Moreover, cell cycle analyses also provide appropriate information on the presence of damaged cells. Results are reported in Table 1. No significant differences between the cell grown in the tubular moulds and the control cells grown in a tissue culture Petri were observed. The G_0G_1 and S phases were statistically similar thus indicating a very similar cell cycle state. Only the percentage of cells in the phase G_2M is significantly higher for cells grown in the tubular mould. Furthermore, results revealed the presence of only a very few percentage of damaged cells in both cases (data not shown).

Platelet Adhesion

In order to verify if the construct represented an adequate surface for endothelial cell proliferation and, also, if extracted endothelial cells still possessed their natural antithrombotic properties, platelet adhesion testing was performed. Endothelial cells reached a confluent layer after 1 week, thereby confirming the suitability of the construct for endothelial cell adhesion and proliferation. Figure 3(a) shows platelets adhesion on the construct before and after endothelial cell seeding. In absence of the endothelial cell lining, a high number of platelets adhered to the collagen surface. Moreover, they appeared highly activated and highly spread. On the other hand, as expected, only few not-spread and single platelets can be observed on the endothelial cell lined-construct. Moreover, the presence of these few platelets was limited almost exclusively to intercellular gaps.

Table 1. Cell cycle analyses.

	G_0G_1	S	G_2M
	%	%	%
Control	76 ± 2	2 ± 6	11 ± 3
Scaffold	69 ± 3	9 ± 4	22 ± 1

The count of adhered platelets [Figure 3(b)] revealed that a mean of 64 ± 4 platelets was present on the non-endothelialized construct, whereas more than five-fold less were counted on the endothelial cell lined construct. The low standard deviation indicates a very high reproducibility among all the samples tested.

Compliance Measurements

Figure 4 shows results obtained from compliance tests performed on cylindrical collagen scaffolds after 1 week of culture in the rotating device. In all the experiments performed the diameter increased proportionally with the pressure applied. The rupture of the scaffold was reached when the pressure overcame 18 ± 1 mmHg. The diameter increased from an initial value of roughly 8 mm to a final value of 12 mm, corresponding to an increase of pressure from 11 to 18 mmHg. Further calculations, taking into account the initial pressure and diameter and the final pressure and diameter, revealed a compliance of $8 \pm 2\% \cdot \text{mmHg}^{-1}$.

Discussion

In the past 20 years, biomaterial scientists and tissue engineers have been focusing on the development of vascular substitutes with biological and mechanical characteristics as close as possible to those of native vessels.[15] Several techniques requiring long and complex protocols for the development of cylindrical scaffolds made of natural collagen have been developed. In general, these scaffolds were not easy to handle, especially when hydrated, due to the mechanical weakness of the collagen. Moreover, the structure was usually firstly matured in a Petri dish and then transferred into a cylindrical geometry. The required manipulations may damage the scaffold and/or contaminate its environment.[2–4] In this context, the aim of this work was to develop a simple one-step procedure to assembly collagen and cells into a scaffold directly in it cylindrical geometry. One of the main advantages of this method is that the scaffold is not processed in Petri dishes, but directly into the tube-mandrel system without any requirement of adding or transferring cells. This intrinsically decreases the risk of contamination caused by repeatedly transferring cells from the Petri dishes to the cylindrical mould, as it is generally required by the processes previously reported in literature. In addition, all the procedures described from other groups required a culture time from minimum 3 weeks to up to 3 months before being able to manipulate the collagen scaffold.[2–4] In this work, the seeded scaffold was easily manipulated in its cylindrical geometry already after 1 week of culture. However, for further maturation in the bioreactor (which was not explored in this study) the
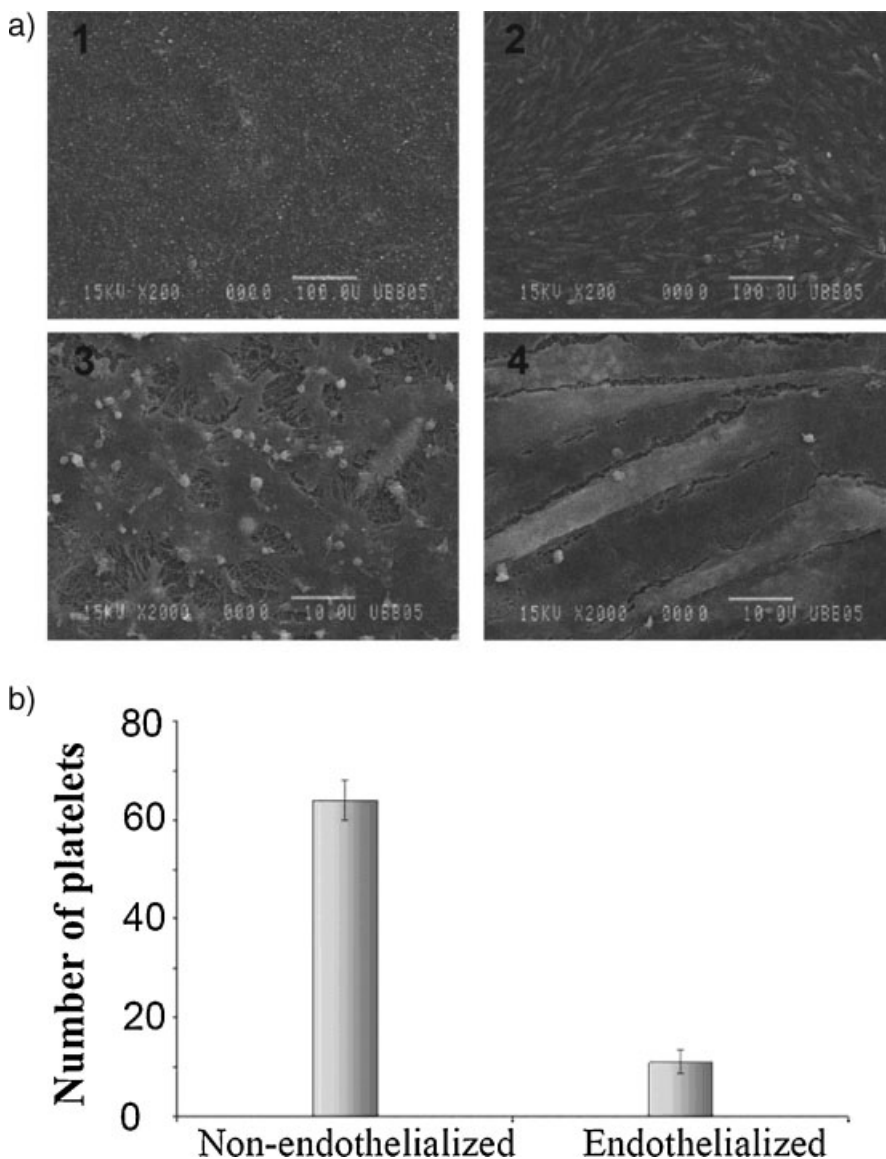
Figure 3. (a) Platelet adhesion on collagen gel seeded with smooth muscle cells without (1, 3) and with (2, 4) endothelial cell layer on the surface. Pictures were acquired with different magnifications with SEM: 200× (1, 2) and 2 000× (3, 4). (b) Platelet adhesion on collagen gel seeded with smooth muscle cells without and with endothelial cell layer on the luminal surface. Results are expressed as mean ± standard deviation. All the results are statistically significant as determined by the ANOVA test ($p = 0.001$).

the proximities of cells clearly shows that they are constantly reorganizing. Although this is the case in native vessels, smooth muscle cells did not seem to have synthesizes elastine after 1 week of culture in the mandrel-tube. It is reasonable to expect synthesis of elastin eventually during the further maturation period in the bioreactor, where smooth muscle cells present in the construct will be subdued to physiologic-like mechanical stimuli. Additionally, cell cycle analyses confirmed that the custom-made rotation device does not compromise smooth muscle cell viability and that the three-dimensional tubular moulds provide an adequate environment for viable cell growth. Finally, results from cell cycle analyses demonstrate that no significant perturbations were induced on smooth muscle cells after growing in the mandrel-tube if compared with cells grown under conventional conditions in Petri dishes.

The use of this construct for vascular tissue engineering requires also excellent hematological properties. For this reason, endothelial cells were seeded on the collagen gels in an attempt to mimic the endothelial cell lining present in native arteries. Previous studies already concluded that collagen flat films processed with the same extraction process than that used in this work, already possess excellent hematological properties and provide a suitable substrate for endothelial cell adhesion.[8] However, the highly hydrated conditions and the presence of smooth muscle cells modify the size of collagen fibrils, and it is known from literature that fibril size affects platelet adhesion and activation.[16] Moreover, endothelial cell adhesion and functionality are known to be passage-dependent.[17] Thus, it was important to verify the adequacy of the cylindrical construct to allow endothelial cell lining as well as to show antithrombotic properties. In this context, results from platelet adhesion tests confirmed the adequacy of the substrate for endothelial cell growth and, moreover, the antithrombotic

cell-based scaffold we developed also needs to be transferred. Additionally, for all the culture period, the scaffold remains easily accessible for further biochemical stimulations.

The use of this construct for vascular tissue engineering requires the preservation of adequate environmental conditions for further cell activity. In this context, histology performed after 1 week shows that the cells are uniformly distributed and spread in the construct. Moreover, the presence of higher concentration of collagen in

Preparation and Characterization of a Scaffold for Vascular Tissue Engineering . . .
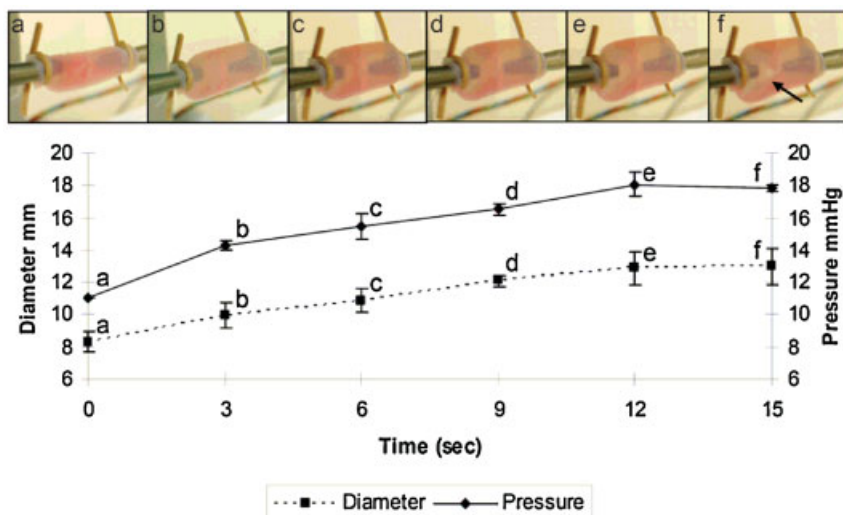
Macromolecular
Bioscience

Figure 4. Compliance test. The diameter of the scaffold was measured at six different times of loading pressure. For each time point (a–f) the pressure, the diameter, and corresponding images are shown. The arrow indicates the point of rupture in the collagen tube. Results are expressed as mean ± standard deviation.

properties of the endothelial cells even after their extraction and after some in vitro passages. Consequently, adequate hematological properties have been observed in vitro. However, it is necessary to further confirm the adequacy in vivo, the in vivo environment being more complex and conditioned by several factors that were not considered in this work. In the perspective to ultimate the maturation of the construct with the further use of a bioreactor, the aim of reaching the complete endothelial cell layer grow under a dynamic flow, could be very interesting since this will closely mimic the natural vascular environment.

The use of this construct for vascular tissue engineering requires also significant mechanical resistance. For synthetic vascular prostheses, for example, it is well known that (mechanical) compliance mismatch is one of the factors that lead to failure.[18] The circumferential compliance of the construct was found to be $8 \pm 2\% \cdot \text{mmHg}^{-1}$. It has to be underlined that the diameter compliance is a function of the applied pressure. For canine abdominal aorta for example, the diameter compliance decreases from $0.8\% \cdot \text{mmHg}^{-1}$ at 14 mmHg to $0.2\% \cdot \text{mmHg}^{-1}$ at 140 mmHg.[13] Therefore, it can be concluded that the construct is ten times more compliant than the canine abdominal aorta. Considering that we use only natural material, without the additional support of any synthetic material, and that the time required for its development in the cylindrical for is of 1 week only, the mechanical properties of the construct are particularly encouraging. After only 1 week of culture in the tubular mould, the construct was solid enough to be handled. Although not comparable with the intraluminal pressure of native vessels, the luminal

pressure applied inside the mandrel-tube might already influence cell activity. In fact, exposure of a cell-seeded scaffold to a pulsatile laminar flow improves the structural integrity and increases the biomechanical properties.[19,20] In this context, the construct obtained after 1 week of culture is expected to strongly beneficiate from further maturation into a bioreactor. This could improve the mechanical properties obtained so far.

In conclusion, the custom-made rotating device provides an adequate environment for cell growth. The biological and hematological properties seem to be adequate for further maturation in the bioreactor. Furthermore, the scaffold possesses adequate mechanical properties which allow future improvements of the structure applying mechanical stresses. Finally, the simplicity and efficiency of the rotating device used to consolidate the collagen gel with smooth muscle cells is an interesting approach for applications in vascular tissue engineering. Future works will focus on the investigation of further strategies to enhance the mechanical properties of the scaffold.

[1] R. Langer, J. P. Vacanti, *Science* **1993**, *260*, 920.
[2] C. B. Weinberg, E. Bell, *Science* **1986**, *231*, 397.
[3] N. L'Heureux, S. Paquet, R. Labbe, L. Germain, F. A. Auger, *FASEB J.* **1998**, *12*, 47.
[4] J. D. Berglund, M. M. Mohseni, R. M. Nerem, A. Sambanis, *Biomaterials* **2003**, *24*, 1241.

[5] G. Goissis, E. Marcantonio, Jr., R. A. Marcantonio, R. C. Lia, D. C. Cancian, W. M. de Carvalho, *Biomaterials* **1999**, *20*, 27.

[6] J. Habermehl, J. Skopinska, F. Boccafoschi, A. Sionkowska, H. Kaczmarek, G. Laroche, D. Mantovani, *Macromol. Biosci.* **2005**, *5*, 821.

[7] N. Rajan, J. Habermehl, M. F. Coté, C. Doillon, D. Mantovani, *Nature Protocols* **2006**, *1*, 2753.

[8] F. Boccafoschi, J. Habermehl, S. Vesentini, D. Mantovani, *Biomaterials* **2005**, *26*, 7410.

[9] K. Bilodeau, F. Couet, F. Boccafoschi, D. Mantovani, *Artif. Organs* **2005**, *29*, 906.

[10] A. Carrillo, *Vet. Immunol. Immunopathol.* **2002**, *89*, 91.

[11] O. Varela, J. Martinez-Gonzalez, L. Badimon, *Eur. J. Clin. Invest.* **1998**, *28*, 313.

[12] J. C. Voyta, D. P. Via, C. E. Butterfield, B. R. Zetter, *J. Cell. Biol.* **1984**, *99*, 2034.

[13] O. Skalli, P. Ropraz, A. Trzeciak, G. Benzonana, D. Gillessen, G. Gabbiani, *J. Cell. Biol.* **1986**, *103*, 2787.

[14] S. F. Stewart, D. J. Lyman, *J. Biomech.* **1990**, *23*, 629.

[15] A. Ratcliffe, *Matrix Biol.* **2000**, *19*, 353.

[16] Y. Kawamoto, M. Kaibara, *Biochim. Biophys. Acta* **1990**, *1035*, 361.

[17] Q. Shi, K. Aida, J. L. Vandeberg, X. L. Wang, *Cell. Biol.* **2004**, *23*, 502.

[18] J. D. Kakisis, C. D. Liapis, C. Breuer, B. E. Sumpio, *J. Vasc. Surg.* **2005**, *41*, 349.

[19] C. A. Thompson et al. *Tissue Eng.* **2002**, *8*, 1083.

[20] A. D. McCulloch, A. B. Harris, C. E. Sarraf, M. Eastwood, *Tissue Eng.* **2004**, *10*, 565.

Macromolecular
Journals

Accepted Manuscript

Title: Effect of different growth factors on human osteoblasts activities: A possible application in bone regeneration for tissue engineering

Authors: Michela Bosetti, Francesca Boccafoschi, Massimiliano Leigheb, Mario F. Cannas

Please cite this article as: Bosetti, M., Boccafoschi, F., Leigheb, M., Cannas, M.F., Effect of different growth factors on human osteoblasts activities: A possible application in bone regeneration for tissue engineering, *Biomolecular Engineering* (2007), doi:10.1016/j.bioeng.2007.08.019

EFFECT OF DIFFERENT GROWTH FACTORS ON HUMAN OSTEOBLASTS ACTIVITIES: A

POSSIBLE APPLICATION IN BONE REGENERATION FOR TISSUE ENGINEERING

Michela Bosetti°^, Francesca Boccafoschi°, Massimiliano Leigheb#°, Mario F. Cannas°*

^DISCAFF, School of Pharmacy, University of Eastern Piedmont, Novara, Italy.

°Department of Clinical an Experimental Medicine, School of Medicine, University of Eastern

Piedmont, Novara, Italy.

#SCDO, Department of Orthopaedics and traumatology, Novara Hospital, Novara, Italy.

*Corresponding author:

Professor Mario F. Cannas M.D. 0039.0321.660632 (Phone and fax)

Via Solaroli 17,

28100 Novara, ITALIA

E-Mail: cannas@med.unipmn.it

RUNNING TITLE: GROWTH FACTORS FOR BONE REGENERATION

KEYWORDS: human primary osteoblast, growth factors, active Vitamin D, proliferation, alkaline

phosphatase, mineralization

ABSTRACT

Cultured human primary osteoblasts reproduce in vivo the phenotypic differentiation and maturation of cells. We have investigated the influence of three isoforms of transforming growth factor beta (TGF-β1, -β2, -β3), three fibroblast growth factors (FGF-2, FGF-4, FGF-6) and the active metabolite of Vitamin D [1,25-(OH)$_2$D3] on proliferation, alkaline phosphatase activity and mineralization of human osteoblast during a period of 24 days of culture. TGF-β isoforms and three FGFs examined have been proved to be inducers of osteoblasts proliferation (higher extent for TGF-β and FGF-2) and inhibitors of alkaline phosphatase activity and osteoblasts mineralization. Combination of these growth factors with the active form of Vitamin D induced osteodifferentation. Infact Vitamin D showed an additive effect on alkaline phosphatase activity and calcium content, induced by FGF-2 and TGF-β in

human osteoblast. These results highlight the potential of proliferating cytokines combination with mineralizing agents for *in vitro* bone growth induction in bone tissue engineering.

INTRODUCTION

Functional bone tissue with a normal structure can be obtained in vitro mimicking the conditions of normal *in vivo* tissue development, offering to clinicians a promising alternative strategy for the treatment of osseous defects and anomalies (Mistry and Mikos, 2005).

The aim of this work was to study growth factors to be used alone or in combination in order to potentiate bone formation. The cellular events involved in bone formation are chemotaxis and proliferation osteoblast precursors, their differentiation to the mature osteoblast with synthesis of extracellular matrix proteins and mineralization of the resulting matrix (Blonder et al., 2006). All these events are controlled by both systemic hormones and local growth factors. Growth factors and cytokines that regulate osteoblast differentiation include TGFs, FGFs, platelet-derived growth factor and insulin-like growth factor (Janssens et al., 2005; Frechette te al., 2005); while endocrine factors regulate bone formation include sex steroid hormones, calcitonin and parathormon, the active metabolite of Vitamin D [1,25-$(OH)_2D3$], leptin and heparan sulfate (Qin et al., 2004; Suda et al. 2003; Karsenty, 2006; Jackson et al., 2007). These mediators of bone functions regulate the phenotype of osteoblasts and other bone cells by binding to cell-surface receptors, which, in turn, activate cellular responses such as proliferation and differentiation (Harada et al., 2003). Data from numerous *in vitro* experiments have descibed conflicting effects of TGF-β and FGFs in different stages of bone formation (Janssens et al., 2005; Erlebacher et al., 1995) probably because obtained from different cell types, at different cell density and different concentrations of growth factors used.

In this paper we have compared the effects of the three mammalian isoforms of TGF-β (-β1, -β2, - β3) and three members of FGFs family (FGF-2, FGF-4, FGF-6) on human osteoblasts proliferation, differentiation and mineralization. Some experiments have been performed using a combination of growth factors showing higher

proliferation ability with the active metabolite of Vitamin D ($1,25(OH)_2D3$) in order to increase osteoblast differentiation and extracellular matrix mineralization for bone tissue engineering applications.

MATERIALS AND METHODS

Cell Culture

Primary osteoblasts were grown from explants of human trabecular bone fragments from knee joints taken at surgery (kindly provided by the Orthopedic Institute, Major Caritas Hospital, Novara, Italy). The osteoblasts were cultured in Iscove's modified Dulbecco's medium supplemented with 10% fetal calf serum (Hyclone, USA), 2 mM L-glutamine, and antibiotics for 2–3 weeks as previously described (Bosetti et al., 2001). Cells from up to three passages were used for all experiments.

Cell proliferation assay

For proliferation assay ViaLight Plus Kit (Cambrex Bio Science Milan, Italy) has been used. The cells were plated at a density of 2×10^3 cells/well in 96-multiwell plates and cultured 1, 4, 8, 16 and 24 days in 2% FCS containing Iscove's modified Dulbecco's medium supplemented with the following growth factors: FGF-2, FGF-4, FGF-6, TGF-β1, β2 and β3. All these growth factors were added to culture media at 10^{-7} M concentration; in experiments aimed at testing the combined effect of proliferating factors with a mineralizing agent, cells were incubated in culture media with the addition of $1,25(OH)_2D3$ at 10^{-6}M in addition to the studied growth factor. At the end of different incubation time points, cells were treated with Cell Lysis Reagent for 10 min and then with ATP monitoring Reagent that utilizes the enzyme luciferase which catalyses the formation of light from ATP and luciferin. The emitted light intensity was linearly related to the intracellular ATP concentration, it was measured using a luminometer and reported as Relative Luminescence Units (RLUs).

Cell differentiation

Alkaline phosphatase activity was determined by an assay based on the hydrolysis of pnitrophenylphosphate to p-nitrophenol. Human osteoblasts were seeded in 24-well culture dishes at 2×10^4 cells/well. After the different treatments with the growth factors described in cell proliferation methods and at the different incubation times cells were collected, rinsed three times with PBS and lysed with 60 μl of a hot solution composed by 75% H_2O, 2.5% SDS, 25% Tris-HCl pH 6.8. 50 μl of this solution has been added to 50 μl of substrate (1mM paranitrophenylphosphate in 1 M diethanolamine + 1 mM $MgCl_2$ pH 9.8 all from Sigma). The mixture was incubated at 37°C until the color was comparable with a standardized series of paranitrophenol solution (Sigma) in about 15-30 min. All samples, including

the standardized series, were measured on a Bio-Rad microplate photospectrometer reader at 405 nm (Bio-Rad, Milan, Italy) and results (n=3) expressed in μM p-nitrophenol. Results were normalized per microgram of cell protein. Protein content was measured in cell lysate by Bicinchoninic Acid (BCA) protein assay reagent kit (Pierce Biotechnology, Rockford, IL, USA).

Cell mineralization

For calcein assay, cells were seeded at 2 x 10^4 cells/well in 24-well culture dishes. Cells were cultured in growth medium for 1 day and then switched to calcification medium [maintenance medium also containing 10 mM β-glycerophosphate (Sigma) and 50 μg/ml L-ascorbic acid (Sigma)]. The medium and growth factors (FGF-2, FGF-4, FGF-6, TGF-β1, β2, β3 and 1,25(OH)$_2$D3) were replaced twice a week. Cells cultured in calcification medium have been used as a basal control, while cells cultured in calcification medium stimulated with 10 mM dexamethasone (DEX) have been used as a positive control. On day 24, osteoblast monolayers were assayed by calcein staining. Cells were treated overnight at 5% CO$_2$/95% air at 37°C with culture medium containing 5 μg/ml calcein, washed 2 times with PBS and examined microscopically using a 515-560 excitation filter. Measurement of mineralized nodules formed in cultures was determined by acquiring 8 random calcein fluorescence images in fields of 1.0912 μm2 surface in each experiment that has been repeated 4 times (n=32). Images have been acquired using a Leica Q550FW camera and analyzed using Qwin Image Analysis software (Leica, Heidelberg, Germany).

Statistical analysis

Statistical analysis of data was carried out using the SPSS for windows software. Bonferroni t-test was applied to evaluate differences in cell proliferation results, APA activity and cell mineralization. P<0.05 was considered to reflect statistical significance.

RESULTS

Proliferation

Human primary osteoblasts evidenced statistically higher intracellular ATP (index of cell proliferation) compared to control cultures when cultured in the presence of TGF- β1, TGF-β2 and TGF-β3; with no differences resulted in the potency of three homodimers isoforms (Figure 1A). This increase in cell proliferation was present starting at short incubation time (1 day) and it was particularly evident at longer incubation times (16-24 days). Figure 1B reported cell proliferation for osteoblasts cultured in control conditions or in TGF-β2 supplemented medium (positive proliferation control), compared to proliferation occured in the presence of FGF-2 or FGF-4 or FGF-6. FGF-2 evidenced the highest proliferation induction as indicated by ATP activity that was comparable to that observed in TGF-β treated cells. On the other hand FGF-4 induced an increase of cell proliferation only at 24 days as well as FGF-6 that induced cell

proliferation after 16 and 24 days of treatment. When $1,25(OH)_2D3$ was added together with FGF-2 or TGF-β, no further increase in osteoblast proliferation was observed compared to cells treated only with growth factors (Figure 1C).

Differentiation

Alkaline phosphatase activity increased from day 8 of culture in both control and growth factors treatd cells. When growth factors were added to culture media a reduced increase of activity was shown after 16 and 24 days (Figure 2A). The inhibition of alkaline phosphatase activity was particularly evident in the presence of TGF-β and FGF-2, the two growth factors that resulted as more effettive activators of human osteoblasts proliferation. As for proliferation experiments, also in alkaline phosphatase activity tests no differences were observed between the potency of the three homodimers of TGF-beta (result not shown); TGF-β2 result was reported in Figure 2A only as representative. When human osteoblasts were cultured in the presence of $1,25(OH)_2D3$ alkaline phosphatase activity increased significantly (p<0.01) compared to control cells starting from day 8 of treatment and reaching an activity plateau at 24 days. Also cells cultured with a combination of FGF-2 or TGF-β2 with $1,25(OH)_2D3$ show an increased (p<0.01) enzyme activity compared to control cells (untreated) and cells cultured in the presence of FGF-2 or TGF-β (Figure 2B).

The combination of FGF-2 and $1,25(OH)_2D3$ evidenced a synergism of activity only at longer incubation times (> 16 days) reaching a plateau of activity at 36 days while the combination of TGF-β2 and $1,25(OH)_2D3$ showed increased alkaline phosphatase activity after 4 days reaching a plateau of activity at 24 days of incubation (Figure 2B).

Mineralization

None of the tested growth factors were able to stimulate mineralization when used alone, while Vitamin D was able to stimulate mineralization compared to untreated cells and cells exposed to tested growth factors. A clear additive effect of FGF-2 and Vitamin D was observed and, at higher extent, between TGF-β and Vitamin D (Figure 3).

DISCUSSION

I*n vivo* bone tissue regeneration is characterized by sequential stages that start with osteoblasts proliferation, followed by their differentiation, and mineralization of the extracellular matrix produced as the endpoint of osteoblast phenotypic expression. Biochemical and molecular studies of bone cells *in vitro* have documented the importance of specific growth and differentiation factors, signaling mediators and transcription factors in bone development (Skjodt et al., 1992). Several fibroblast growth factors (FGFs) are expressed at early stages of bone development and fracture repair

i.e. FGF-8 was shown to increase osteoblast proliferation, mineralization and alkaline phosphatase activity (Valta et al., 2006), while FGF-2 has anabolic effects on bone *in vivo* and was shown to stimulate bone regeneration when implanted into an adequate matrix (Franceschi, 2005). Conflicting results were reported about the effects of TGFβ on osteoblastogenesis and bone formation *in vitro* that probably can be attributed to differences in the osteoblastic cell model system (tumorigenic vs. nontumorigenic, animal vs. human), culture conditions (e.g. serum concentration, presence of other growth factors), differentiation stage of the target cell (mesenchymal, mature) (Janssens et al., 2005).

We tested proliferative and differentiating activity of different growth factors to individuate their potential osteoinductive effect in bone tissue engineering. Our data indicate that TGF-β isoforms and the three FGFs examined (FGF-2, FGF-4 and FGF-6) enhanced human primary osteoblast proliferation with TGF-β and FGF-2 showing an higher activity compared to FGF-6 and FGF-4. All these growth factors inhibited alkaline phosphatase activity and osteoblast mineralization (Sobue et al., 2005).

From recent reports TGF-β and FGF-2 induction of cell proliferation seems to be mediated by MAPK-dependent signaling through phosphorylation of ERK, JNK and p38 and activation of transcription factors that dimerize into AP-1 complexes which bind to AP1 sites in the DNA, inducing an immediate increase in cell proliferation (Spector et al., 2005). Molecular mechanisms that explain TGF-β actions in bone formation revealed a role for both MAPK- and Smad-dependent signaling that interact with each other; on the other hand crosstalk occurs with pathways initiated by other local and systemic factors that probably have synergistic or antagonistic mechanisms (Sowa et al., 2002).

Alkaline phosphatase activity is an important enzyme during the maturation of bone extracellular matrix, as it contributes to bone mineralization by hydrolyzing phosphate ester, stimulating calcium phosphate precipitation, and hydrolyzing inorganic pyrophosphate (an inhibitor of hydroxyapatite formation) (Ho et al., 1999). Alkaline phosphatase expression is known to peak after the end of the proliferative stage and before matrix maturation during osteoblast differentiation. Cytokines e.g. platelet-derived growth factor and BMP-2, play important roles in alkaline phosphatase expression during bone remodeling; Vitamin D has a stimulatory effect on osteoblast alkaline phosphatase activity (Gonnerman et al., 2006), whereas conflicting results exist for TGF-β and FGF-2. TGF-β has been recently proposed as a growth factor to be incorporated into biomaterials in order to improves bone-healing efficacy (Lee et al., 2006; Lilli et al., 2002) evidencing increased alkaline phosphatase activity and mineralization of osteoblasts. Our results, according to most recent data (Vanderschueren et al., 2004), indicate that TGF-β increases bone formation *in vitro* mainly by expanding the pool of committed osteoblasts but on the other hand it blocks later phases of differentiation (reduced alkaline phosphatase activity) and mineralization (reduced calcium content in extracellular matrix). These later stages of bone metabolism seem to be regulated by other growth factors (Jorgensen et al., 2004) that could be hypothetically added in the osteoinductive support together with the proliferating agent in tissue engineering applications.

To increase the second and third step of osteoblast osteodifferentiation, tested respectively using alkaline phosphatase activity and mineralization, we have used a combination of the growth factors with high proliferation activity together to the active form of Vitamin D, an osteodifferentiative factor (Van Leewen et al., 2001). The active metabolite of Vitamin D [1,25-(OH)$_2$D3] stimulates bone formation through the up-regulation of osteoblast differentiation and extracellular matrix mineralization. TGF-β and 1,25-(OH)$_2$D3 can both synergize or antagonize each other's functions and it appears that signals transmitted through Smad and MAPK pathways evoke opposite effects on 1,25-(OH)$_2$D3 functioning (Gurlek and Kumar, 2001). Results obtained evidenced additive effects of both FGF-2 and TGF-β on Vitamin D alkaline phosphatase activity and osteoblasts calcium content, indicative of increased osteodifferentiation. TGF-β synergy to calcitriol could be mediated by cross-talk between the growth factor and the lipophilic hormone by Smad3, a downstream component of the TGF-β signaling pathway that acts as a co activator of Vitamin D receptor and positively regulates the Vitamin D signaling pathway (Gurlek et al., 2002). The FGF-2 synergy with 1,25-(OH)$_2$D3 is more complex to explain as the only report about interactions between FGF-2 and Vitamin D describes as FGF-2 inhibition of osteoclast-like formation induced by 1,25-(OH)$_2$D3 (Zuo et al., 2004); therefore only some hypotheses can be postulated to try to explain FGF-2 synergy to calcitriol. FGF/FGF receptor signaling induces the expression of Runx2 (Kim et al., 2003), a transcription factor in osteoblast differentiation. Furthermore recent studies have identified Runx2-VDR protein-protein interactions with the co regulatory Smad proteins for Vitamin D enhanced transcription (Parades et al., 2004). Thus FGF-2 treatment could potentiate 1,25-(OH)$_2$D3 activity on osteoblast alkaline phosphatase activity and mineralization upregulating the transactivating activity of Runx2 (Figure 4).

In conclusion, the combinations tested of growth factor and Vitamin D could be useful for *in vitro* bone growth induction in the field of bone tissue engineering.

REFERENCES

Blonder, J., Xiao, Z., Veenstra, T.D., 2006. Proteomic profiling of differentiating osteoblasts. Expert Rev Proteomics 3, 483-496.

Bosetti, M., Vernè, E., Ferraris, M., Ravaglioli, A., Cannas, M., 2001. In vitro characterisation of zirconia coated by bioactive glass. Biomaterials 22, 987-994.

Erlebacher, A., Filvaroff, E.H., Gitelman, S.E., Derynck, R., 1995. Toward a molecular understanding of skeletal development. Cell 80, 371-378.

Franceschi, R.T., 2005. Biological approaches to bone regeneration by gene therapy. J Dent Res 84, 1093-1103.

Frechette, J.P., Martineau, I., Gagnon, G., 2005. Platelet-rich plasmas: growth factor content and roles in wound healing. J Dent Res 84, 434-439.

Gonnerman, K.N., Brown, L.S., Chu, T.M., 2006. Effects of growth factors on cell migration and alkaline phosphatase release. Biomed Sci Instrum 42, 60-66.

Gurlek, A., Kumar, R., 2001. Regulation of osteoblast growth by interactions between transforming growth factor$-\beta$ and 1α,25-dihydroxyvitamin D3. Crit Rev Eukaryot Gene Expr 11, 299-317.

Gurlek, A., Pittelkow, M.R., Kumar, R., 2002. Modulation of growth factor/cytokine synthesis and signaling by 1a,25-dihydroxyvitamin D3: implications in cell growth and differentiation. Endocr Rev 23, 763-786.

Harada, S., Rodan, G.A., 2003. Control of osteoblast function and regulation of bone mass. Nature 423, 349-355.

Ho, M.L., Chang, J.K., Chuang, L.Y., Hsu, H.K., Wang, G.J., 1999. Effects of nonsteroidal anti-inflammatory drugs and prostaglandins on osteoblastic functions. Biochem Pharmacol 58, 983-990.

Jackson, R., Murali, S., Van Wijnen, A.J., Stein, G.S., Nurcombe, V., Cool, S.M., 2007. Heparan sulfate regulates the anabolic activity of MC3T3-E1 preosteoblast cells by induction of runx2. J Cell Physiol 210, 38-50.

Janssens, K., Dijke, P., Janssens, S., Van Hul, W., 2005. Transforming growth factor-β1 to the bone. Endocrine Reviews 26, 743-774.

Jorgensen, N.R., Henriksen, Z., Sorensen, O.H., Civitelli, R., 2004. Dexamethasone, BMP-2, and 1,25-dihydroxyvitamin D enhance a more differentiated osteoblast phenotype: validation of an in vitro model for human bone marrow-derived primary osteoblasts. Steroids 69, 219-226.

Karsenty, G., 2006. Convergence between bone and energy homeostases: leptin regulation of bone mass. Cell Metab 4, 341-348.

Kim, H.J., Kim, J.H., Bae, S.C., Choi, J.Y., Ryoo, H.M., 2003. The protein kinase C pathway plays a central role in the fibroblast growth factor-stimulated expression and transactivation activity of Runx2. J Biol Chem 278, 319-326.

Lee, J.Y., Kim, K.H., Shin, S.Y., Rhyu, I.C., Lee, Y.M., Park, Y.J., Chung, C.P., Lee, S.J., 2006. Enhanced bone formation by transforming growth factor-beta1-releasing collagen/chitosan microgranules. J Biomed Mater Res A 76, 530-539.

Lilli, C., Marinucci, L., Stabellini, G., Belcastro, S., Becchetti, E., Balducci, C., Staffolani, N., Locci, P., 2002. Biomembranes enriched with TGFbeta1 favor bone matrix protein expression by human osteoblasts in vitro. J Biomed Mater Res 63, 577-582.

Mistry, A.S., Mikos, A.G., 2005. Tissue engineering strategies for bone regeneration. Adv Biochem Eng Biotechnol 94, 1-22.

Parades, R., Arriagada, G., Cruzat, F., Villagra, A., Olate, J., Zaidi, K., van Wijnen, A., Lian, J.B., Stein, G.S., Stein, J.L., Montecino, M., 2004. Bone-specific transcription factor Runx2 interacts with the 1alpha,25-dihydroxyvitamin D3 receptor to up-regulate rat osteocalcin gene expression in osteoblastic cells. Mol Cell Biol 24, 8847-8861.

Qin, L., Raggatt, L.J., Partridge, N.C., 2004. Parathyroid hormone: a double-edged sword for bone metabolism. Trends Endocrinol Metab 15, 60-65.

Skjodt, H., Russel, G., 1992. Bone cell biology and the regulation of bone turnover. In: Growen, M., eds. Cytokines and Bone Metabolism. Boca Raton, FL: CRC Press, pp. 1-70.

Sobue, T., Naganawa, T., Xiao, L., Okada, Y., Tanaka, Y., Ito, M., Okimoto, N., Nakamura, T., Coffin, J.D., Hurley, M.M., 2005. Over-expression of fibroblast growth factor-2 causes defective bone mineralization and osteopenia in transgenic mice. J Cell Biochem 95, 83-94.

Sowa, H., Kaji, H., Yamaguchi, T., Sugimoto, T., Chihara, K., 2002. Activations of ERK1/2 and JNK by transforming growth factor b negatively regulate Smad3-induced alkaline phosphatase activity and mineralization in mouse osteoblastic cells. J Biol Chem 277, 36024-36031.

Spector, J.A., Mathy, J.A., Warren, S.M., Nacamuli, R.P., Song, H.M., Lenton, K., Fong, K.D., Fang, D.T., Longaker, M.T., 2005. FGF-2 acts through an ERK1/2 intracellular pathway to affect osteoblast differentiation. Plast Reconstr Surg 115, 838-852.

Suda, T., Ueno, Y., Fujii, K., Shinki, T., 2003. Vitamin D and bone. J Cell Biochem 88, 259-266. Valta, M.P., Hentunen, T., Qu, Q., Valve, E.M., Harjula, A., Seppanen, J.A., Vaananen, H.K., Harkonen, P.L., 2006. Regulation of osteoblast differentiation: a novel function for fibroblast growth factor 8. Endocrinology 147, 2171-2182.

Van Leeuwen, J.P., Van Driel, M., Van den Bemd, G.J., Pols, H.A., 2001. Vitamin D control of osteoblast function and bone extracellular matrix mineralization. Crit Rev Eukaryot Gene Expr 11, 199-226.

Vanderschueren, D., Vandenput, L., Boonen, S., Lindberg, M.K., Bouillon, R., Ohlsson, C., 2004. Androgens and bone. Endocr Rev 25, 389-425.

Zuo, J., Jiand, J., Dolce, C., Holliday, L.S., 2004. Effects of basic fibroblast growth factor on osteoclasts and osteoclast-like cells. Biochem Biophys Res Commun 318, 162-167.

FIGURE LEGENDS

FIGURE 1. Cell proliferation has been evaluated by the ATP monitoring technique on human osteoblasts plated on 96-well microtiter plates in the presence of different growth factors at 10^{-7} M TGF-β1, TGF-β2, TGF-β3 (**A**), FGF-2, FGF-4, FGF-6 (**B**) and growth factors combined with the active form of Vitamin D (**C**). The experiments have been performed in the presence of 2% FCS; cells cultured without growth factors represented control. The effect of the molecules has been evaluated at 1, 4, 8, 16 and 24 days. Results are expressed as relative luminescence units and values represent the average ± standard deviation (SD) of each treatment performed in triplicate for three independent experiments. *p < 0.01 vs. control.

FIGURE 2. Alkaline phosphatase activity has been evaluated by biochemical method on human osteoblasts cultured in the presence or absence of growth factors at 10^{-7} M (**A**) and growth factors combined with 1,25-(OH)$_2$D3 (**B**). The effect of the molecules has been evaluated at 1, 4, 8, 16 and 24 days. Results are expressed as µM/µg protein and values

represent the average ± standard deviation (SD) of each treatment performed in triplicate in three independent experiments. *p < 0.01 vs. control.

FIGURE 3. Confluent human osteoblasts, cultured with ascorbic acid and β−glycerophosphate, have been treated or not with the tested growth factors for 24 days. The formation of mineralised nodules has been detected on cells using calcein staining. Photomicrographs have been obtained by a digital Leica camera connected to a fluorescence microscope (**A**). Quantitative analysis of mineralized nodules has been performed measuring the surface areas of mineralization on a computer-assisted image analyzer (**B**). Results represent the average ± standard deviation (SD) of three independent experiments. *p < 0.01 vs. control.

FIGURE 4. Signaling by the growth factors through the MAPK-dependent (A) and Smaddependent (B) pathways and hypothetic mechanism of $1\alpha,25\text{-}(OH)_2D3$ on Smad pathway involving Runx2-VDR protein-protein interactions for Vitamin D enhanced transcription for osteoblast differentiation. VDR ($1\alpha,25\text{-}(OH)_2D3$ receptor); Runx2 (runt-related transcription factor 2, a transcription factor that promotes osteoblast differentiation); AP-1 (activator protein 1); SBEs (Smad-binding elements); GFsR (growth factors receptor, P phosphorylation state).
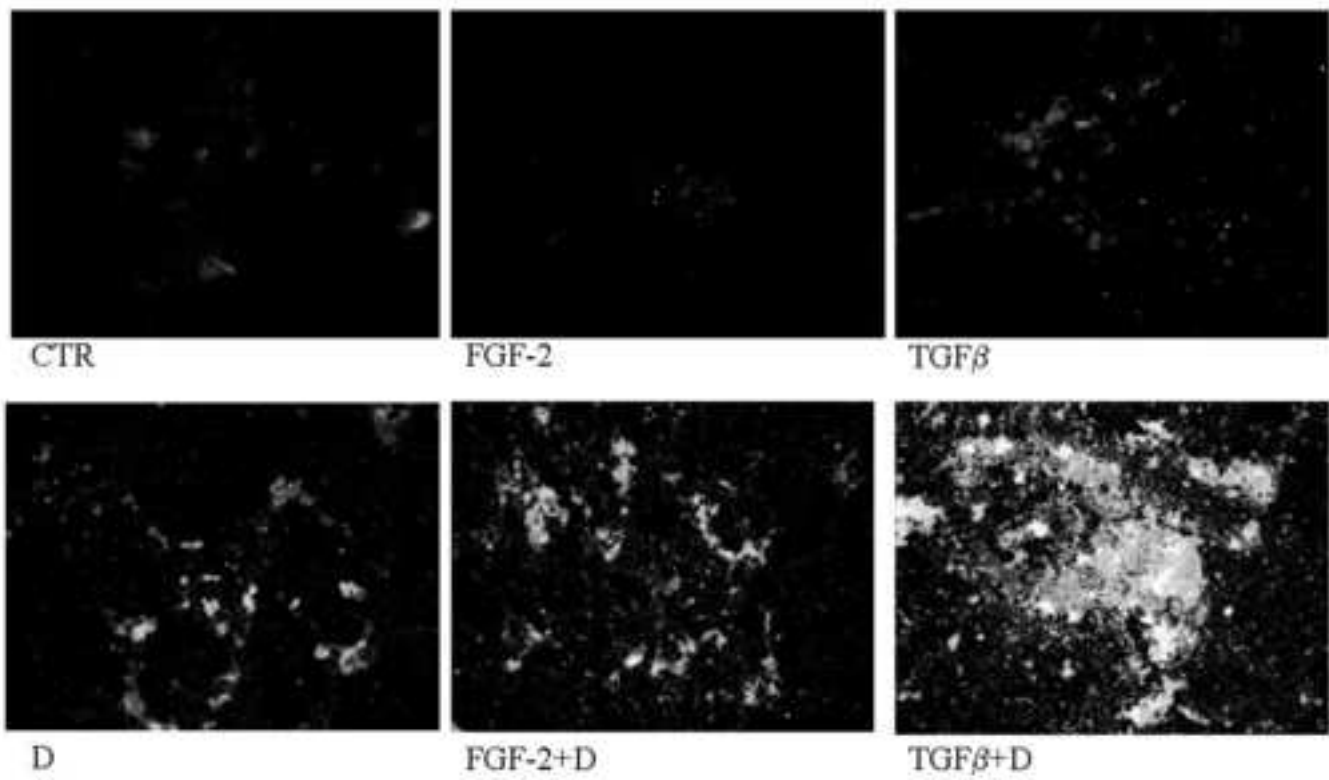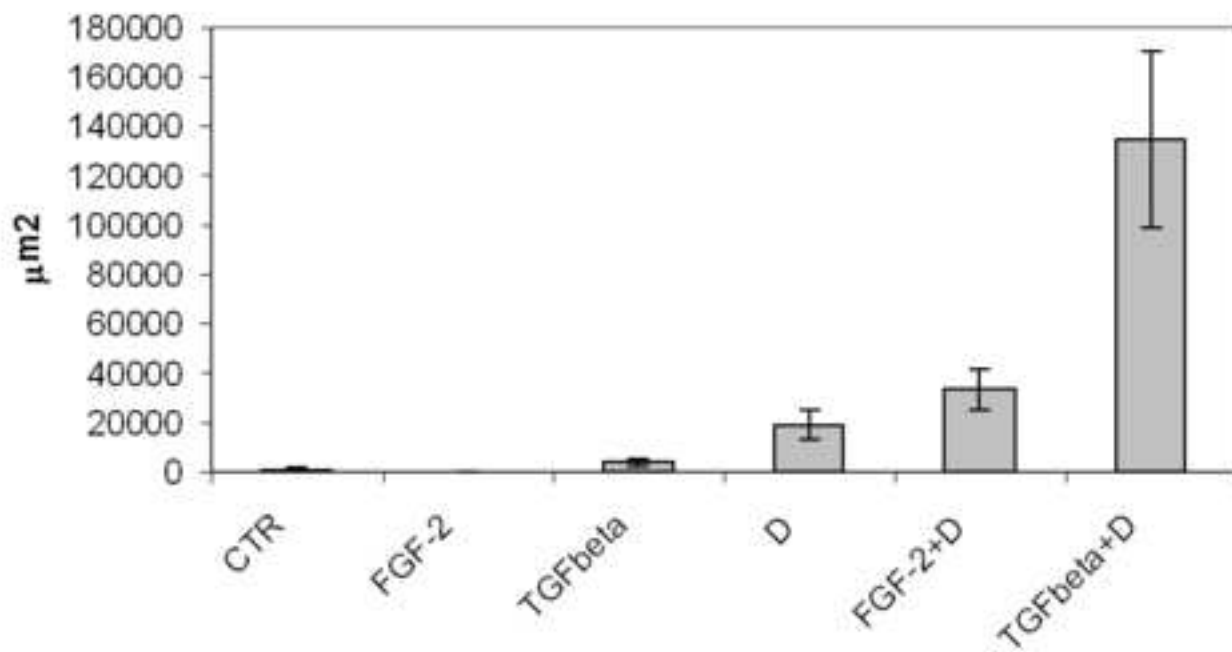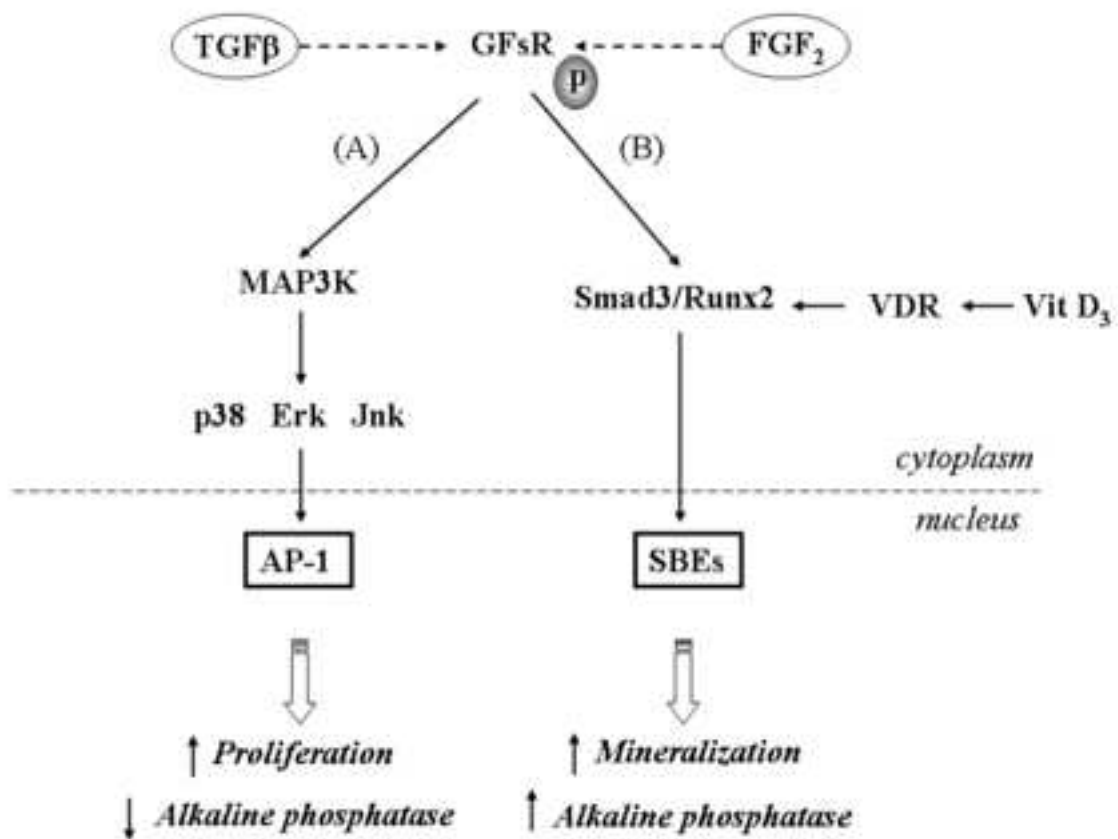
A

B

CTR   FGF-2   TGFβ

D   FGF-2+D   TGFβ+D
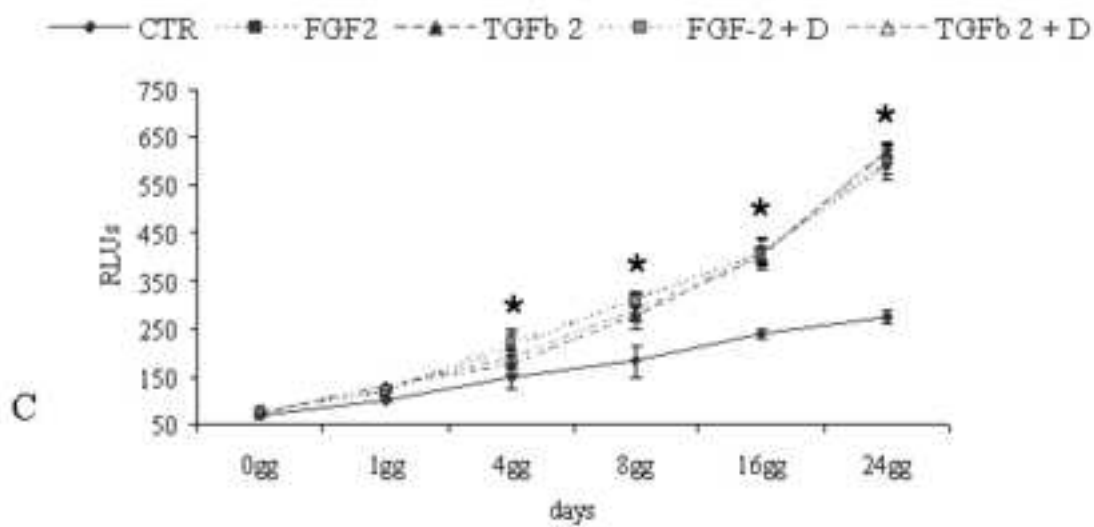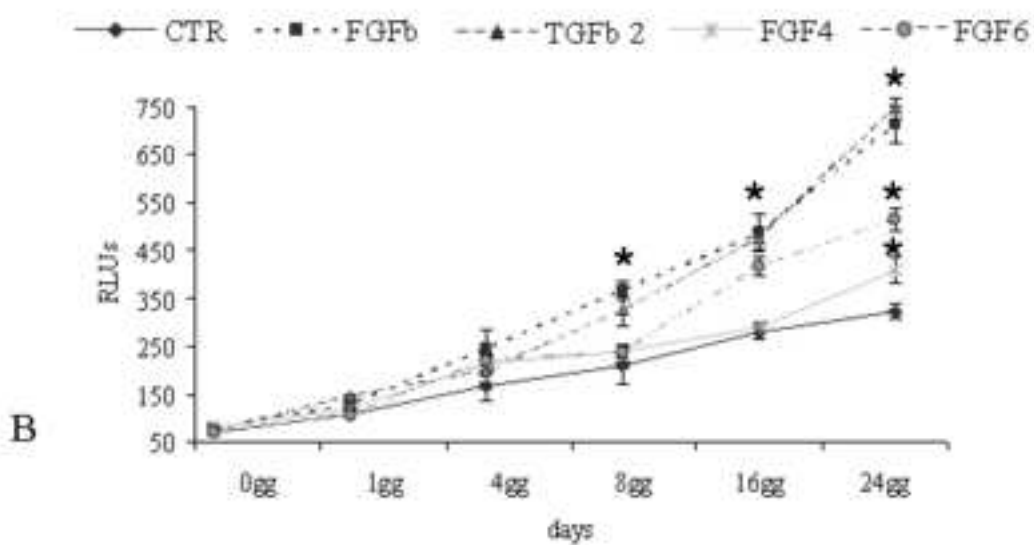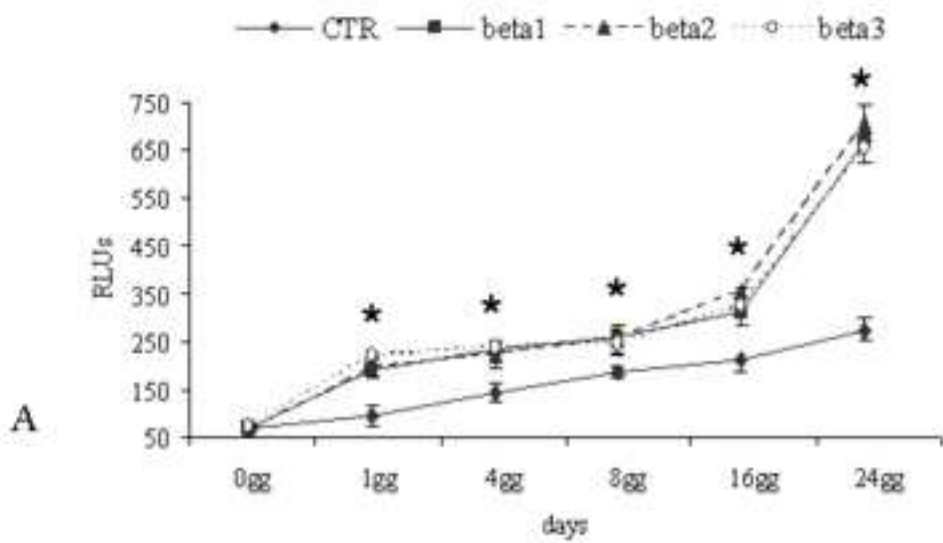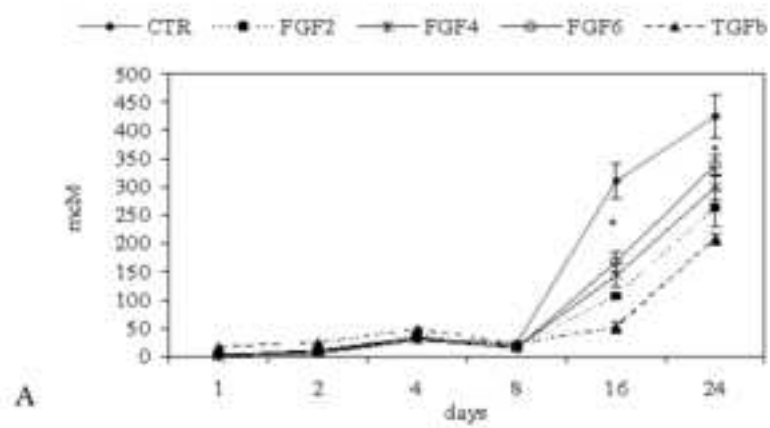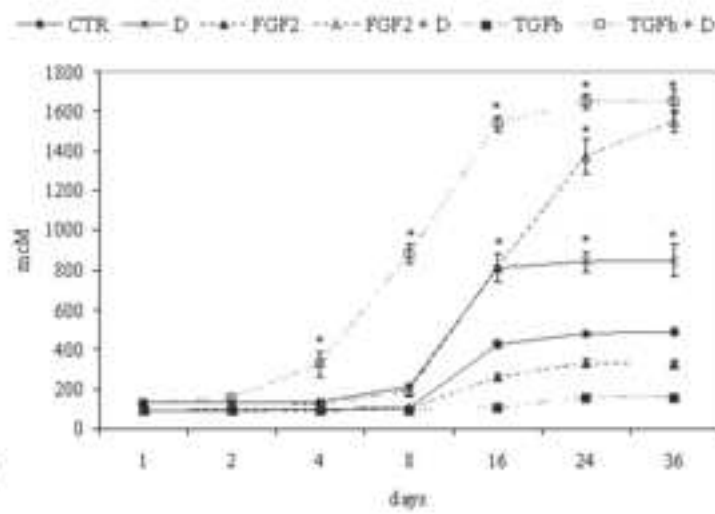
Research Paper

Dynamic Fibroblast Cultures

Response to Mechanical Stretching

F. Boccafoschi

M. Bosetti

S. Gatti

M. Cannas*

Department of Clinical and Experimental Medicine; Human Anatomy; University of Eastern Piedmont; Novara, Italy

*Correspondence to: M. Cannas; Via Solaroli 17; Novara 28100 Italy; Tel./Fax: +39.0321.660632; Email: cannas@med.unipmn.it

KEY WORDS

ABSTRACT

Mechanical forces play an important role in the organization, growth and function of tissues. Dynamic extracellular environment affects cellular behavior modifying their orientation and their cytoskeleton. In this work, human fibroblasts have been subjected for three hours to increasing substrate deformations (1–25%) applied as cyclic uniaxial stretching at different frequencies (from 0.25 Hz to 3 Hz). Our objective was to identify whether and in which ranges the different deformations magnitude and rate were the factors responsible of the cell alignment and if actin cytoskeleton modification was involved in these responses. After three hours of cyclically stretched substrate, results evidenced that fibroblasts aligned perpendicularly to the stretch direction at 1% substrate deformation and reached statistically higher orientation at 2% substrate deformation with unmodified values at 5–20%, while 25% substrate deformation induced cellular death. It was also shown that a percentage of cells oriented perpendicularly to the deformation were not influenced by increased frequency of cyclical three hours deformations (0.25–3 Hz). Cyclic substrate deformation was shown also to involve actin fibers which orient perpendicularly to the stress direction as well. Thus, we argue that a substrate deformation induces a dynamic change in cytoskeleton able to modify the entire morphology of the cells.

INTRODUCTION

Native tissues are composed of three-dimensional matrices and well aligned cellular layers. This composition enables the tissues to operate with proper functionality, for instance to move peristaltically and to be compliant in vascular and visceral tubular-structured tissues. The orientation of cells and the alignment of cytoskeleton elements are affected by the dynamic extracellular environment that results from the application of mechanical stress.[1] It is well established that connective tissues adapt to changes in mechanical environment, i.e., in bones trabeculae align in response to compressive and tensile stresses.[2]

More recently in vitro studies evidenced that cyclic substrate deformations cause changes in cell orientation[3-6] and in actin cytoskeleton.[6,8] Cyclic substrate deformation was shown to induce alignment of fibroblast perpendicular to the stretch direction; osteoblasts,[9] smooth muscle cells,[5] embryonic myoblasts[10] and endothelial cells[6,11] have also shown to modify the alignment when cultured on stretched substrate.

Thus, literature reports large evidences which support cell alignment after applying a substrate deformation but a comparison between different deformations and frequencies applied to cell lines is not reported yet. In this work, human fetal lung fibroblasts have been subjected to increasing substrate deformations (from 1% to 25%) and different frequencies (from 0.25 Hz to 3 Hz) in order to identify whether and in which ranges the different deformations magnitude and rate were the factors responsible of the cell alignment and if actin cytoskeleton modification was involved in these responses.

MATERIALS AND METHODS

Materials. Silicone sheets 0.010" non-reinforced vulcanized (SMI Specialty Manufacturing Inc. Saginaw, Michigan, USA) have been used as deformable substrates. Sheets (1 x 1 cm) have been sterilized by autoclaving for 20 minutes at 121°C and coated with sterile fibronectin 10 μg/ml (Sigma, Milan, Italy) for one hour at room temperature

before cell seeding. Unless otherwise specified, all chemical reagents were purchased from Sigma.

Cell culture. Human fibroblasts MRC5 (ATCC CRL 171) derived from normal lung tissue have been used at 15×10^3 cells/cm^2. Cells have been cultured in DMEM enriched with 10% fetal bovine serum, glutamine (2 mM), penicillin (100 U/ml) and streptomycin (100 μg/ml) (Euroclone, Italy). In order to obtain the optimal attachment to the membrane, cells have been maintained on silicon at 37°C in humidified atmosphere with 5% CO_2 in static conditions for 24 hours before applying mechanical stress.

Application of mechanical stretching to the cells. Instron 5564 testing Instrument (Instron Corporation, Canton, Massachusets, USA) has been used to tensing silicon substrates on which cells have been allowed to adhere. The device comprises an electronic control console and a loading frame with a load capacity of 2.5 N in tension or in compression and 2,500 mm/minute–0.05 mm/minute respectively maximum and minimum speed of the moving crosshead. Silicon samples with cells, connected with tweezers to the Instron's load cell, have been immerged for all the experimental time (three hours) in a culture vertical chamber (Ugo Basile, Milan, Italy) filled with culture medium and maintained at 37°C with 5% CO_2 in a closed bath. Different substrate deformations have been applied as cyclic uniaxial stretching and compared with a not stressed control. The range of magnitude tested was from 1 to 25% at 0.5 Hz, whereas different frequencies tested were from 0.25 to 3 Hz at 2% magnitude. The orientation and number of cells were determined from photographs of cells obtained in random fields from at least three separate experiments as described in next section.

MTT test. MTT (3-[4,5-dimethylthiazol-2-yl]-2,5-diphenyl-tetrazolium bromide) is a water-soluble chemical. Active mitochondrial dehydrogenases of living cells convert the yellowish MTT to an insoluble purple formazan. This conversion does not take place in dead cells. This water-insoluble formazan can be solubilized using dimethylsulfoxide (DMSO), and the dissolved material can be measured spectrophotometrically. After applying mechanical stress on cell, cells were incubated for additional three hours with a MTT solution (50 μg/ml final concentration). Samples were rinsed and formazan salt formed were dissolved. Absorbance at 570 nm was read. Data obtained were expressed as mean percentage with respect to control ± standard deviation.

Orientation counting. Cell orientation has been considered by the longest aspect of the cells. To evaluate the percentage of oriented cells, samples have been fixed with 3.7% formaldehyde for 30 minutes and stained ten minutes with toluidine blue 0.01% in dH$_2$O pH8. Seven pictures for each sample have been acquired and tests for each stress condition have been performed in triplicate (n = 21). A grid with different oriented angle (0–30°; 30–60° and 60–90°) has been applied on each picture and the cellular orientation has been measured and reported in graphs as percentage of oriented
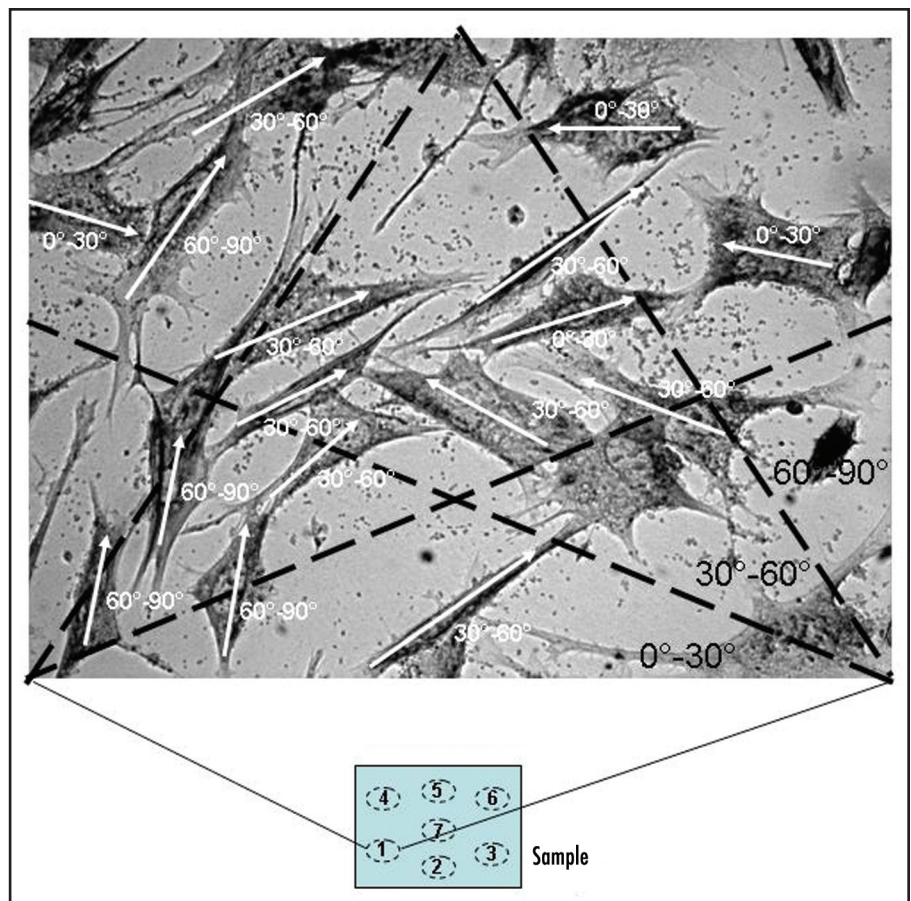

Figure 1. Example of cell orientation counting. This method has been used for measure cell and actin filaments orientation.

cells in each of the three angle considered. The direction of uniaxial deformation has been considered as 0°. The picture below shows an example of the method used to define and measure cell orientation (**Fig. 1**).

Actin filaments. To determine the role of the actin cytoskeleton in cell alignment, separate experiments performed in the same conditions described above have been used. Cells cultured on unstretched control or on silicon stretched for three hours in different conditions have been fixed in formaldehyde 3.7% for 30 minutes and then labeled with phalloidin-TRITC conjugated (Sigma, Italy). Actin filaments have been observed by fluorescence microscopy (Leica, DM 2500) at 40x magnification. A grid with different oriented angle (0–30°; 30–60° and 60–90°) has been applied on pictures acquired and the actin filaments orientation has been measured and reported in graphs as percentage of oriented filaments in each of the three angles considered.

Statistical analysis. Means of group were compared by analysis of variance, and the significance of differences was obtained by post hoc testing using Bonferroni's method. p value was obtained from the ANOVA table; the conventional 0.05 level was considered to reflect statistical significance.
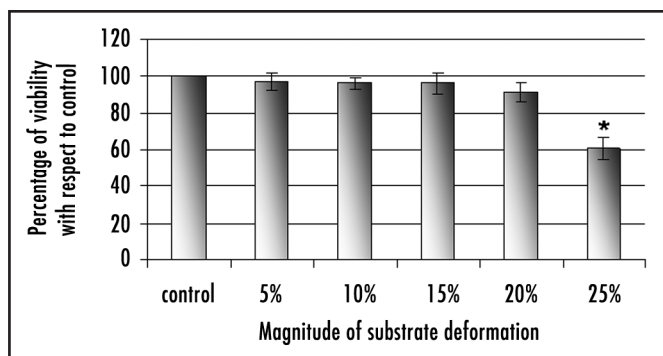
Figure 2. MTT test. Cell viability has been verified after applying different deformation magnitude for three hours. Results are expressed as mean of percentage with respect to control ± standard deviation.

RESULTS

Cell viability. Figure 2 shows results obtained from viability test. Mechanical stress did not interfere with cells viability until 20% of magnitude deformation was reached, as the mean of percentages close to 100% showed in all the cases. At 25% of deformation magnitude cells viability decreased reaching a mean of 60% ± 6 with statistical relevance. In this case, the decreasing value was due to both cell detachment and damage of the cellular structure as confirmed in (Fig. 3D).

Cell alignment on deformed substrate. Pictures shown in Figure 3 (magnification 25x) are representative of the morphology and the distribution of cells when subjected to a substrate deformation (Fig. 3B–D) compared with cells cultured in a static control (Fig. 3A). Cells were randomly distributed on control not deformed substrata while cells subjected to a mechanical stress ≥2% of substrate deformation align perpendicularly to the stress direction. No modifications in cell morphology were seen from 2 to 20% of silicon deformation while cells subjected to a 25% deformation shown a severely altered morphology (Fig. 1D).

Figure 4 shows percentage of oriented cells in the three angles considered to study cell alignment modifications after three hours of different degrees of deformation. Cells cultured on control, not deformed substrata, showed a random distribution with no statistical differences between cell numbers in the three degrees of alignment. Starting from the 2% deformation, 60% of fibroblasts aligns perpendicularly to the stretch direction, as shown by a statistically higher number of cells in the range 60–90° together with lower percentage of cells in the range 0–30° and 30–60° orientation. No statistically significant differences were observed between cells stressed from 2 to 20% while when 25% of substrate deformation was applied, cell morphology, as shown in Figure 3D, was altered thus cell reorientation was technically difficult to quantify for the high percentage of cells damaged and detached (Fig. 4).

Cells subjected for three hours to 2% of substrate deformation were then tested modifying the frequency of substrate deformation from 0.25 Hz to 3 Hz. As shown in Figure 5, when comparing the percentage of oriented cells in control not stressed culture with stressed substrata it was evident a statistically increase of cells oriented in the range 60–90°. No statistical differences were seen when comparing all the frequency applied.
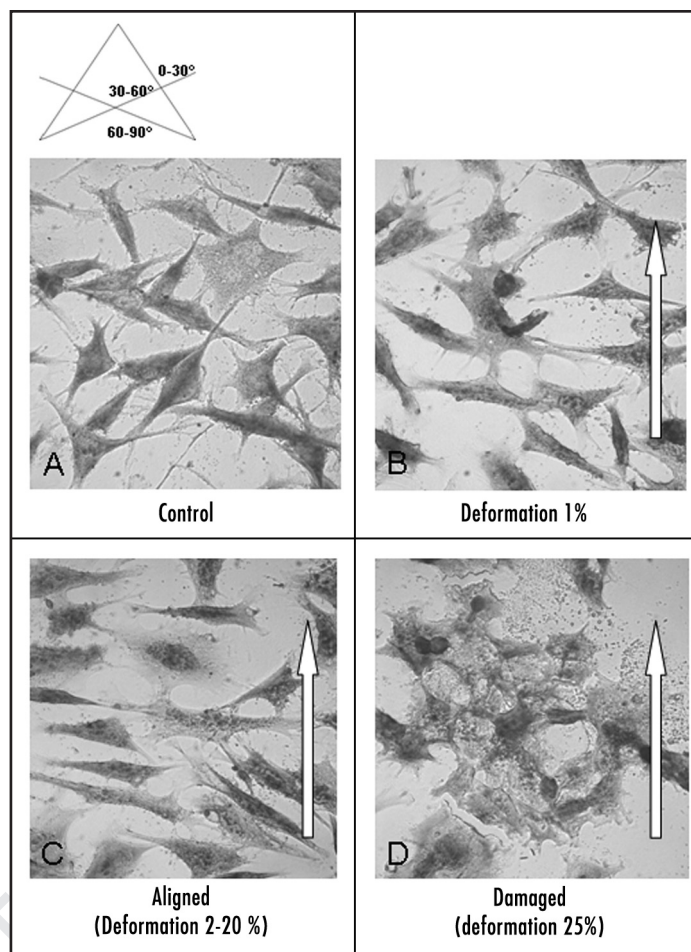

Figure 3. Picture shows a cellular random distribution in the control (A) and when 1% substrata deformation was applied (B). (C) represents the morphology and alignment of cells cultured on substrata deformed from 2 to 20%. (D) evidenced damaged cells at 25% substrate deformation. (At the top of the figure the grid used to measure the cell alignment).
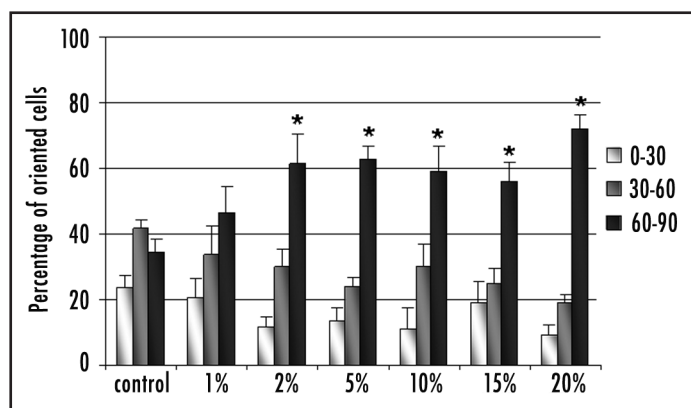

Figure 4. Percentage of oriented cells in the three angle-range considered varying the degrees of substrate deformation. (* indicates significant results compared with the control with $p \leq 0.05$).

Actin filaments. Figure 6 shows fluorescent micrographs (40x magnification) of cells stained with phalloidin-TRITC labeling actin filaments and morphometrical measures of actin filaments. Human fibroblasts cultured on stretched substrata showed that
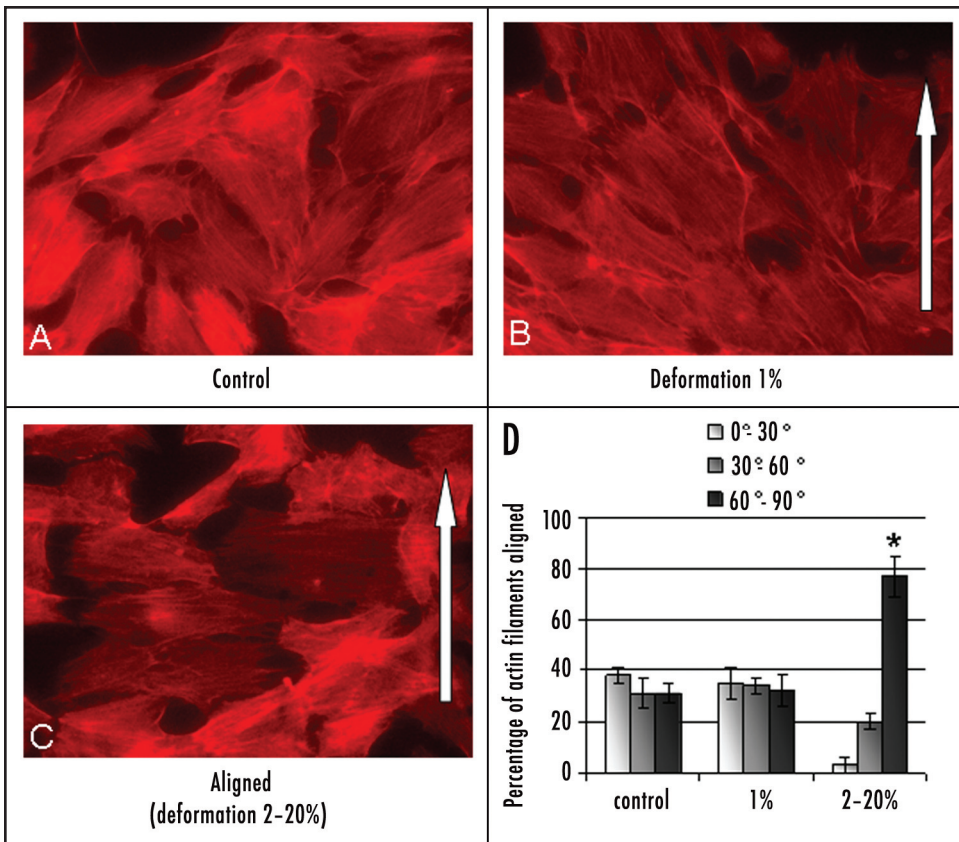
Figure 6. Fluorescence microscopy of phalloidin-TRITC stained cells for actin filaments on control (A) and when 1% substrata deformation was applied (B). (C) represents the morphology and alignment of actin stress fibers when cells were cultured on substrata deformed from 2 to 20%. (D) shows the graph obtained from the morphometric measures on actin filaments reorientation after applying mechanical stress (2% 0.5 Hz three hours). (* indicates significant results compared with the control with p ≤ 0.05).
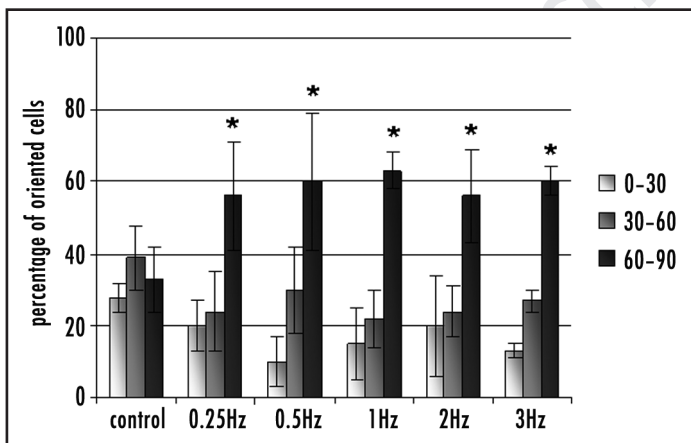

Figure 5. Percentage of oriented cells in the three angle-range considered varying the frequency of substrate deformation. (* indicates significant results compared with the control with p ≤ 0.05).

the actin cytoskeleton remodeling follows cell alignment. Control unstretched cells (Fig. 6A) and cells cultured on 1% deformed silicon (Fig. 6B) evidenced dense and randomly oriented actin filaments while after three hours of elongation in a deformation range between 2 and 20%, cells formed bundles of stress fibers oriented near perpendicular to the deformation direction (Fig. 6C). Seventy-seven ± 8%

of actin filaments was oriented in the range of 60–90° angle with respect to the uniaxial stretch direction. A significant lower percentage of cells was in the range of 0–30° angle (2 ± 3%) and 30–60° (34 ± 3%) (Fig. 6D). At 25% substrate deformation, cell sufferance shown in contrast microscopy (Fig. 3D) was evidenced also in fluorescence microscopy (data not shown) where cells became smaller with few actin filaments randomly oriented.

DISCUSSION

Cyclic stretching plays an important role in creating the architecture of tissues (e.g., bone, arteries, ligament) but the mechanisms involved in cell orientation as response to mechanical stress remains for certain aspects unclear even if actin cytoskeleton seems to be strongly involved. Literature reported several studies concerning cell response to mechanical stretching[12-15] but in none of them cell response to different stretching magnitude or to different stretching frequencies have been compared. In the present work, silicon deformable substrates have been elongated for three hours uniaxially and magnitudes have been applied from values that produce no response on cellular behavior (1%) until a cellular damage that was reached where many cells are detached, damaged or round-shaped (25%). Cell counting of oriented cells after applying a mechanical stress showed that a substrate deformation from 2 to 20% is well tolerated by the cells and enable more than 60% of cells to align perpendicularly to the stress direction with a percentage of cell orientation significantly higher respect to cells cultured on control. Our results, obtained after three hours of substrate deformation, suggest that the molecular mechanism which regulates cell orientation involves a really quick response affecting directly cytoskeleton proteins and other structural components (i.e., focal adhesions sites) which have an established role in mechanotransduction, being able to transmit and modulate tension within the cell.

Moreover, within few hours of mechanical stimuli applied to cells cultured on deformable substrates, cells flatten and spread and active filaments form actin stress fibers.[16] The actin filaments resulted aligned perpendicularly to the stress direction, confirming data obtained by Wang and colleagues, which stated that stress fibers can only be formed in a direction with minimal substrate deformation, probably guiding cell spreading in the same direction. In fact, the time frame for formation of this new cell morphology and reorganization of actin microfilaments is consistent with the duration of the experiments used in our work. Our data show that, short stressing time (three hours) is sufficient to induce fibroblasts reorientation and 1% substrate deformation is not sufficient to evidence statistical significant reorientation obtained at ≥2% substrate deformation.

After three hours of stretching we found that at constant percentage of substrate deformation, different frequencies applied do not modify cell alignment. These findings support the hypothesis that cell orientation is a defense which allows minimizing the stress on cells. In fact, the alignment direction corresponds to the less strength applied on the cells, thus the substrate deformation has a stronger role compared to the frequency. Thus, at short stretching time, the frequency of mechanical stress applied seems not to have a key role for cell orientation which resulted influenced by stretching magnitude. In fact, it has been evidenced that cell orientation in the angle range 60–90° occur from a 2% to a 20% substrate deformation, with no differences if the stress is applied at low (0.25 Hz) or high (3 Hz) frequencies. Cells do not sustain substrate deformations higher than 25% and do not modify their orientation at magnitude lower than 2% substrate deformation. Actin filaments work as a guide to modify cell alignment, orienting their direction as well perpendicularly to the stress direction. These findings are useful considering their application in tissue engineering in order to mimic as close as possible the physiological conditions as for instance in the cardiovascular system.

References

1. Wang JHC, Goldschmidt-Clermont P, Wille J, Yin FCP. Specificity of endothelial cell reorientation in response to cyclic mechanical stretching. J Biomech 2001; 34:1563-72.
2. Mullender MG, Huiskes R. Proposal for the regulatory mechanism of Wolff's law J. Orthop Res 1995; 13:503-12.
3. Buck RC. Reorientation response of cells to repeated stretch and recoil of the substratum. Exp Cell Res 1980; 127:470-4.
4. Buckley MJ, Banes AJ, Levin LG, Sumpio BE, Sato M, Jordan R, Gilbert J, Link GW, Tran Son Tay R. Osteoblasts increase their rate of division and align in response to cyclic mechanical tension in vitro. Bone Miner 1988; 4:225-36.
5. Dartsch PC, Hammerle H, Betz E. Orientation of cultured arterial smooth muscle cells growing on cyclically stretched substrates. Acta Anat 1986; 125:108-13.
6. Dartsch PC, Betz E. Cellular and cytoskeletal response of vascular cells to mechanical stretch. In: Plank H, Dauner M, Renardy M, eds. Medical Textiles for Implantation. Berlin: Springer, 1992:193-218.
7. Pender N, McCulloch CA. Quantitation of actin polymerization in two human fibroblast subtypes responding to mechanical stretching. J Cell Sci 1991; 100:187-93.
8. Hayakawa K, Sato N, Obinata T. Dynamic reorientation of cultured cells and stress fibers under mechanical stress from periodic stretching. Exp Cell Res 2001; 268:104-14.
9. Banes AJ, Gilbert J, Taylor D, Monbureau O. A new vacuum operated stress-providing instrument that applies static or variable duration cyclic tension or compression to cell in vitro. J Cell Sci 1985; 75:35-42.
10. Vandenburgh HH. A computerized mechanical cell stimulator for tissue culture: Effects on skeletal muscle organogenesis. In Vitro 1988; 24:609-19.
11. Tba T, Sumpio BE. Morphological response of human endothelial cells subjected to cyclic strain in vitro. Microvasc Res 1991; 42245-54.
12. Wang JHC, Grood ES, Florer J, Wenstrup R. Alignment and proliferation of MC3T3-E1 osteoblasts in microgrooved silicone substrata subjected to cyclic stretching. J Biomech 2000; 33:729-35.
13. Moretti M, Prina-Mello A, Reid AJ, Barron V, Prendergast PJ. Endothelial cell alignment on cyclically-stretched silicone surfaces. J Mater Sci Med 2004; 15:1159-64.
14. Shirinky VP, Antonov AS, Birukov KG, Sobolevsky AV, Romanov YA, Kabaeva NV, Antonova GN, Smirnov VN. Mechano-chemical control of human endothelium orientation and size. J Cell Biol 1989; 109:331-9.
15. Shikata Y, Rios A, Kawkitinarong K, DePaola N, Garcia JGN, Birukov KG. Differential effects of shear stress and cyclic stretch on focal adhesion remodelling, site-specific FAK phosphorylation, and small GTPases in human lung endothelial cells. Exp Cell Res 2005; 304:40-9.
16. Hynes RO, Destree AT. Relationships between fibronectin and actin (LETS protein). Cell 1978; 15:875-86.